NOTICE

The quality of this microform is heavily dependent upon the quality of the original thesis submitted for microfilming. Every effort has been made to ensure the highest quality of reproduction possible.

If pages are missing, contact the university which granted the degree.

Some pages may have indistinct print especially if the original pages were typed with a poor typewriter ribbon or if the university sent us an inferior photocopy.

Previously copyrighted materials (journal articles, published tests, etc.) are not filmed.

Reproduction in full or in part of this microform is governed by the Canadian Copyright Act, R.S.C. 1970, c. C-30.

AVIS

La qualité de cette microforme dépend grandement de la qualité de la thèse soumise au microfilmage. Nous avons tout fait pour assurer une qualité supérieure de reproduction.

S'il manque des pages, veuillez communiquer avec l'université qui a conféré le grade.

La qualité d'impression de certaines pages peut laisser à désirer, surtout si les pages originales ont été dactylographiées à l'aide d'un ruban usé ou si l'université nous a fait parvenir une photocopie de qualité inférieure.

Les documents qui font déjà l'objet d'un droit d'auteur (articles de revue, tests publiés, etc.) ne sont pas microfilmés.

La reproduction, même partielle, de cette microforme est soumise à la Loi canadienne sur le droit d'auteur, SRC 1970, c. C-30.

Design and Finite Element Analysis of Switched Reluctance Motors

Arumugam Rengasamy

A Thesis

in

The Department

of

Electrical Engineering

Presented in Partial Fulfillment of the Requirements
for the Degree of Doctor of Philosophy
Concordia University
Montréal, Québec, Canada

October 1987

ISBN 0-315-41587-8

ABSTRACT

Design and Finite Element Analysis of Switched Reluctance Motors

Arumugam Rengasamy, Ph.D.

Concordia University, 1987

In this thesis, it is noted that although the principle of producing mechanical motion by reluctance variation is not new, practical drives using such a principle could not be developed until 1970's. During the last decade interest in switched reluctance motor drives was revived in the United Kingdom and as a result a commercial switched reluctance motor drive appeared in 1983.

After a review of existing analyses of the switched reluctance motor, the thesis develops an analysis that overcomes many of their limitations. In particular, a finite element analysis is used to determine parameters such as self and mutual inductances. This analysis is used to compare the characteristics of two forms of construction. It is also used to determine the influence of the airgap geometry on the performance of the switched reluctance motor by varying the pole arc/pole pitch ratios of both the stator and rotor.

A design procedure for the switched reluctance motor is developed. This is in a form similar to that for conventional machines in that an output equation is obtained.

End effects are investigated using a three dimensional finite element analysis on one machine. This is used to provide a comparison of the two and three dimensional finite element analyses.

ACKNOWLEDGEMENTS

The author wishes to express his gratitude to his research advisor Dr. J. F. Lindsay for his guidance, support and encouragement during all the stages of this research.

The author's indebtedness to Dr. R. Krishnan, his research advisor, who initiated this research and had been a source of inspiration is acknowledged.

The author expresses his deep appreciation to Dr. D. A. Lowther, McGill University, with whom he had valuable discussions on finite element analysis.

The author wishes to acknowledge the financial support provided by the Natural Sciences and Engineering Research Council of Canada (NSERC) throughout the period of this research. The computational facilities provided by M/S. Infolytica Corporation, Montreal, and McGill University in their Computer Aided Design Laboratory are acknowledged.

Thanks are due to his colleagues Prof. M. A. Panneerselvam, Mr. S. Sriraman and Dr. A. Sambandan of Anna University, Madras for their encouragement and willingness to share the author's personal responsibilities.

Thanks are expressed to Mr. B. Forghani and Mr. D. Seward of Infolytica Corporation with whom the author had the pleasure of working on finite element analysis. Thanks are also due to all the friends in Power Laboratory, Concordia University and in CAD Laboratory, McGill University whose friendship the author will cherish in the years to come.

The author expresses his deep appreciation to his wife (Mangayarkarasi) and his children (Jaikumar and Subashini) who endured long period of separation. But for their patience and understanding he could not have accomplished this research.

TABLE OF CONTENTS

		PAGE
ABSTRACT		iii
ACKNOWLEDGEMENT		v
TABLE OF CONTENTS		vi
LIST OF TABLES		ix
LIST OF FIGURES		x
CHAPTER 1	INTRODUCTION	1
1.1	Introduction to SR motor drives	1
1.2	History of SR motor development	3
1.3	Contributions	8
1.4	Organization of the thesis	8
CHAPTER 2	FINITE ELEMENT ANALYSIS OF SR MOTORS	10
2.1	Introduction	10
2.2	Assumptions	11
2.3	Derivation of partial differential equation	11
2.4	Boundary conditions	15
2.5	MagNet CAD Package	17
2.6	Modeling of magnetization characteristic curve	21
2.7	Postprocessing	23
2.7.1	Calculation of flux linkages	23
2.7.2	Terminal inductance calculation	25
2.7.3	Coenergy calculation	27
2.7.4	Calculation of torque	27
2.8	Conclusion	29

CHAPTER 3	APPLICATION OF FINITE ELEMENT ANALYSIS TO SR MOTOR PERFORMANCE PREDICTION		30
	3.1	Introduction	30
	3.2	Motor specifications	30
	3.3	Analysis of 6/4 motor	37
	3.4	Analysis of 12/10 motor	44
	3.5	Comparison of 6/4&12/10 motor performances	58
	3.6	Conclusion	61
CHAPTER 4	SENSITIVITY OF POLE ARC/POLE PITCH RATIO ON SR MOTOR PERFORMANCE		64
	4.1	Introduction	64
	4.2	Basis of sensitivity study	65
	4.3	Methods of torque calculation	66
		4.3.1 Analytical method	66
		4.3.2 Finite element analysis	69
	4.4	Results	70
	4.5	Conclusion	70
CHAPTER 5	DESIGN PROCEDURE FOR SR MOTORS		80
	5.1	Introduction	80
	5.2	Output equation	81
	5.3	Design considerations	88
		5.3.1 Number of poles	89
		5.3.2 Pole arcs on the stator and rotor	90
		5.3.3 Starting torque	90
		5.3.4 Windings	90
		5.3.5 Airgap	91
		5.3.6 Losses	91

5.4	Selection of design parameters		91
	5.4.1	Speed	91
	5.4.2	Diameter and length	91
	5.4.3	Airgap length	92
	5.4.4	Number of turns	92
	5.4.5	Thermal considerations	94
5.5	Design verification		95
5.6	Operational limits		100
5.7	Conclusion		102
CHAPTER 6	COMPARISON OF 2D AND 3D FINITE ELEMENT ANALYSIS OF A SR MOTOR		104
6.1	Introduction		104
6.2	Problem specification		109
	6.2.1	Two dimensional model	109
	6.2.2	Three dimensional model	109
6.3	Results		112
	6.3.1	Inductance	112
	6.3.2	Flux density	120
	6.3.3	End effects	126
6.4	Conclusion		131
CHAPTER 7	CONCLUSIONS		136
7.1	Conclusion		136
7.2	Recommendations for future work		140
CHAPTER 8	REFERENCES		141
APPENDIX I			149

LIST OF TABLES

		PAGE
Table 3.1	Motor specifications	31
Table 4.1	Average torque values for various stator and rotor pole arc/pole pitch ratios (Analytical Method)	71
Table 5.1	Motor main dimensions	100
Table 6.1	Inductance values calculated using 2D and 3D finite element methods	115

LIST OF FIGURES

		PAGE
Fig. 2.1	Two dimensional region R	13
Fig. 2.2	Finite element subdivisions (6/4 motor) Aligned position	16
Fig. 2.3	Finite element subdivisions (6/4) motor Rotor pole axis at 25 degrees from the aligned position	18
Fig. 2.4	Finite element subdivisions in the airgap region S-stator R-rotor A-airgap	20
Fig. 2.5	Winding arrangement in SR motor	24
Fig. 2.6	Typical flux linkages vs current characteristic	28
Fig. 3.1	Motor configuration in aligned position (6/4 motor)	32
Fig. 3.2	Motor configuration in aligned position (12/10 motor)	33
Fig. 3.3	Magnetization curve (M-19 Steel)	35
Fig. 3.4	Finite element subdivision of the motor model 6/4 motor (aligned position).	36
Fig. 3.5	Flux plot. Aligned position.	38
Fig. 3.6	Flux plot. Unaligned position.	39
Fig. 3.7	Flux plot. Rotor pole axis at 10 degrees from the aligned position	40
Fig. 3.8	Flux plot. Rotor pole axis at 20 degrees from the aligned position.	40
Fig. 3.9	Flux plot. Rotor pole axis at 30 degrees from the aligned position.	41
Fig. 3.10	Flux linkages per pole vs current characteristic	41
Fig. 3.11	Terminal inductance vs rotor position	43
Fig. 3.12	Leakage inductance vs rotor position, due to leakage	

	flux to yoke of one phase	43
Fig. 3.13	Leakage inductance vs rotor position, due to leakage flux to adjacent pole winding of one phase	45
Fig. 3.14	Average torque vs rotor position for 9 A excitation	45
Fig. 3.15	Average torque per ampere characteristic (a) 33% excitation (b) 40% excitation (c) 50% excitation	46
Fig. 3.16	Finite element subdivision of 12/10 motor model in the aligned position	48
Fig. 3.17	Flux plot. Aligned position	49
Fig. 3.18	Flux plot. Unaligned position	50
Fig. 3.19	Flux plot. Rotor pole axis at 4 degrees from the aligned position	51
Fig. 3.20	Flux plot. Rotor pole axis at 8 degrees from the aligned position	51
Fig. 3.21	Flux plot. Rotor pole axis at 12 degrees from the aligned position	52
Fig. 3.22	Total flux linkages vs excitation of one pole winding	52
Fig. 3.23	Comparison of flux linkages	53
Fig. 3.24	Terminal inductance vs rotor position	55
Fig. 3.25	Leakage inductance vs rotor position, due to leakage flux to yoke of one phase	55
Fig. 3.26	Leakage inductance vs rotor position, due to leakage flux to adjacent pole winding of one phase	56
Fig. 3.27	Average torque vs rotor position for 6 A excitation	56
Fig. 3.28	Average torque per ampere characteristic (a) 33% excitation (b) 40% excitation (c) 50% excitation	57
Fig. 3.29	Comparison of flux linkages of 6/4 and 12/10 motors	59

Fig. 3.30	Total leakage inductance vs rotor position per phase (a) 6/4 motor. (b) 12/10 motor.	60
Fig. 4.1	Flux linkages vs excitation characteristic (Analytical Method)	72
Fig. 4.2	Average torue vs stator pole arc/pole pitch ratio (Excitation at 12 ampere)	73
Fig. 4.3	Average torque vs pole arc/pole pitch ratio (stator and rotor ratios are equal)	74
Fig. 4.4	Average torque vs pole arc/pole pitch ratios of stator and rotor (Excitation at 2 amperes)	75
Fig. 4.5	Average torque vs pole arc/pole pitch ratios of stator and rotor (Excitation at 4 amperes)	76
Fig. 4.6	Average torque vs pole arc/pole pitch ratios of stator and rotor (Excitation at 8 amperes)	77
Fig. 4.7	Average torque vs pole arc/pole pitch ratios of stator and rotor (Excitation at 12 amperes)	78
Fig. 5.1	Typical SR motor configuration (6/4 motor)	83
Fig. 5.2	Approximate flux linkages vs current characteristic	84
Fig. 5.3	Flux linkages vs excitation characteristic of the designed motor obtained using finite element analysis	97
Fig. 5.4	Terminal inductance vs excitation	98
Fig. 5.5	k_2 and $\frac{L_a^s}{L_u}$ vs excitation	99
Fig. 5.6	$k_2 B$ vs excitation	101
Fig. 6.1	Motor configuration used for 2D analysis Aligned position	105
Fig. 6.2	2D Finite element mesh for aligned position	106

Fig. 6.3	Motor confoguration used for 2D analysis	
	Unaligned position	107
Fig. 6.4	2D Finite element mesh for unaligned position	108
Fig. 6.5	Side view of the motor model used for 3D analysis	110
Fig. 6.6	3D finite element model for unaligned position	111
Fig. 6.7	Contours used for flux calculation	113
Fig. 6.8	B-H Curve used for 2D and 3D analysis	114
Fig. 6.9	Flux density plot for 2D solution	
	Aligned position	116
Fig. 6.10	Flux density plot for 3D solution	
	Plane at z=0 cm, aligned position	117
Fig. 6.11	Flux density plot for 3D solution	
	Plane at z=4.5 cm, aligned position	118
Fig. 6.12	Flux density plot for 3D solution	
	Plane at z=5.4 cm, aligned position	119
Fig. 6.13	Flux density plot for 2D solution	
	Unaligned position	121
Fig. 6.14	Flux density plot for 3D solution	
	Plane at z=0, unaligned position	122
Fig. 6.15	Flux density plot for 3D solution	
	Plane at z=4.5 cm, unaligned position	123
Fig. 6.16	Flux density plot for 3D soultion	
	Plane at z=5.4 cm, unaligned position	124
Fig. 6.17	Flux under a stator pole in the axial direction	
	Aligned position	125
Fig. 6.18	Flux under a stator pole in the axial direction	
	Unaligned position	125

Fig. 6.19	Line showing longitudinal slice at 75 degrees Aligned position	127
Fig. 6.20	Outline of longitudinal slice, showing zoom area Aligned position	128
Fig. 6.21	Flux density plot along longitudinal slice Aligned position	129
Fig. 6.22	Flux density plot over zoomed area Aligned position	130
Fig. 6.23	Line showing longitudinal slice at 63 degrees Unaligned position	132
Fig. 6.24	Outline of longitudinal slice, showing zoom area Unaligned position	133
Fig. 6.25	Flux density plot along longitudinal slice Unaligned position	134
Fig. 6.26	Flux density plot over zoomed area Unaligned position	135

CHAPTER 1

INTRODUCTION

1.1 Introduction to SR motor drives

With the advent of semiconductor power devices, there had been considerable innovations in the development of variable speed drives. Switched Reluctance (SR) motor drives are one of such developments. They have been under active research and development during the past two decades [1]-[4]. The first motor operating on the principle of reluctance variation was built in 1842 [5]. Until the recent past, the reluctance motors were considered to be highly inefficient with low specific power output. The present developments are primarily due to the availability of reliable semiconductor power switches and the modern computer aided design process. The power density of SR motor drive is high and they operate with high power factor and efficiency. Their controllers are simple with a minimum number of switching devices compared with induction motor controllers [6],[7].

The doubly salient switched reluctance motor resembles the variable reluctance stepper motor in construction. The stator and rotor of the motor have even but unequal number of salient poles. The stator poles carry windings and there are no windings on the rotor so that there is no rotor copper loss. Each concentrated winding on the stator poles when connected with the diametrically opposite pole winding in series constitutes one phase of the motor. Each phase winding is excited at appropriate times such that the motor develops torque in the required direction. Rotor position sensors are used to generate control signals to switch currents into the phase windings.

The air gap length of the motor is made very small so that the motor can

be operated under saturated conditions. This results in higher coenergy change as the rotor moves from the maximum reluctance position towards the minimum reluctance position, compared with that in unsaturated conditions. Hence, the motor develops more torque [8].

The doubly salient switched reluctance motor operates on the principle of the rotor poles getting themselves aligned along the axis of minimum reluctance when the appropriate stator pole windings are excited. Since the torque is produced due to the change of reluctance in the motor, the direction of current flow in the excited winding is immaterial. This results in the unipolar operation of the motor with only one switching device required in each phase of the motor. The number of switching operations for each revolution of the motor depends on the number of phases and the number of rotor poles. The direction of rotation of the motor depends on the sequence of switching the stator phase windings.

The speed of the motor can be varied by altering the switching frequency when the torque is held constant. The developed torque at constant power can be controlled by the instant and duration of switching. Thus, the switching angles are controlled to achieve the desired speed and torque and to stabilize the operation of the motor. At low speeds chopping is used to limit the peak current.

For convenience, the position when a stator tooth is opposite a rotor tooth such that the reluctance is minimum is defined as the aligned position. The unaligned position is defined as that when the stator tooth is opposite the rotor slot such that the reluctance is maximum.

1.2 History of SR motor development

The method of electromagnetic energy conversion used in SR motor is not new. From the day Faraday demonstrated the possibility of obtaining mechanical motion by electromagnetic means in 1821 there had been several attempts to build electric motors which were then called as 'electromagnetic engines'. In 1840 W.H.Taylor made a motor utilizing the force of magnetic attraction between the soft iron armatures and the electromagnets [9]. The special feature of his motor was that the electromagnets were simply switched on and off and were never reversed. Charles Wheatstone, then Professor of Experimental Philosophy at King's College, London, who visited Taylor's machine with his students, later constructed motors which he called 'eccentric electromagnetic engines'. His motors which are now in the Science Museum, London were not developed further as a practical source of energy conversion.

In 1842, Robert Davidson made a motor based on similar operating principles as the earlier versions, for driving a battery powered vehicle [10]. Later Charles Grafton Page of U.S.A. made a large switched field machine in 1851 for traction purposes [11]. The above attempts were not successful due to poor electromagnetic and mechanical designs and the unavailability of suitable switching devices. They used the commutator as the rotor position sensor to switch currents into the windings and there was no provision to change the duty cycle of the excitation.

Practical application of the above energy conversion principle was made to develop other type of motors early in this century. It was used to build high frequency alternators known as pulsating field or induction alternator type machines [12],[13]. The later versions of these machines were known as the vernier slotting machines [14].

Due to the availability of reliable semiconductor switches such as the transistors and thyristors, the interest in switched field machines was revived in the 1960's. Several patents were filed in U.S.A. in early 1970's [2]-[4].

The first commercial version of the switched reluctance machine appeared in the form of single phase shaver motors with mechanical contactors. More recently, a number of researchers have directed their attention to various particular design developments of variable reluctance stepper motors aimed at increasing their power levels considerably.

Lawrenson and others [15]-[17] investigated the reluctance machines in the 1960's and published papers on various types of low inertia rotor, variable reluctance motors. In 1965, Lawrenson has reported that these motors, when given suitable design and development opportunity, could surpass at least in some aspects, the induction motors [18]. A considerable amount of work on variable reluctance stepper motors [19]-[24] has been done and has later been extended to the design of doubly salient switched reluctance motors.

It has been pointed out by Byrne and Lacy [25], and O'Connor [26] that the saturation profoundly affects the force tending to align the partially overlapped teeth in doubly salient structures. If the magnetic material has square loop B-H curves and the saturation is confined to the pole faces then the force developed could be almost twice that in the unsaturated conditions.

Byrne and Lacy [4] in their patent specification have described a single stack, 2 phase stator and 2 pole rotor variable reluctance machine which was unidirectional. They have shaped the rotor poles such that there is uniform rate of flux increase with mechanical displacement of the rotor. The airgap length was made small so that saturation could be produced in the pole faces with the objective of increasing the torque output as proposed by Jarret [27].

Among the developments of variable reluctance motors was an axial air-gap motor developed by Unnewehr and Koch [28] for battery powered traction. Originally conceived as a low power motor, this reluctance motor has subsequently been developed for many high power applications such as traction, fans, blowers and pumps. Due to mechanical complexities and cost, there were not much further improvements. Koch [29] subsequently described a 3 phase, single stack pulsating field reluctance motor, very similar to those of the present SR motors. The motor had salient poles on the stator and rotor and was supplied from a fixed voltage dc source. He presented an analysis of the operation of the motor to determine the current waveforms, controller power output, shaft power output of the motor, gating angles to control the speed torque characteristics. He has also described the determination of an optimum pole and gap dimensions based on the linear permeance values of doubly salient devices [30]. But, he has not considered the fundamental effects of negative torque developed during part of the operating cycle and the possibility of switching current into the phase winding before the onset of increasing inductance period, which are essential in practical systems.

Bausch and Relke [31] extended the stepping motor strategies to a 4 phase double stack reluctance motor using a drive system proposed by them [32] for low speed operation. They were particularly interested in the inherent series motor characteristic of the vehicle drive.

Harris et al. [22],[23] have proposed a theory for the static reluctance torque produced by a doubly salient machine when its magnetic circuit is strongly saturated as that occurs in the majority of stepping motors. They have used the linear permeance values derived by Mukherji et al. [30] from the unpublished work of F.W.Carter, to predict the performance of the doubly salient machines. They also have shown that saturation sets a theoretical limit

to the torque that can be obtained per unit rotor volume. The relative proportions of tooth, slot and airgap that produce the maximum torque are investigated using the linear permeance data. Subsequently, they have reported a unifying approach for predicting static torque in stepping motor structures. They developed an expression for the holding torque, duly introducing factors to account for (a) the fraction of the rotor volume effectively utilized for torque production at a time, (b) the shape of the torque angle characteristic and (c) the finite magnitude of excitation current in the windings that do not cause saturation in the unaligned position.

In 1974, a feasibility study of ac drives for battery vehicles was conducted by Nottingham University [6]. In that study, it was pointed out that an inverter feeding a doubly salient reluctance motor was more promising than an induction motor system. During that time, research on SR motor was already in progress at Leeds University. In 1975, Chloride Technical Ltd. sponsored a combined project on the analysis, design and development of SR motors to both these universities. The outcome of their research was the first commercial SR motor variable speed drive in 1983 [33]-[35].

Stephenson and Corda of Leeds University have described a more accurate method to compute the torque and current of doubly salient reluctance motors from the measured or predicted magnetization data [36]. The other methods of performance prediction [22],[23] used linear permeance values presented in references [30] and [37]. The accuracy of the method depends mainly on the permeance values in the aligned and unaligned positions. Subsequently, Corda and Stephenson [38] proposed an analytical method to estimate the aligned and unaligned permeances from the motor geometry and the winding distribution. Their method of calculation assumes that the flux lines

consist of straight line segments and concentric circular arcs, similar to the assumptions of Chai [39].

Ray and Davis of Nottingham University [6] described an inverter for a doubly salient SR motor. An analysis was presented using a linear model for the SR motor to predict the approximate current waveforms and to determine the control strategy of the inverter system. The details of the power converter design were reported by Davis et al. [7], subsequently, for both 3 phase and 4 phase SR motors.

In 1980, Lawrenson et al. [1] have presented the principles of operation, design considerations and test results for SR motors. This is the first paper published on the design considerations of SR motors. The papers published by them later on SR motors [40]-[51] present the development in the motor design, performance, cost comparison, traction application and the power controllers from time to time. There have been several patents associated with the work on SR motors [52]-[56].

Finch et al. [57],[58] have extended the design method developed for stepping motors [23] to design a SR motor with two teeth per stator pole in 1984.

Miller [59] described a nonlinear analysis of SR motor drive system. The basis for the determination of the kVA requirements of the SR motor power converter were discussed. Bose et al. [60] of General Electric described a microcomputer based four quadrant control of a SR motor. A review of the capabilities of different SR motor drives and induction motor drives has been presented by Harris et al. [61]. A unipolar power converter for SR motor was presented by Bass et al. [62]. This converter is designed such that it returns the entire trapped energy in the phase windings to a capacitor when the power switch is commutated.

1.3 Contributions

The following are the major contributions of this thesis.

(a) A 2 dimensional finite element analysis is applied to the analysis of switched reluctance motors.

(b) Two different motor configurations are analyzed, their performance evaluated and compared. Same main dimensions are used for both the configurations to give first true comparison.

(c) The interpolar leakage fluxes are clearly indentified and their magnitudes calculated.

(d) Sensitivity of stator and rotor pole arcs variation on switched reluctance motor performance is investigated.

(e) A design procedure for switched reluctance motors is developed.

(f) A 3 dimensional finite element analysis has been performed to asses the approximations involved in 2 dimensional analysis, due to end effects. A comparison of 2D and 3D results is made.

1.4 Organization of the thesis

This thesis is presented in seven chapters. Most of the chapters are provided with an introduction and a conclusion. This is intended to provide the reader with a brief summary of the materials covered in each chapter.

In Chapter 2, an account of the finite element analysis of SR motors is given. This includes the derivation of the basic equation which defines the magnetic field problem, setting up of boundary conditions, the various steps involved in the use of the MagNet CAD package, modeling of the magnetization curve and the postprocessing of the finite element field solution.

Chapter 3 deals with the application of finite element analysis for the prediction of SR motor performance. Two types of SR motors with different configurations are analyzed. A comparison of the performance parameters such as the flux linkages, terminal inductances, leakage inductances and the torque characteristics are presented.

The sensitivity of the change in pole arc/pole pitch ratio of the stator and rotor on SR motor performance is given in Chapter 4. In addition to the use of finite element analysis an analytical method of sensitivity study is also described.

A step by step design procedure for SR motors is developed and presented in Chapter 5. An output equation similar to that used for the conventional ac machine design is derived. A discussion on some of the design considerations, the selection of design parameters, design verification and an operational limit are given.

Chapter 6 deals with a comparison of 2D and 3D finite element analysis of SR motors. A local parameter such as the flux density and a global parameter such as the inductance are evaluated and compared.

A comprehensive summary of the conclusions reached from this research are presented in Chapter 7. A few suggestions for further research on SR motor drive are given.

CHAPTER 2

FINITE ELEMENT ANALYSIS OF SR MOTORS

The design of SR motors must satisfy certain specific requirements with regard to rating, torque, peak current, temperature rise, etc. The power supply requirements and the intended use of the motor as a fixed or variable speed drive are to be considered. These requirements coupled with the need for design optimization necessitate accurate performance prediction at the design stage.

This chapter deals with the finite element analysis which is used to determine the magnetic field distribution in SR motors. Classical analytical solutions [63],[64] are possible only for idealized cases of grossly simplifying assumptions concerning the machine geometries and material properties. Traditional approaches are generally not suitable for complex geometries and material nonlinearities and therefore, require the use of numerical methods.

2.1 Introduction

With the advent of modern digital computers, numerical methods have become practical in engineering design and are, nowadays, extensively being used to improve the accuracy of magnetic field computations. The finite element analysis has emerged in the past decade as a useful numerical method for magnetic field analysis of electrical machines.

The method is based on formulating the magnetic field equations in terms of magnetic vector potential. The solution is obtained by reformulating the resulting partial differential equation using variational terms and extremizing the associated energy functional by a set of trial functions. To implement the variational formulation, the entire problem region is divided into numerous

subregions called finite elements. In this thesis triangular elements are used. Inside each elemental triangle the magnetic vector potential is linearly interpolated by a first order polynomial from the three vertex values. The complex motor configuration and the nonlinear material characteristic are taken into account in finite element analysis.

2.2 Assumptions

To determine the magnetic field distribution inside the motor, the following assumptions are made:

(a) The magnetic field outside the motor periphery is negligible and hence the outer periphery of the motor can be treated as a zero vector potential line.

(b) The magnetic material of the stator and rotor cores is isotropic and the magnetization curve is single valued, i.e., hysteresis effects are neglected.

(c) The magnetic vector potential, A and the current density vector, J have only axially directed components and are invariant in that direction.

(d) The magnetic field distribution is constant along the axial direction of the motor.

(e) The electromagnetic field is quasistationary, i.e., displacement currents are neglected.

(f) Time harmonic effects are absent.

(g) In the two dimensional analysis the end effects are neglected.

2.3 Derivation of Partial Differential Equation

The fundamental laws governing all electromagnetic fields can be expressed by the well known Maxwell's equations. With the above assumptions the Maxwell's equation become,

$$Curl\ H = J \tag{2.1}$$

$$Div\ B = 0 \tag{2.2}$$

The constituent relation is

$$B = \mu H \tag{2.3}$$

where μ is the permeability of the magnetic material which is a single valued function of magnetic flux density B.

By defining the magnetic vector potential, A as

$$B = Curl\ A \tag{2.4}$$

and by using Coulomb's convention, we assume that

$$Div\ A = 0 \tag{2.5}$$

From equations (2.1) and (2.3)

$$Curl\ (\gamma B) = J \tag{2.6}$$

where γ is the reluctivity of the magnetic material which is reciprocal of the permeability.

Substituting equation (2.4) into equation (2.6), we get

$$Curl\ (\gamma\ Curl\ A) = J \tag{2.7}$$

which may be regarded as more general, because the problem region may include non zero current densities. The reluctivity γ is field dependent and thus equation(2.7) is nonlinear in iron regions.

Since A has only z-directed components $A_z(x, y)$,

$$Curl\ A = \frac{\partial A}{\partial y}\vec{i} - \frac{\partial A}{\partial x}\vec{j} \tag{2.8}$$

From equations (2.7), (2.5) and (2.8), we get

$$\frac{\partial}{\partial x}(\gamma\frac{\partial A}{\partial x}) + \frac{\partial}{\partial y}(\gamma\frac{\partial A}{\partial y}) = -J \tag{2.9}$$

Consider Fig. 2.1 where a two dimensional finite region,R in the x,y plane which represents a typical problem region, bounded by S, has been shown. The region R contains a current region, an iron region having nonlinear materials

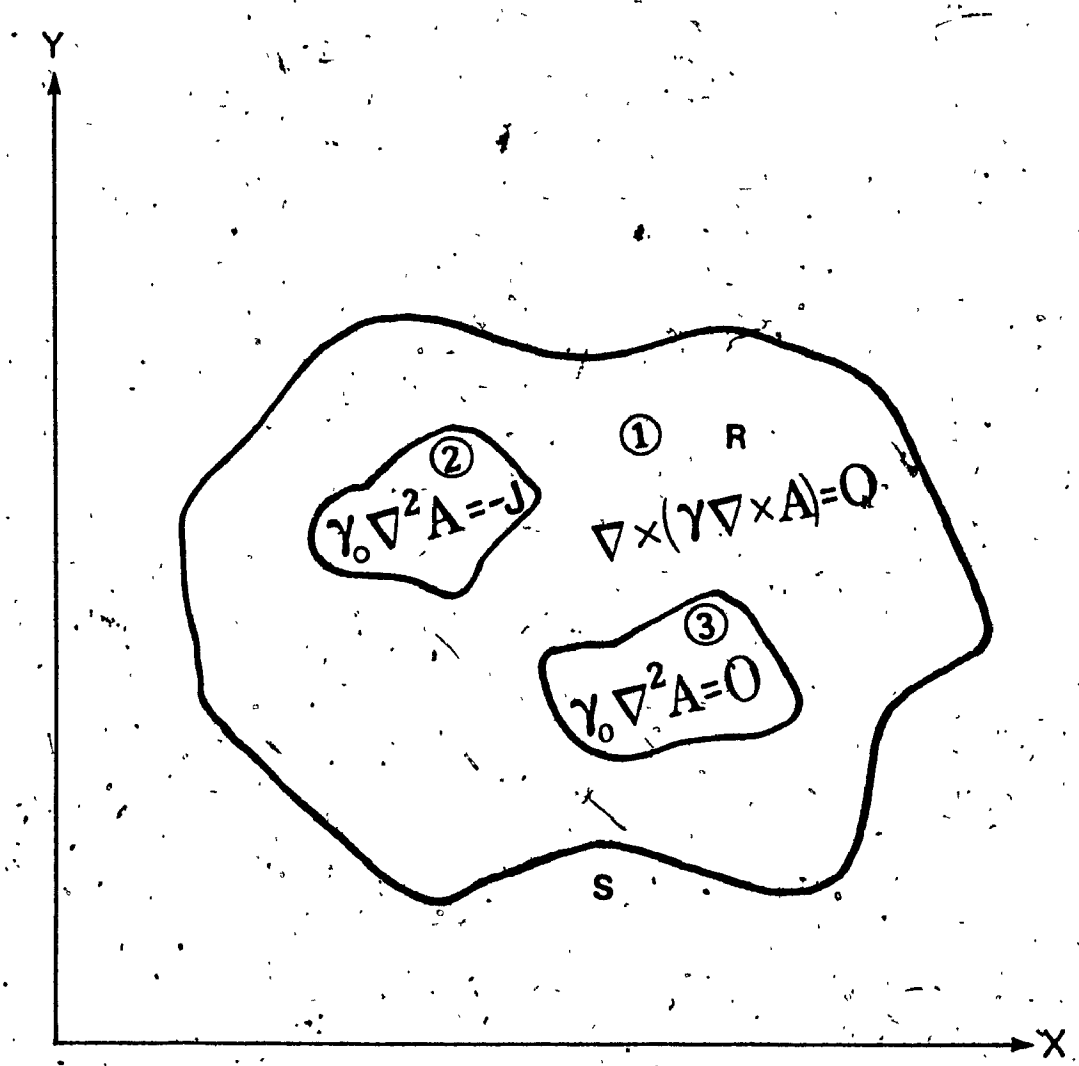

Fig. 2.1. Two dimensional region R

and a non-iron current free region. The equation(2.9) is the general partial differential equation applicable to all the above three regions within the problem region R.

When we consider the SR motor in the x,y plane as the problem region R, then for the stator and rotor core regions where there are material nonlinearities present due to saturation but have no excitation current density present, the equation(2.9) can be written as,

$$\frac{\partial}{\partial x}(\gamma\frac{\partial A}{\partial x}) + \frac{\partial}{\partial y}(\gamma\frac{\partial A}{\partial y}) = 0 \tag{2.10}$$

The winding regions carrying excitations have no iron parts and hence equation(2.9) reduces to

$$\gamma\,(\frac{\partial^2 A}{\partial x^2} + \frac{\partial^2 A}{\partial y^2}) = -J \tag{2.11}$$

The equation(2.9), for the airgap regions where there are no current carrying conductors or iron parts, becomes

$$\gamma\,(\frac{\partial^2 A}{\partial x^2} + \frac{\partial^2 A}{\partial y^2}) = 0 \tag{2.12}$$

The equation(2.9) is the two dimensional nonlinear partial differential equation which is to be solved to get the magnetic vector potential values when the excitation current density is specified. The solution of this equation in closed form is very difficult to obtain due to the complex geometry of the SR motor and the nonlinear nature of the core material. Hence, numerical methods such as finite difference and finite element are particularly useful. In this thesis, the finite element method is used to obtain the field solution.

To obtain a numerical solution to the field problem which is free from topological and geometrical restrictions a variational formulation is used [65]. This formulation incorporates the boundary conditions during its solution process and also permits triangular finite elements of any size and material

property. From the known boundary conditions, an interpolation technique is used to determine the the nodal magnetic vector potential. The solution is obtained by minimizing the nonlinear energy functional

$$F = \int_R \left[\int_0^B H.dB - J.A \right] dR \qquad (2.13)$$

where R is the problem region of integration.

The entire problem region is subdivided into triangular finite elements. The elements are defined such that the sides of the triangle coincide with the boundary of each material. Smaller elements are used where the magnetic flux density is expected to change very much. Such regions are the pole tips and the airgap between the overlapping poles.

2.4 Boundary Conditions

In SR motor analysis, based on the assumptions made earlier, there are certain nodes lying on a contour having a specified potential value. In some cases, the potential of the nodes on a specified line may be constrained to have a certain value of the potential on another line segment. Or, the difference in potential may be specified without knowing the exact value of the potential itself. The nodal potentials specified may be for exterior or interior boundary nodes. Depending on the nature of constraints they are classified as Neumann, Dirichlet or Periodic boundary conditions.

In order to identify these boundary conditions, let us consider one quarter of the cross section of the SR motor, shown in Fig. 2.2. When the rotor is in the aligned position, the pole axis of the stator and rotor poles has geometric as well as magnetic symmetry. Hence, the aligned pole axis may be considered as an equipotential line of zero magnetic vector potential. Based on the assumption that the flux lines are confined within the motor core only, the

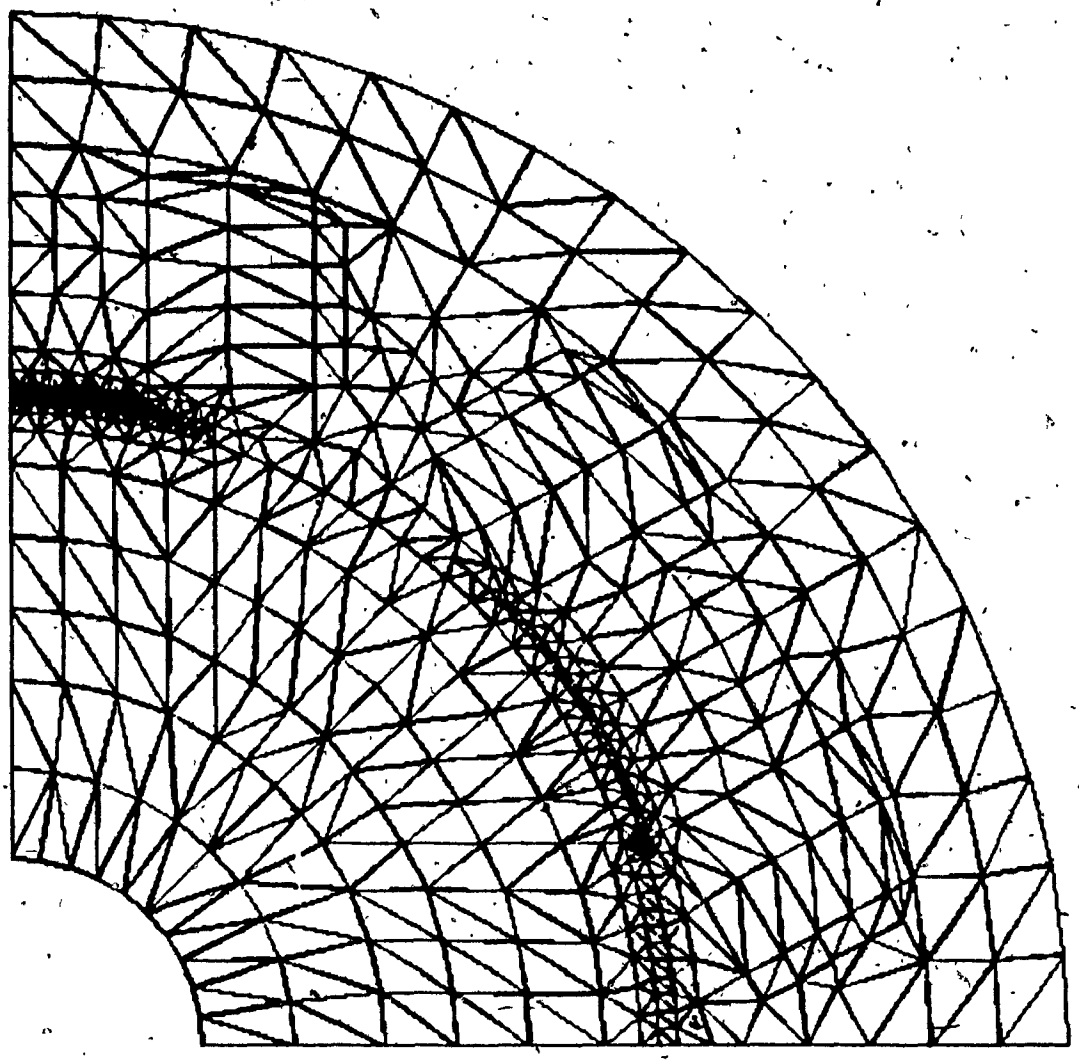

Fig. 2.2 Finite element subdivisions (6/4 motor)

Aligned position

exterior boundary of the stator and rotor shaft are taken as an equipotential line with zero magnetic vector potential magnitude. The nodes on these boundaries are specified by the Dirichlet (A=0) boundary condition. They are specified using unary constraints.

When the rotor is in the aligned position, the radial line on the horizontal axis is a line of even symmetry in A. The flux lines cross this line at right angles. Hence, the normal derivative of the potential A is zero on this line. Also, along the iron air boundaries inside the motor the flux lines impinge on the iron surfaces at right angles due to the very high value of the permeability of iron compared with that of air. These boundaries are called Neumann boundaries where $\frac{\partial A}{\partial n} = 0$. This is also known as natural boundary condition.

Consider Fig. 2.3 where one half of the motor is shown. The rotor is shown to be displaced from the aligned position. In such cases, it can be observed that the symmetry of the magnetic circuit is upset. But the physical conditions repeat after half the motor cross section. This periodic nature of the magnetic circuit condition results in a periodic nature of the flux density and that of the magnetic vector potential. The vector potential and/or its normal derivative are not known along the radial boundary. Still, the corresponding nodes on the radial lines on either side of the shaft are constrained to have the same magnitude of the potential but with opposite polarity, whereas the normal derivatives of the vector potential at these nodes have equal values. These are denoted as periodic boundary conditions and are specified by using binary constraints.

2.5 MagNet CAD Package

The finite element analysis is performed using a MagNet CAD package. It involves preprocessing, problem editing, solving and postprocessing operations.

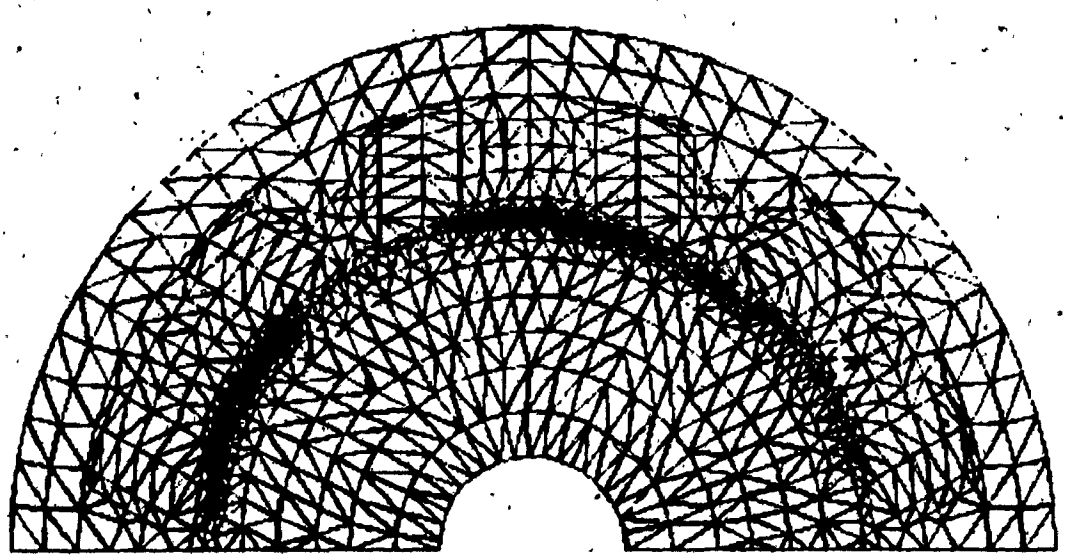

Fig. 2.3 Finite element subdivisions (6/4) motor

Rotor pole axis at 25 degrees from the aligned position

Preprocessing comprises the specification and subdivision of the motor geometry to be analyzed. With the knowledge of the main dimensions, the minimum motor geometry that could be used for analysis is determined based on the geometric and magnetic symmetry that exists for a given rotor position.

The subdivision of the problem region has been done using triangular elements of arbitrary shape and size with the restriction that every single element shall be entirely in one region of the same material and that the union of all elements shall create a problem region without overlapping. Finer meshes are to be used wherever the flux density is likely to change very much. Fig. 2.4 shows the finite element subdivision of the airgap region used for the analysis of a SR motor with six stator poles and four rotor poles. The elements should be such that the included angle of each triangle is not less than 5 degrees. A higher aspect ratio for an element has to be avoided as it may result in numerical instability. It is important to keep in mind that a valid mesh need not be a good mesh approximation.

Preprocessing also includes, the material characteristic modeling and setting up boundary conditions. Cubic Hermite interpolation polynomials are used to represent the B-H curve of the core material. Sufficient data points will result in a better approximation of the characteristic. Best curve fitting is absolutely essential and the material characteristic has to be monotonic for all values of flux density, otherwise, an unique solution can not be guaranteed [66].

Problem editing requires the specification of the excitation in the winding region. The winding region, the excitation in ampere conductors and its polarity are given as the input. The magnetization characteristic for the core

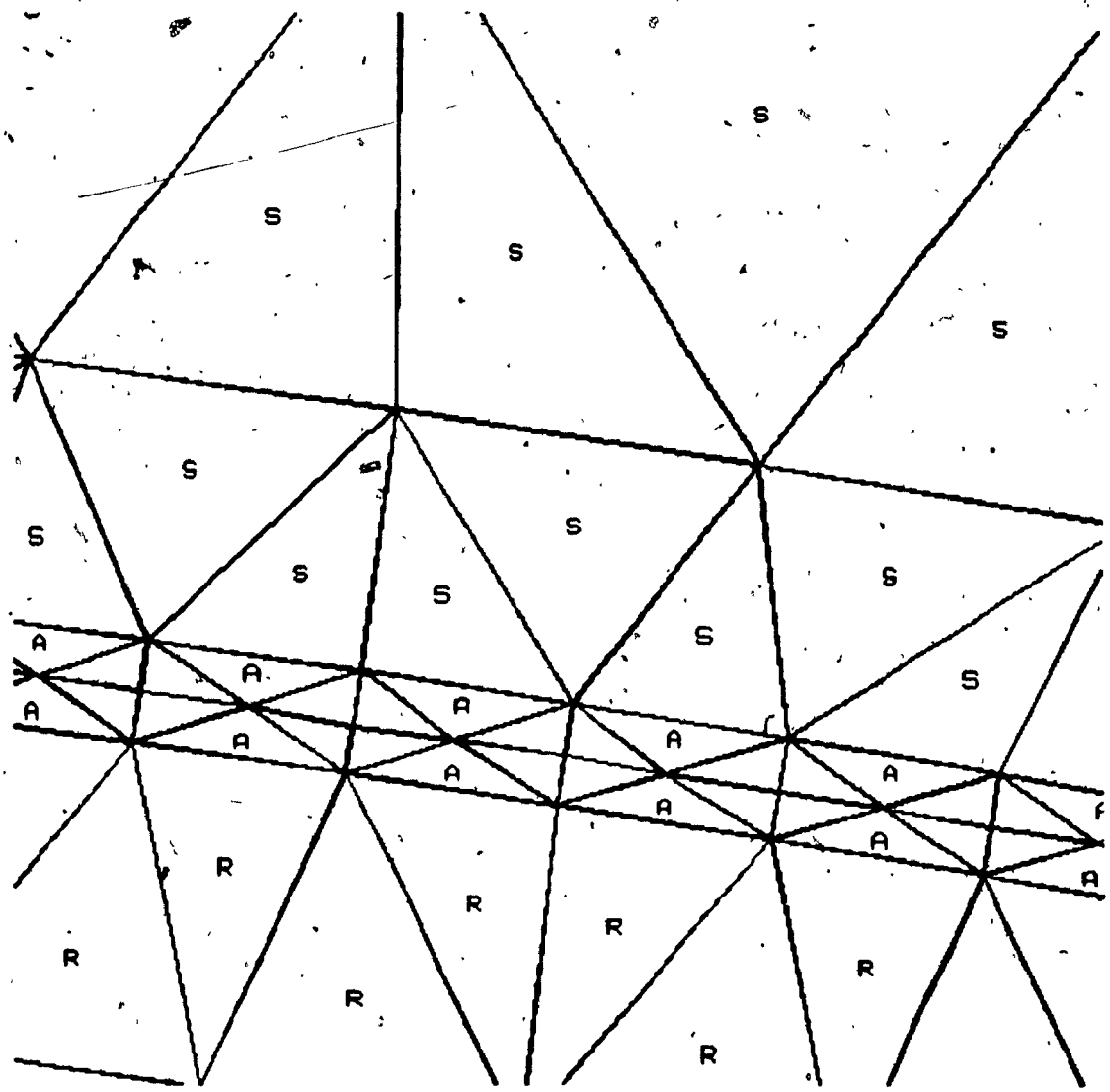

Fig. 2.4 Finite element subdivisions in the airgap region

S-stator R-rotor A-airgap

material, the type of solver to be used and the tolerance during numerical iterations are also specified during problem editing.

Once the problem is edited, then the CAD package does not require user interaction during the solution process. The output of the solver will be a digital version of the magnetic field. Further manipulations are required to extract engineering information from the mathematical solutions.

During postprocessing, the mathematical solution which is in the form of the nodal potential values is processed to obtain specific results such as the flux linkages, inductance, torque, etc. By utilizing the BASIC style programming capability of the CAD package, specific subprogrammes are written. These subprogrammes, known as the User Defined Verb are used to calculate a certain value of the desired result.

2.6 Modeling of Magnetization Characteristic Curve

Finite element analysis of magnetic devices requires the use of a single equation to represent the magnetization characteristic of the core material. A number of methods were proposed in the past to model the magnetic material property [67],[68]. They use power series approximations, transcendental functions, Fourier series, hyperbolas in the form of Frocilch's equation, a sum of exponentials, a rational fraction approximation, etc. These equations contain constants which are to be determined by trial and error. All the iterative methods require repeated evaluation of reluctivity and its first derivative with respect to each elemental flux density. This necessitates the modeling of the B-H curve using a computationally cheap and accurate method.

The Newton Raphson iterative method is used in the finite element analysis of nonlinear magnetic field problems. In order to exploit the quadratic convergence properties of Newton's method the reluctivity of the core material

has to be modeled as a function of squared flux density and the function must have a first derivative. It is shown by Charl that the function must be continuous and should vary monotonically to yield a unique solution. The convergence rate is quite sensitive to the consistency of the curve modeled for reluctivity and its first derivative. Therefore, the iron should be characterized by a single very smooth curve for which its derivative is obtained simultaneously. When cubic splines are used to model the reluctivity characteristic these requirements are well satisfied at low computational cost [69].

In order to model the reluctivity characteristic it is necessary to subdivide the squared flux density axis into a number of segments so that the accuracy can be improved. The following requirements are to be satisfied when a cubic spline fit is used.

(a) The derivative and the curvature must be continuous at all end points.

(b) At B=0 the slope must be zero.

(c) The slope in the rightmost segment must be constant.

A simpler model for the reluctivity characteristic was proposed by Brauer [70]. The characteristic is approximated by the equation

$$H = [k_1 exp(k_2 B^2) + k_3] B \qquad (2.14)$$

It can be seen that the reluctivity and its derivative are obtained by simple equations. They are much easier to employ and have fine convergence properties. The constants k_1, k_2 and k_3 can be evaluated accurately by using a Newton's scheme [71].

The MagNet CAD package used for the analysis of SR motors uses cubic Hermite interpolation polynomials to model the reluctivity characteristic. The reluctivity is expressed as a function of squared flux density.

2.7 Postprocessing

2.7.1 Calculation of Flux Linkages

Consider one pole of the motor carrying a concentrated winding as shown in Fig. 2.5. The flux ϕ, that is linked by a representative turn of a coil can be expressed in terms of the flux density B, and the area enclosed by the coil. Thus,

$$\phi = \int B.dS \tag{2.15}$$

Since the flux density can be expressed in terms of the magnetic vector potential A, as

$$B = Curl\ A \tag{2.16}$$

the expression for the flux will be,

$$\phi = \int Curl\ A.dS \tag{2.17}$$

Using Stoke's theorem,

$$\phi = \int A.dl \tag{2.18}$$

where the integration is around the closed contour of the coil. Since the length of the winding in the axial direction is always greater than the distance between the coilsides, the end contribution in the integral may be neglected. If the vector potential on the right and left hand coilsides of the coil is denoted as A_R and A_L respectively, then the flux

$$\phi = l\ (A_R - A_L) \tag{2.19}$$

where l is the core length. For a multiturn coil having N turns, the flux linkages are

$$\psi = N\phi = Nl\,(A_R - A_L) \tag{2.20}$$

If the current carried by each conductor of the winding is i, then the inductance of the winding will be

$$L = \frac{N\phi}{i} = \frac{Nl\,(A_R - A_L)}{i} \tag{2.21}$$

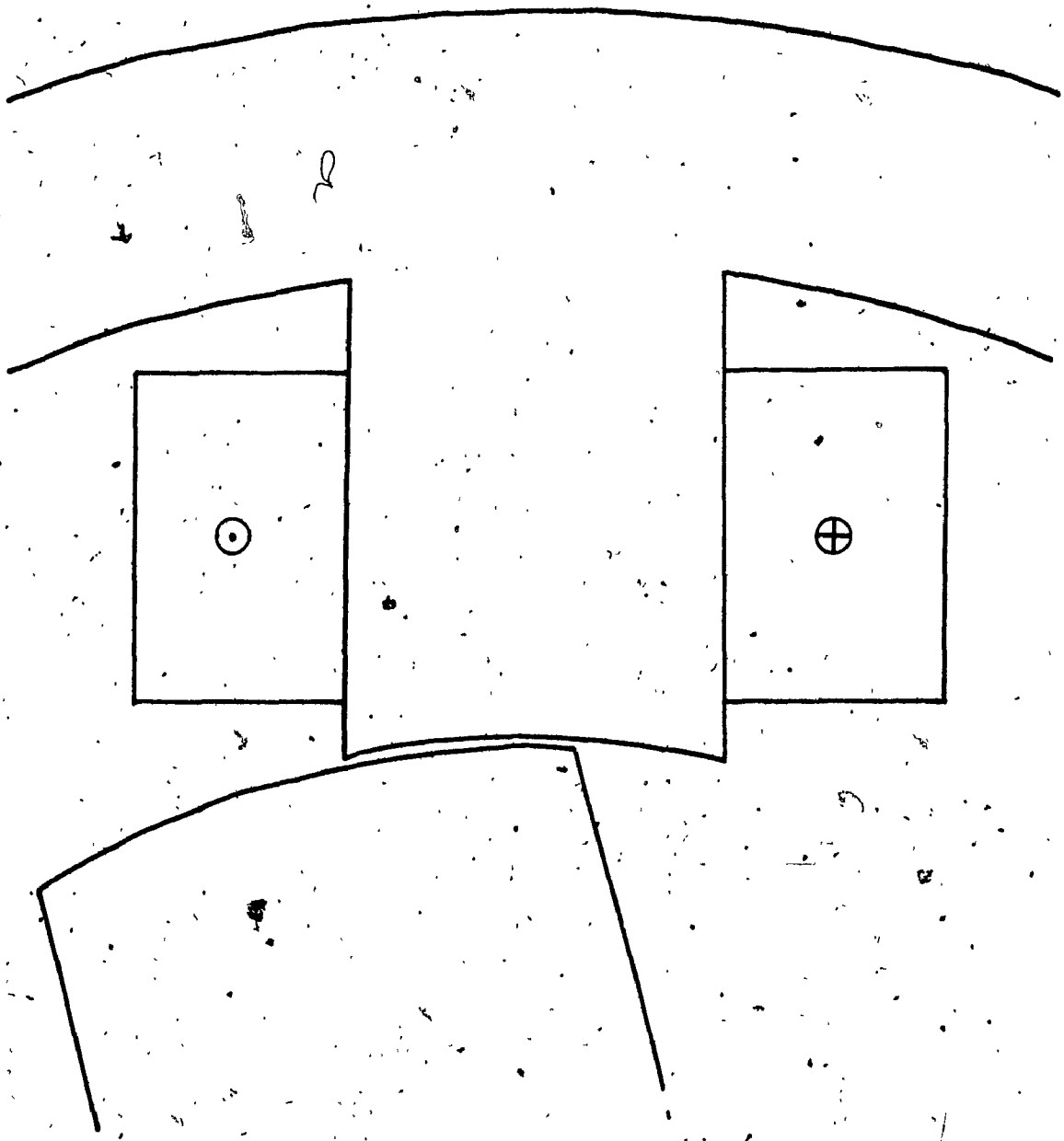

Fig. 2.5 Winding arrangement in SR motor

A similar procedure can be used to determine the flux that leaks to the yoke and the flux that leaks to the adjacent pole winding from the knowledge of the magnetic vector potential differences between appropriate points.

2.7.2 Terminal Inductance Calculation

The inductance due to the flux that links the excited stator pole windings only, the inductance due to the flux that leaks to the yoke and the inductance due to the flux that leaks to the adjacent poles can be added to obtain the terminal inductance of the motor.

For windings that fill a considerable amount of space, the question of choosing the exact points where the vector potential has to be considered is rather ambiguous. In such cases, some sort of average value of the vector potential over the winding space may give a satisfactory value for the inductance.

Consider a thick winding which may be regarded as having a set of smaller, thin, multiturn coil, all connected in series. The total flux linkages of the winding is the sum of flux linkages due to all the sets of coils. Consider the k-th set of coils with N_k turns, its flux linkages are

$$(n\phi)_k = N_k (A_{kR} - A_{kL}) \tag{2.22}$$

where the potentials on the right and left hand sides are A_{kR} and A_{kL} respectively. The total flux linkages, assuming that there are m such sets of coils in the winding, is

$$n\phi = \sum_{k=1}^{m} (n\phi)_k = \sum_{k=1}^{2m} N_k \frac{J}{|J|} A_k \tag{2.23}$$

The last term in the summation is performed over the coilsides, taking appropriate signs for the direction of the current density vector, J. Since, all the turns are in series and carrying a current of i amperes,

$$N_k \frac{J}{|J|} = \frac{\int_{S_k} J \, dS}{Ni} N \qquad (2.24)$$

where the surface integration S_k is the cross sectional area of the k-th elementary collside while the denominator represents the total ampere-turns of the winding.

From equations (2.23) and (2.24)

$$n\phi = \frac{1}{i}\int_S A \; J \; dS \qquad (2.25)$$

The winding inductance for a winding having l meter depth, will be

$$L = \frac{l}{i^2}\int_S A \; J \; dS \qquad (2.26)$$

The above equation has been used to determine the terminal inductance of the phase winding. The listing of the User Defined Verb used is as follows.

```
10 REM INDUCTANCE CALCULATION.
20 GET PR1
30 GET PR1 DENS
40 EMBE
50 DOT
60 INTE
70 STAC NUME
80 PUSH
90 ENTE LNTH
100 PUSH
110 MULT
120 ENTE CUR
130 PUSH
140 DUPL
150 MULT
160 DIVI
170 STAT

VERB INDU
```

In the above subprogramme, PR1 refers to the name of the problem containing the solutions. LNTH is the length of the iron core and CUR is the excitation current used for that problem. The numerical values for LNTH and

CUR have to be entered through the keyboard by the user who is doing the postprocessing. INDU refers to the User Defined Verb which will be stored in the computer for later use.

2.7.3 Coenergy Calculation

The coenergy in the SR motor for a specified excitation current when the rotor is in a given position can be obtained as the area under the flux linkages vs current characteristic curve upto the specified current.

Consider Fig. 2.6 where the flux linkages are plotted against the excitation for a given rotor position θ. If the operating current value is i_0 then the coenergy will be equal to the sum of the areas S_2 and S_3. In finite element analysis, the area S_1 can be calculated using the equation

$$S_1 = l \iint_S \left[\int_0^B H \; dB \right] dS \tag{2.27}$$

The area S_2 can be obtained by considering the linear relationship and using the equation

$$S_2 = \frac{l}{2} \int_S A \; J \; dS \tag{2.28}$$

By making use of equations (2.27) and (2.28) the coenergy, W, is computed as

$$W = 2S_2 - S_1 \tag{2.29}$$

The change of coenergy when the rotor changes its position at a constant current, is obtained as the difference of coenergies at two different rotor positions.

2.7.4 Calculation of Torque

The average torque developed by the SR motor is calculated as the change in coenergy per unit angular displacement of the rotor at a given excitation current.

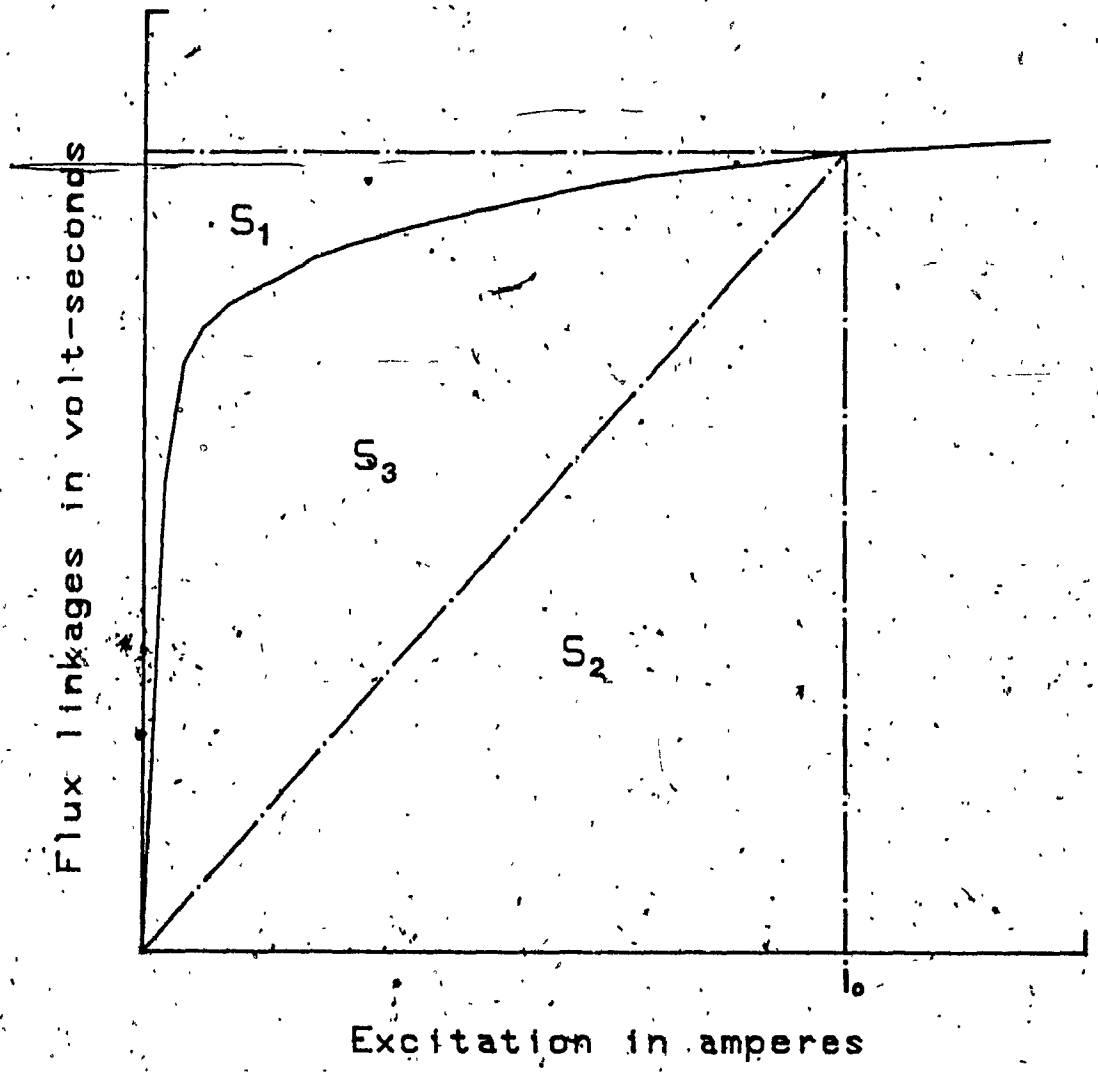

Fig. 2.6 Typical flux linkages vs current characteristic

2.8 Conclusion

In this chapter, a two dimensional finite element formulation is described. The basic equations used to get the magnetic field solution, the assumptions based on which the formulation is done, setting up of the boundary conditions for the SR motor analysis, the modeling requirements of the magnetization characteristic curve for numerical computations are given. The basic principles involved in the calculation of flux linkages, terminal inductance, coenergy and torque are discussed. A brief description of the use of the MagNet CAD package which was used in this thesis and the various steps to be followed during the analysis of SR motors are given.

CHAPTER 3

APPLICATION OF FINITE ELEMENT ANALYSIS TO SR MOTOR PERFORMANCE PREDICTION

3.1 Introduction

In this chapter, the characteristics of two different types of SR motors are pre-determined using a two dimensional finite element analysis. One of the motors , has six poles on the stator and four poles on the rotor (6/4 motor). The other motor has six stator poles having two teeth on each stator pole and ten poles on the rotor (12/10 motor). A comparison of their performance is made.

The main dimensions for the 12/10 motor are taken from Finch et al., [57]. One of the considerations for this choice is that the performance predicted using finite element analysis could be verified by the test results that are already reported in their paper. In order to compare the performance of both the motors, the main dimensions of the 6/4 motor are taken to be the same as those of the 12/10 motor with some modifications. From the results of the finite element analysis their performance parameters such as the flux linkages of an excited pole winding, the terminal inductance of the motor, the leakage inductances and the torque developed by the motor for various excitation currents and rotor positions are determined.

3.2 Motor Specification

The main dimensions for the 6/4 and 12/10 motors are given in Table 3.1. The configurations of the motor laminations for both the motors are shown in Fig. 3.1 and Fig. 3.2 where the stator and rotor poles are in the aligned position. The windings on each stator pole are concentrated.

TABLE 3.1

Motor Specifications

	6/4 motor	12/10 motor
Stator core outer diameter	165.1	165.1
Bore diameter	93	93
Length of iron core	108	108
Back of stator core	12.5	12.5
Length of air gap	0.255	0.255
Stator pole arc	18.8	-
Height of stator pole	23.55	-
Tooth width	-	10.2
Stator pole neck	-	24.5
Rotor pole arc	28.3	10.2
Height of rotor pole	19.5	-
Shaft diameter	28.58	28.58

(All dimensions are in mm)

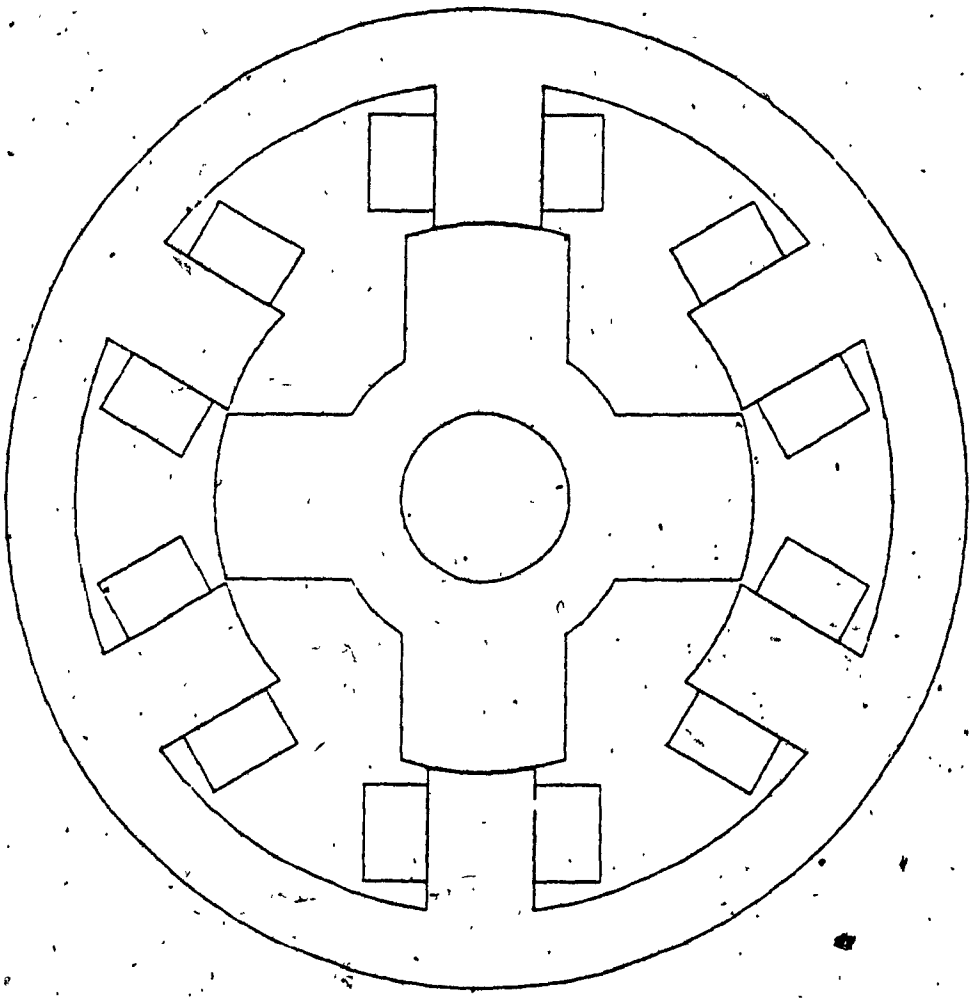

Fig. 3.1 Motor configuration in aligned position (6/4 motor)

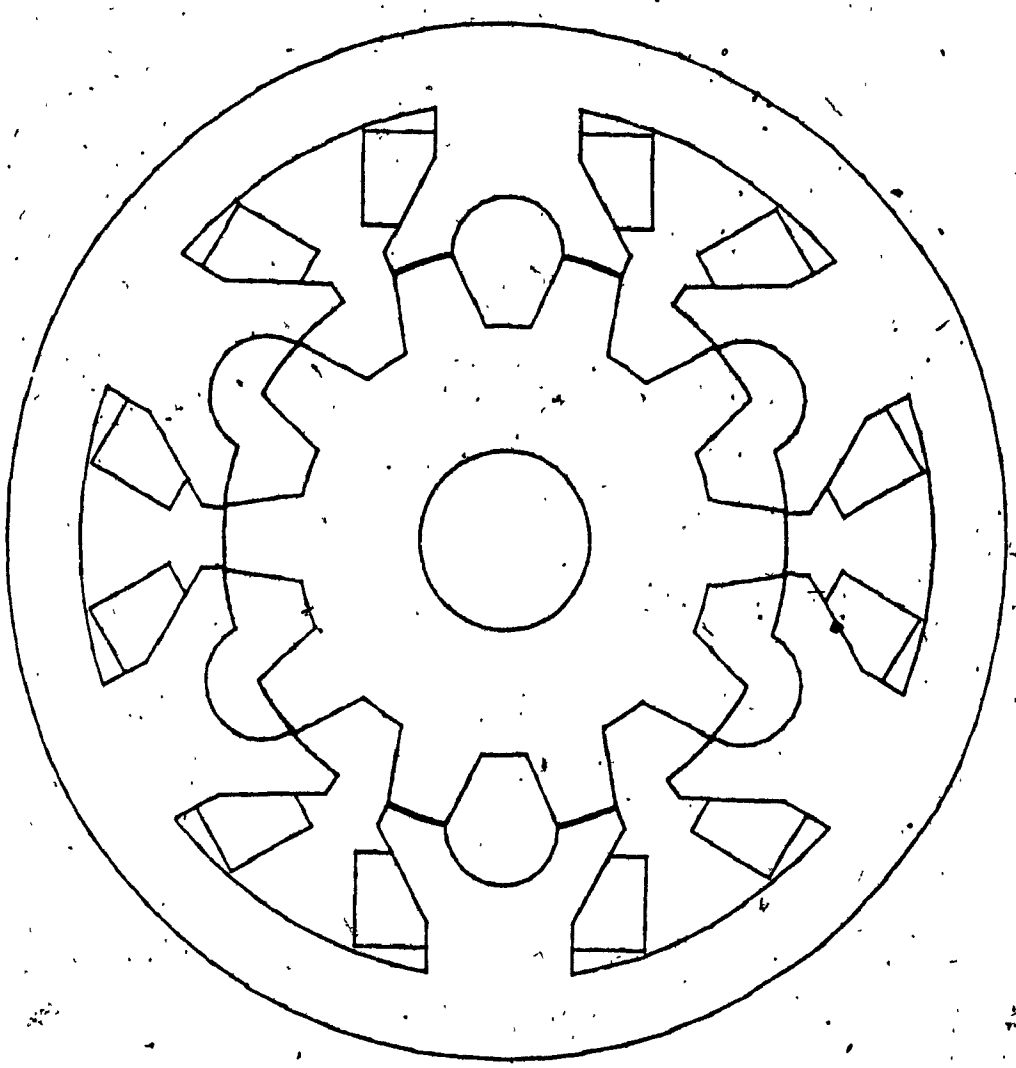

Fig. 3.2 Motor confoguration in allgned posltion (12/10 motor)

The concentrated winding on each stator pole has 222 turns. The stator and rotor core are made up of M-19 non-oriented silicon steel laminations. The magnetization curve for the core is taken from the manufacturer's data sheets and is shown in Fig. 3.3.

To give some measure of the position dependence of the torque developed by the motor, it is modeled for different rotor positions in addition to the aligned and unaligned positions. For the 6/4 motor the field solutions are obtained at the rotor positions of 10, 20 and 30 mechanical degrees from the aligned position. Similarly, for the 12/10 motor the field solutions are obtained when the rotor is at 4, 8 and 12 mechanical degrees from the aligned position. Calculations for more intermediate positions of the rotor would result in better prediction of the torque during its movement from the unaligned to the aligned position. It is presumed that this will not affect the credibility of the results obtained to an appreciable extent.

Owing to the symmetry when the rotor is in aligned and unaligned positions, one quarter of the motor model is used for field analysis. The nodes on the periphery of the stator, the shaft periphery, the maximum permeance axis for the aligned position and the minimum permeance axis for the unaligned position are defined to have zero magnetic vector potential. The Neumann boundary is implicitly applied at the nodes on the iron air boundaries inside the motor and on the nodes along the horizontal axis of the model.

For other intermediate positions of the rotor, a model of one half of the motor is used, since the periodicity condition repeats after three stator pole pitches. The homogeneous Dirichlet boundary condition (A=0) is used along the shaft and motor peripheries. Binary constraints are applied to the nodes on the diametrically opposite points on either side of the motor shaft.

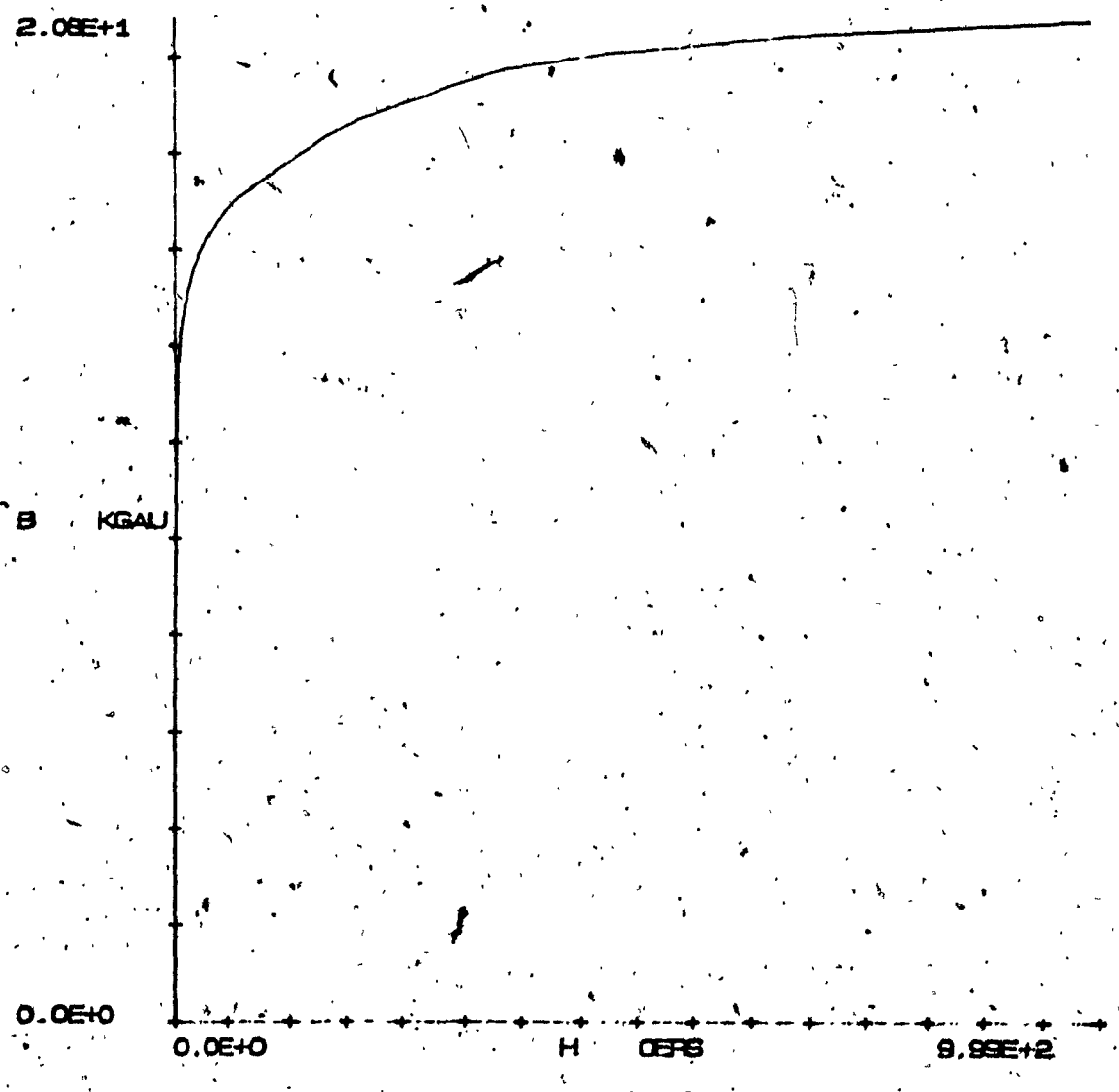

Fig. 3.3 Magnetization curve (M-19 Steel)

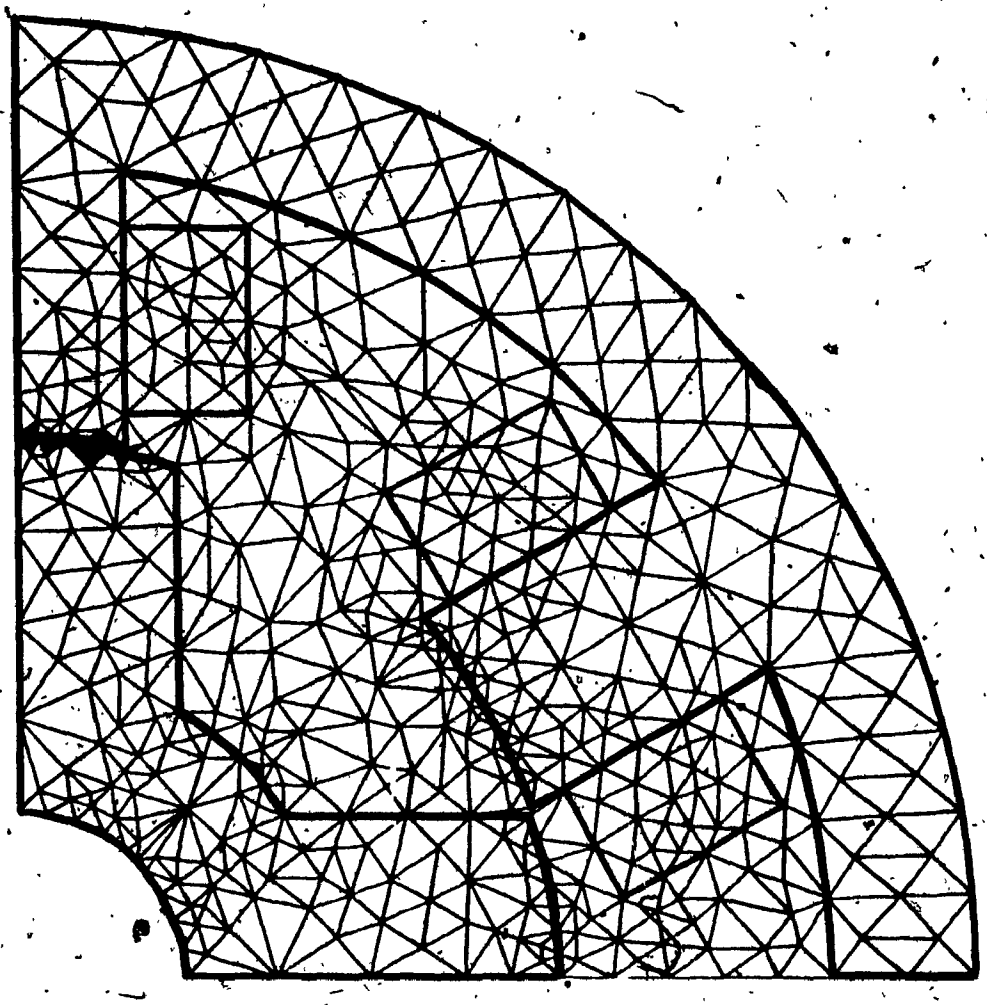

Fig. 3.4 Finite element subdivision of the motor model 6/4 motor (aligned position).

The field analysis is performed using a MagNet CAD package which is based on the variational energy minimization technique for the magnetic vector potential. The field solution is postprocessed to obtain the results such as the energy stored in the field, flux density distribution, etc. The interactive graphic feature of the CAD package facilitates the display of field distribution, flux, energy density distribution, etc.

3.3 Analysis of 6/4 Motor

The configuration of the 6/4 motor is shown in Fig. 3.1 and its main dimensions are given in Table 3.1. The finite element subdivision of the motor in the aligned position is shown in Fig. 3.4. The field solution is obtained by solving equation (2.9), satisfying the assumptions made earlier and the boundary conditions specified.

Typical flux plots obtained for the motor in the aligned and unaligned positions of the rotor and for the intermediate positions of 10, 20 and 30 degrees from the aligned position are shown in Figs. 3.5 - 3.9, respectively. The plots shown are for a steady excitation of 6 amperes in one phase winding. The flux plots obtained for other excitations are not shown but are similar. These equipotential plots represents the flux distribution in the motor. The flux distribution pattern itself gives the nature of saturation that occurs in different parts of the motor. It can be observed that there are fluxes which complete their path through the rotor pole tip and the adjacent stator pole which cause mutual inductance between the adjacent stator pole windings. These fluxes were not considered in earlier investigations. The excited stator poles are heavily saturated compared with the other parts of the motor. At partial overlap of the stator and rotor poles the pole tips have higher flux densities than those in the back of iron cores.

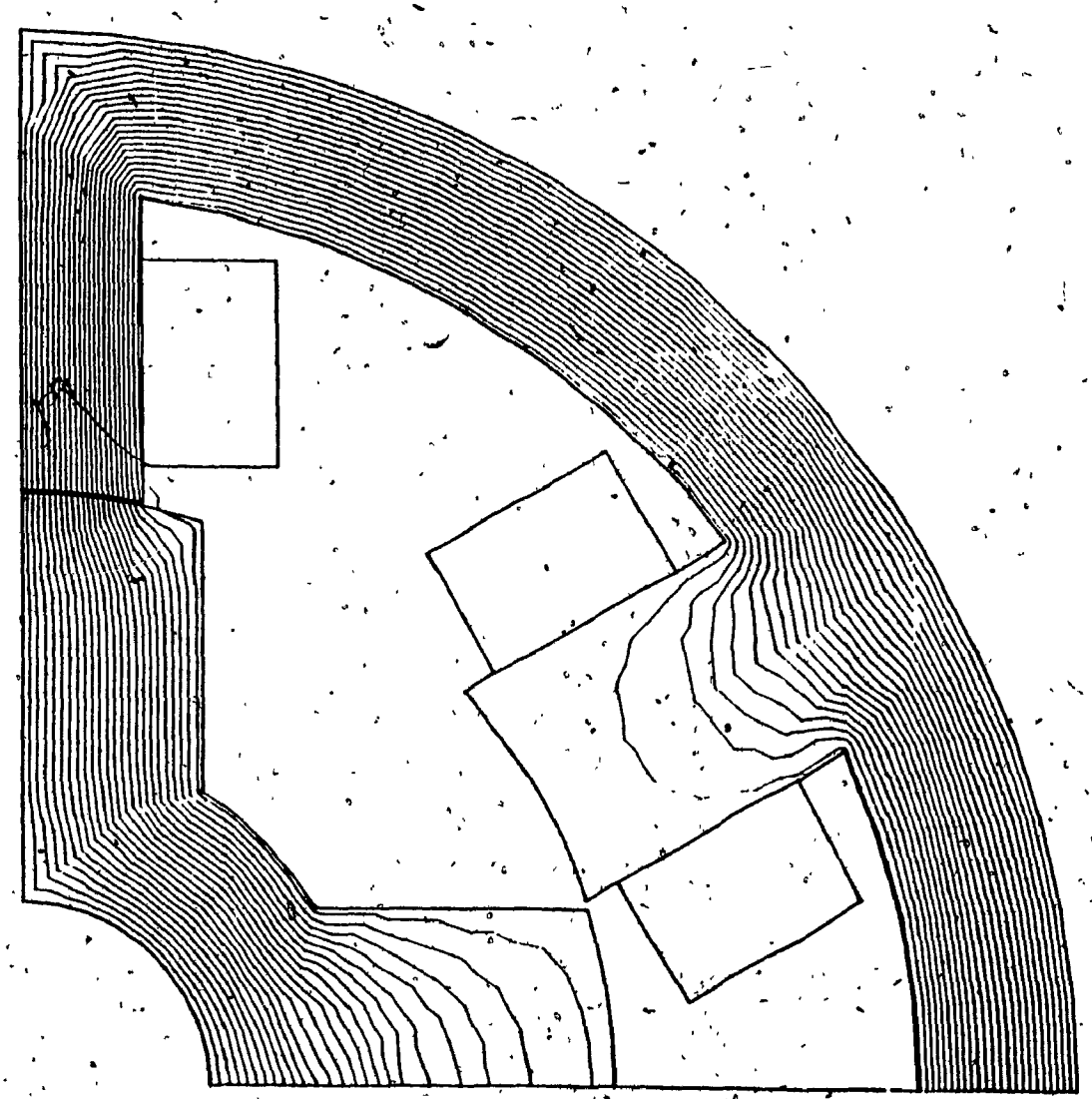

Fig. 3.5 Flux plot. Aligned position.

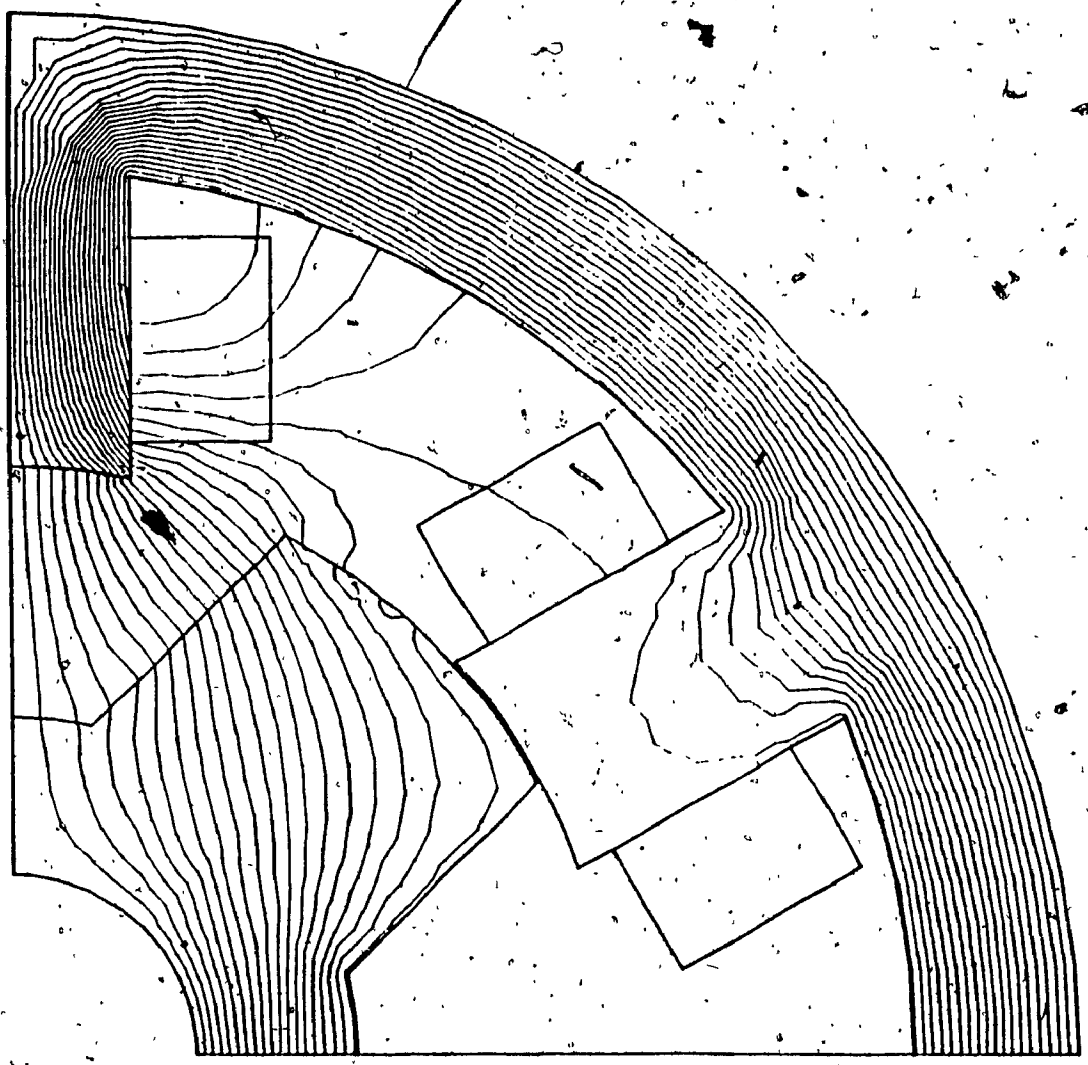

Fig. 3.6 Flux plot. Unaligned position.

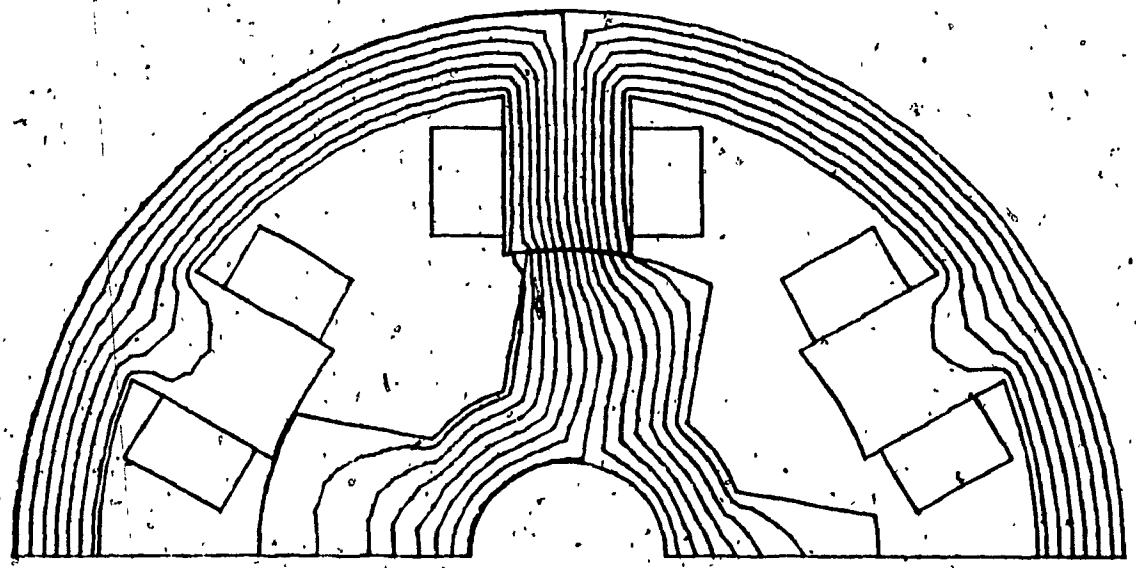

Fig. 3.7 Flux plot. Rotor pole axis at 10 degrees from the aligned position

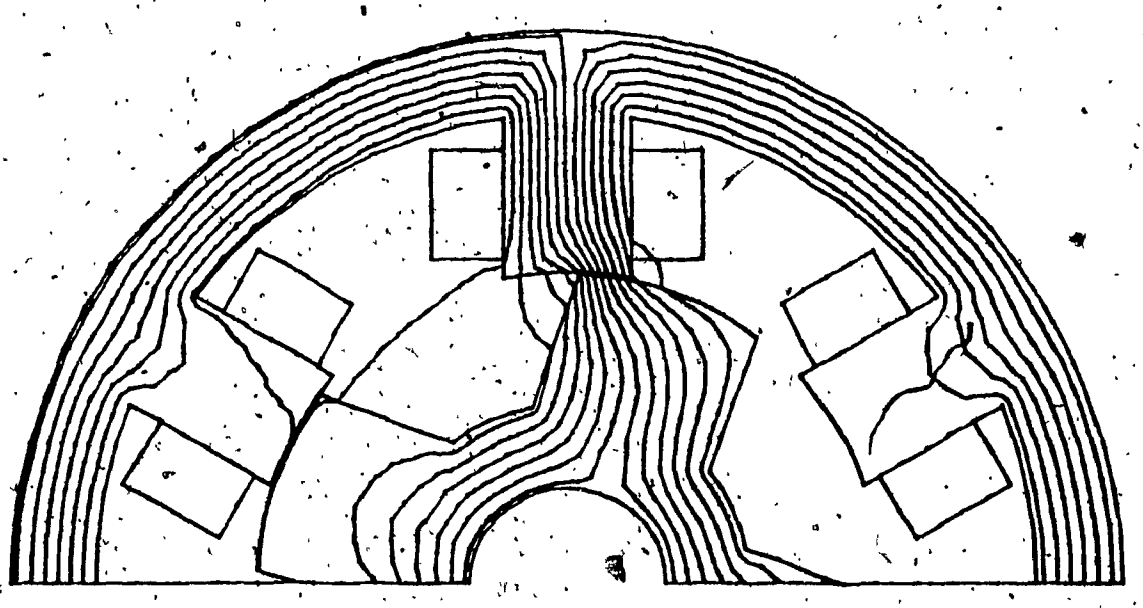

Fig. 3.8 Flux plot. Rotor pole axis at 20 degrees from the aligned position.

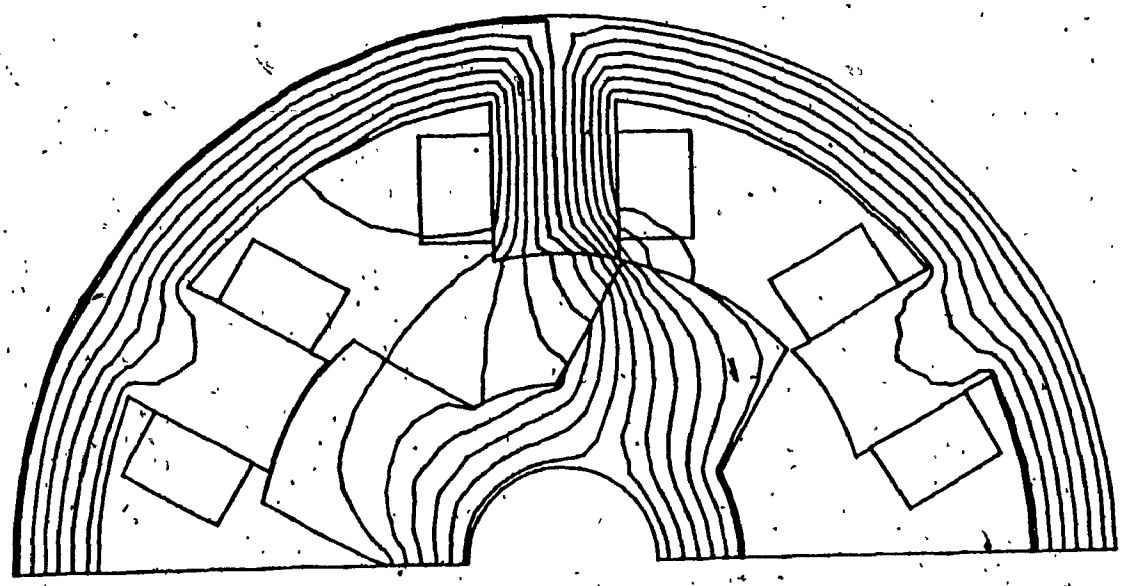

Fig. 3.9 Flux plot. Rotor pole axis at 30 degrees from the aligned position.

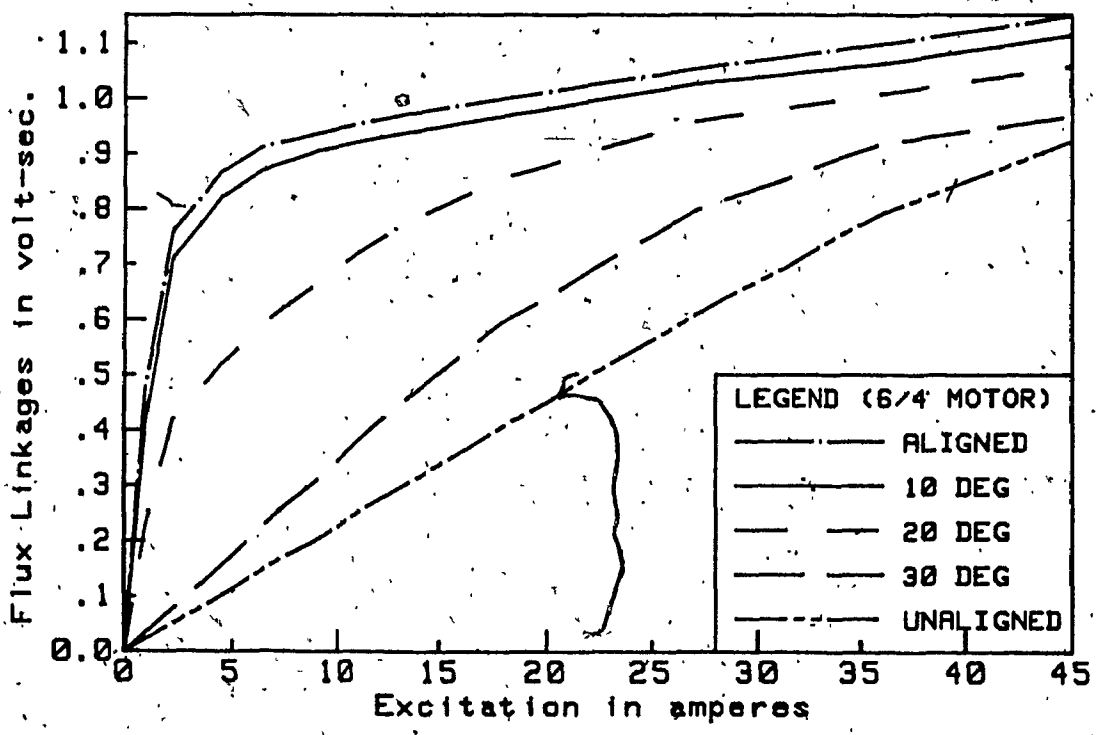

Fig. 3.10 Flux linkages per pole vs current characteristic

The flux linkages of one pole winding for varying excitation currents and rotor positions are shown in Fig. 3.10. They increase monotonically with excitation, but decrease as the rotor moves away from the aligned position. The area under each curve gives the coenergy when the rotor is in a given position. As the torque developed depends on the coenergy change during rotor movement from one position to the other, the areas between these curves are important to the motor designer. It is observed that the change in coenergy when the rotor poles are nearer to the aligned position is considerably smaller than that when the rotor poles are in the partial overlap positions. Hence, the excitation of the windings can be switched off just before the poles reach aligned position without much loss of torque. Similarly, an increase in excitation beyond saturation produces a progressively smaller increase in torque.

The terminal inductance of the SR motor consists of three components. They are, (a) the inductance due to the flux that flows through both the excited stator poles, the rotor and the stator core, (b) the inductance due to the flux that leaks to the yoke and (c) the inductance due to the flux that links the excited and adjacent stator pole windings. The terminal inductance variations with rotor position and excitation are shown in Fig. 3.11.

The leakage inductance which is due to the leakage flux in the interpolar airgap and the yoke of a phase is shown in Fig. 3.12 for different excitations and rotor positions. The amount of leakage flux increases as the rotor moves away from the aligned position, for a given excitation. This does not change the leakage inductance value appreciably but the leakage inductance does decrease slightly at higher excitations.

The leakage inductance due to the flux that links the excited and the adjacent pole windings is shown in Fig. 3.13. The leakage flux increases with

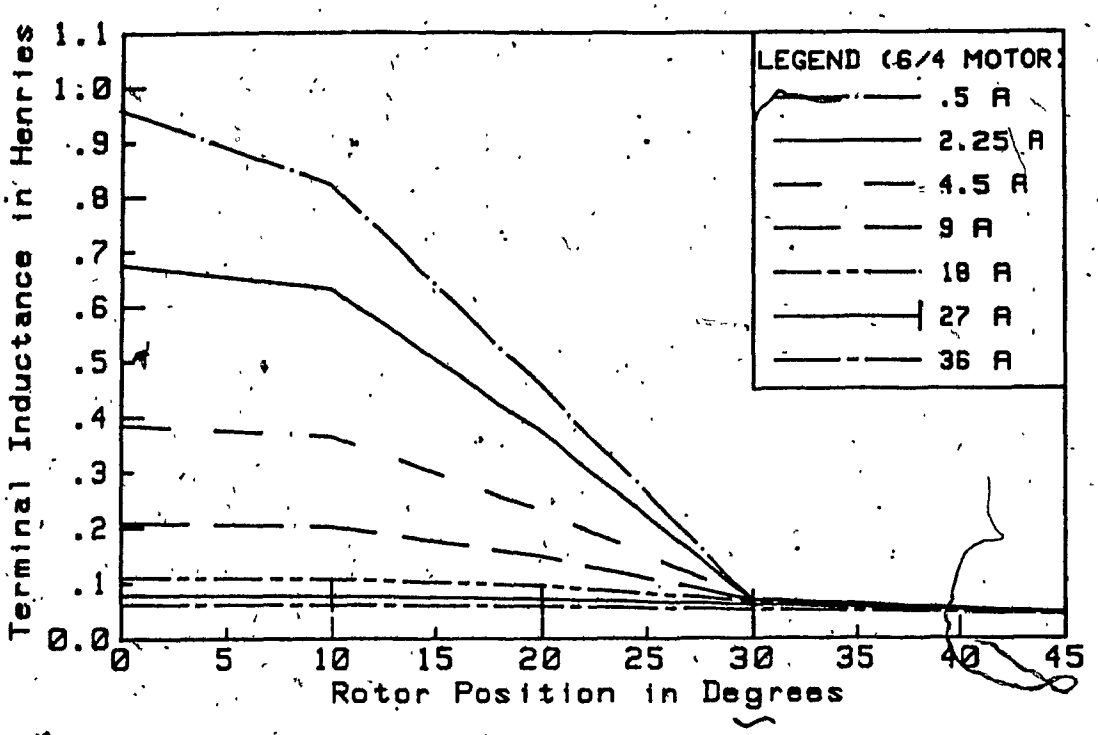

Fig. 3.11 Terminal inductance vs rotor position

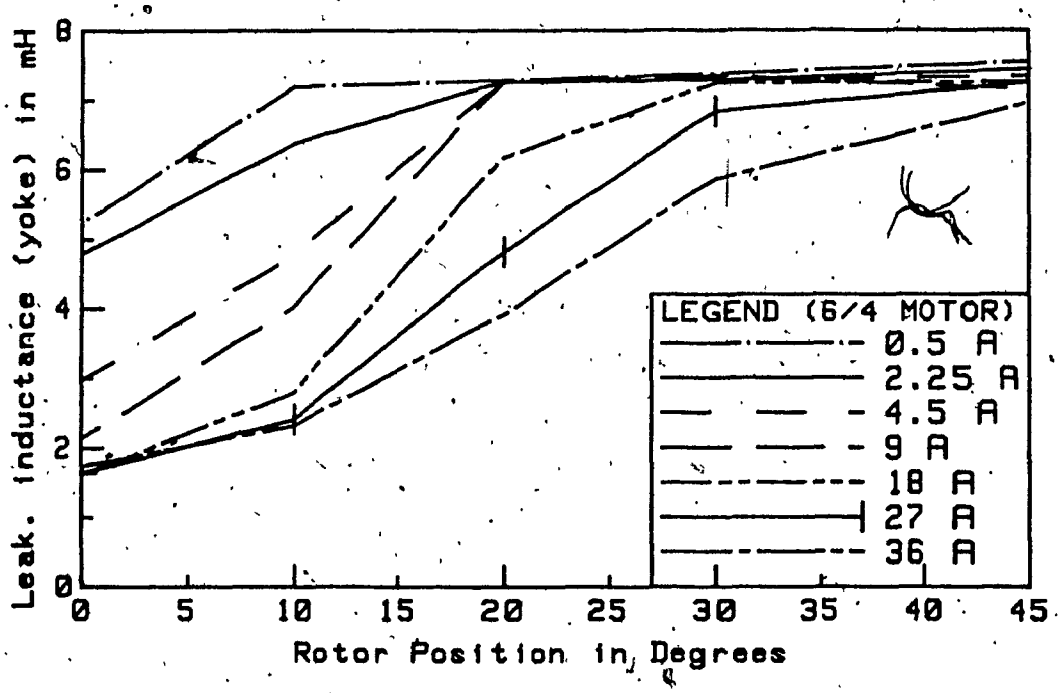

Fig. 3.12 Leakage inductance vs rotor position, due to leakage flux to yoke of one phase

excitation and also as the rotor moves towards the unaligned position. A considerable amount of flux crosses the airgap and travels through the rotor pole tip to the adjacent stator pole. For a given excitation the change in the leakage inductance is very small compared to aligned inductance values.

By using the finite element analysis the energy stored in the motor for a given rotor position and excitation is computed from the calculated flux densities in each element of the motor model and the magnetization characteristic of the core material. The average torques developed during the rotor movement between the rotor positions of 0, 10, 20, 30 and 45 degrees from the aligned position are calculated. The values obtained show clearly that the developed torque is a function of rotor position for a given excitation. A typical torque vs rotor position curve is shown in Fig. 3.14 for a steady excitation of 9 amperes. For convenience, the average torque is shown as constant over the intervals.

Depending on the instant of switching and duration of conduction of the power switches, the average torque developed per rms ampere excitation varies. Fig. 3.15 shows the predicted values of the average torque per ampere for fixed excitation durations of 33, 40 and 50 percent duty cycle. Although the average torque increases as the duration of current conduction is increased, the maximum value of the torque per ampere decreases.

3.4 Analysis of 12/10 Motor

The configuration of the 12/10 motor is shown in Fig. 3.2 and its main dimensions are given in Table 3.2. This motor has six poles on the stator each pole having two teeth and the rotor carries ten poles. The main dimensions of this motor are the same as those used by Finch et al. [57] in their experimental

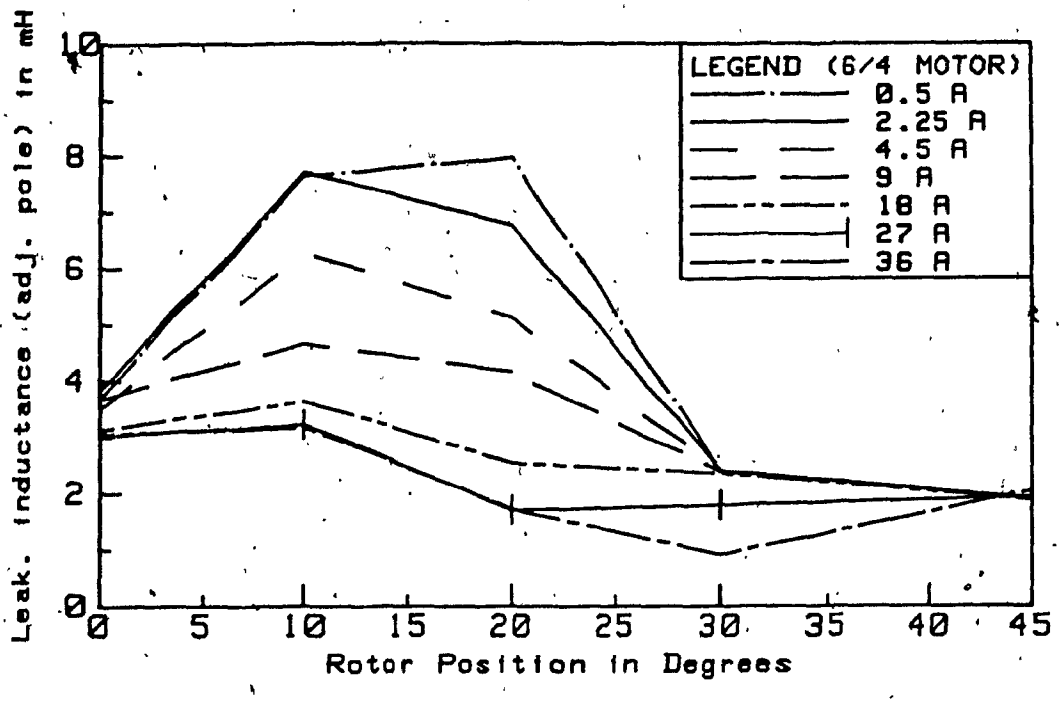

Fig. 3.13 Leakage inductance vs rotor position, due to leakage flux to adjacent pole winding of one phase

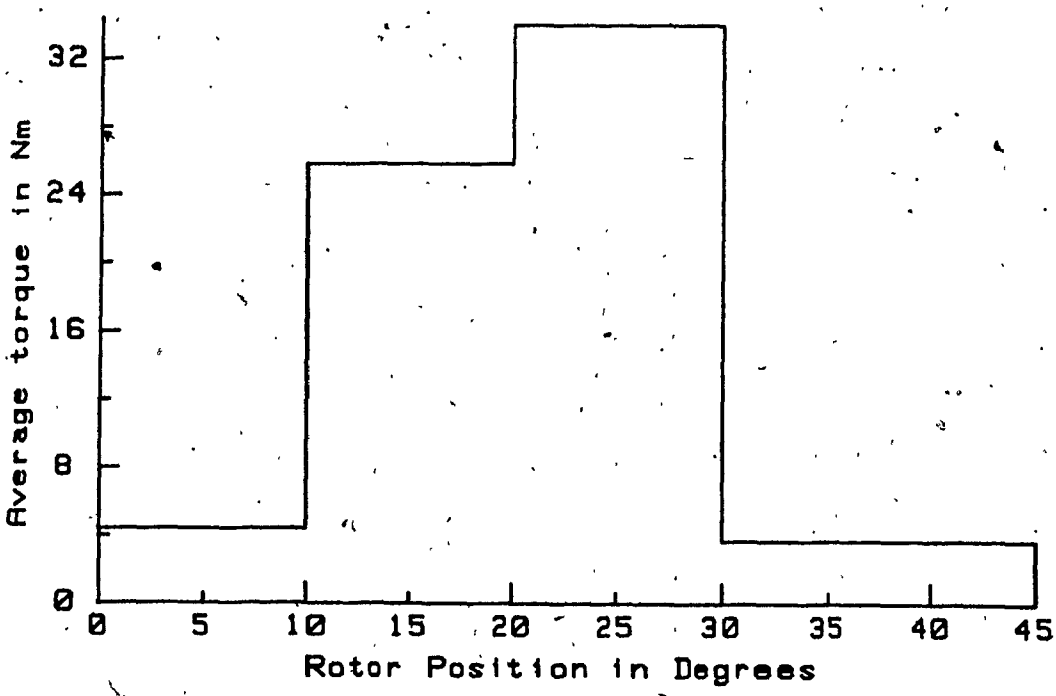

Fig. 3.14 Average torque vs rotor position for 9 A excitation

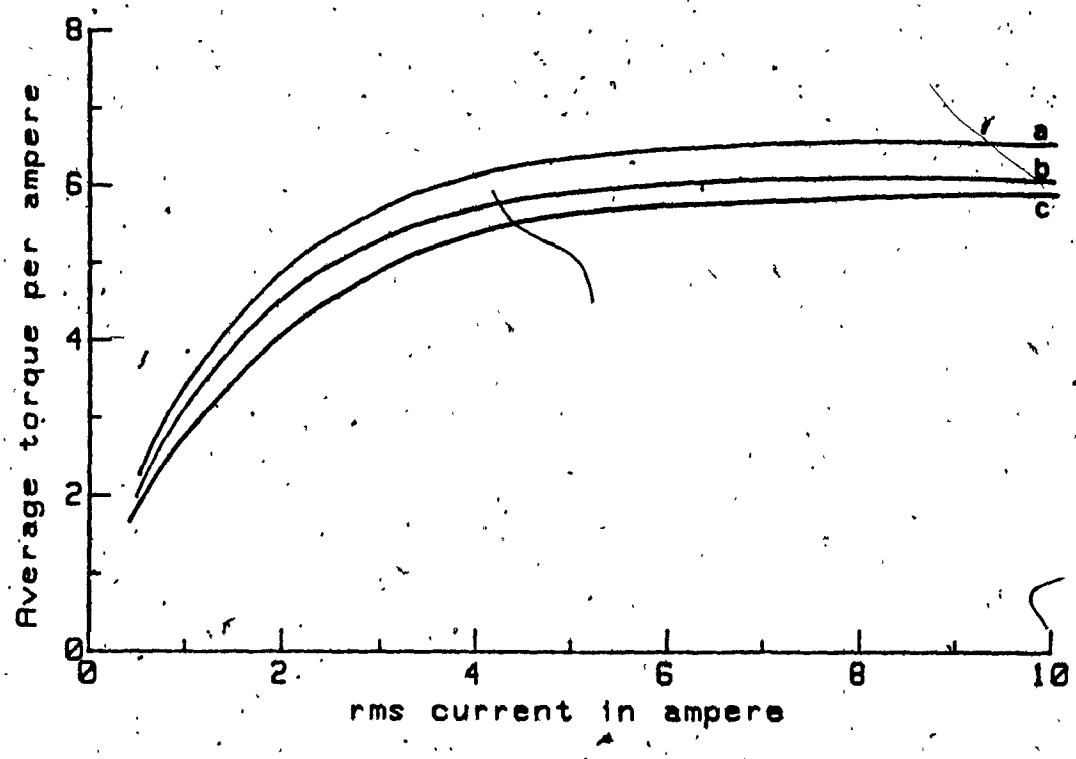

Fig. 3.15 Average torque per ampere characteristic

(a) 33% excitation (b) 40% excitation (c) 50% excitation

motor. The results obtained by the finite element analysis are compared with the experimental results of Finch et al. wherever possible.

The finite element subdivisions of the motor in the aligned position are shown in Fig. 3.16. The stator and rotor core regions are represented with larger elements whereas the stator and rotor pole tips and the airgap between them are subdivided into finer elements.

Finite element field solutions are obtained when the rotor is in the aligned, unaligned and intermediate positions of 4, 8 and 12 degrees from the aligned position. The flux plots obtained for these rotor positions are shown in Figs. 3.17 -3.21, respectively when the excitation is 6 amperes. A detailed study is done to asses the amount of saturation that is present in different parts of the motor under varying excitation conditions. It is observed that the flux density in the excited stator poles and the torque producing rotor poles are higher compared with those in the back of rotor and stator cores for a given excitation. Flux densities in other parts of the motor are very much less.

A plot of the flux linkages of one pole winding for varying excitations and rotor positions are shown in Fig. 3.22. The pattern of flux linkage variation is very similar to the variation obtained for the 6/4 motor. When expressed in normalized form, the aligned and unaligned flux linkages are as shown in Fig. 3.23. The steady excitation (18.1A) that causes saturation in the motor when the rotor is in the unaligned position and the corresponding flux linkages (1.18Vs) are taken as base values. The normalized flux linkages obtained through the finite element analysis show higher values than those of the experimental values reported by Finch et al. when the rotor is in the aligned position. The flux linkages in the unaligned position are the same as those reported by Finch et al. until the beginning of saturation, beyond which the finite ele-

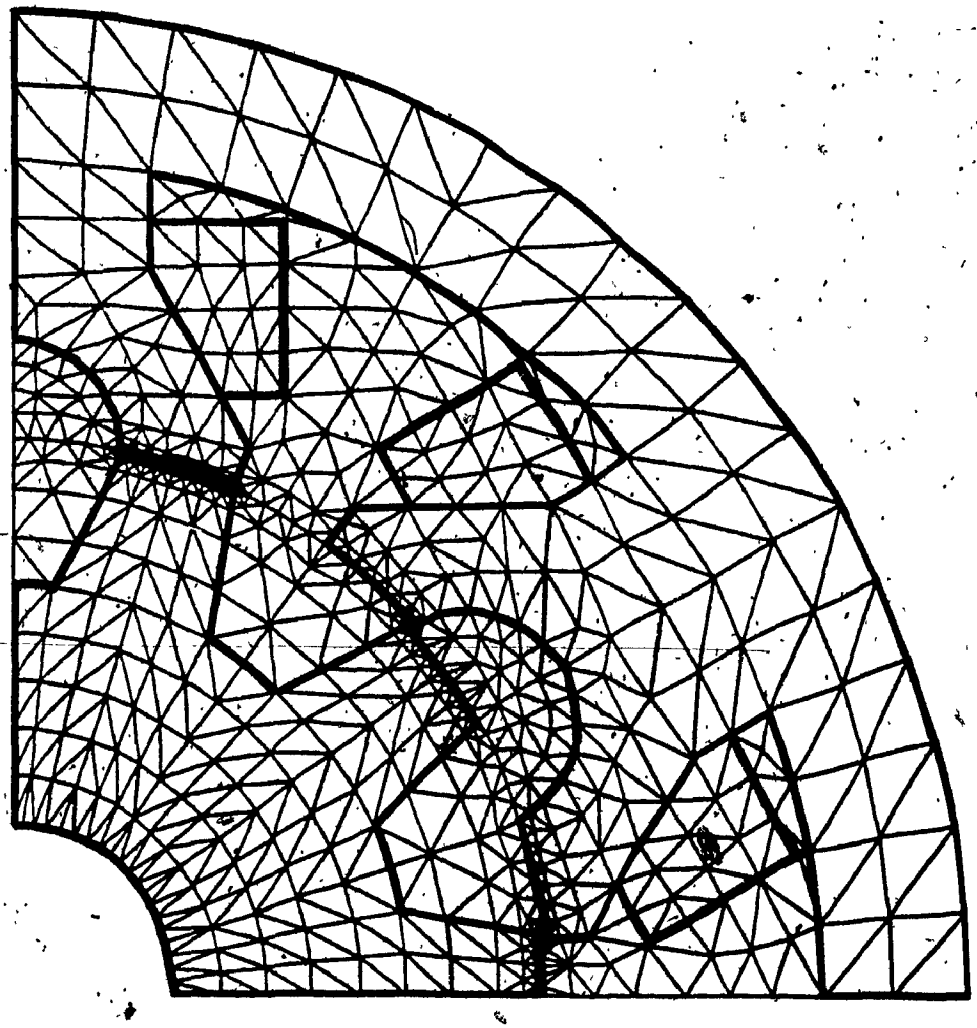

Fig. 3.16 Finite element subdivision of 12/10 motor model in the aligned position

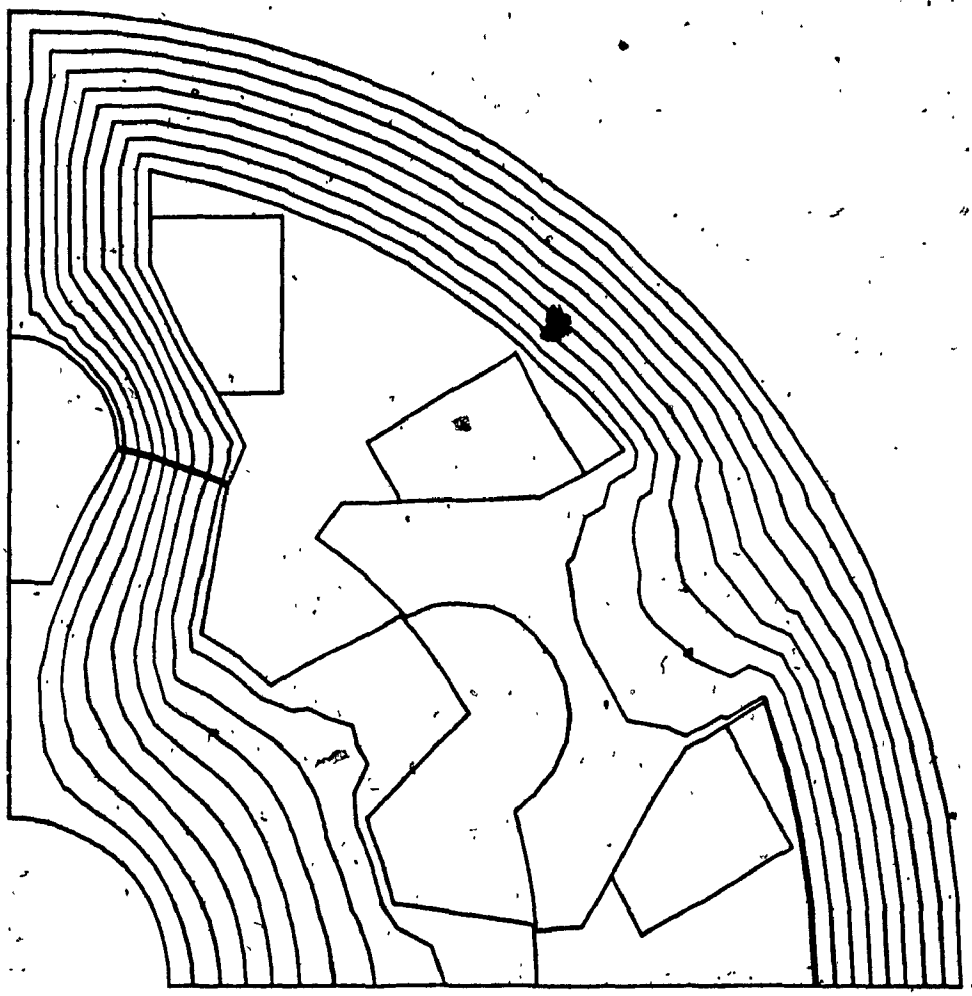

Fig. 3.17 Flux plot. Aligned position

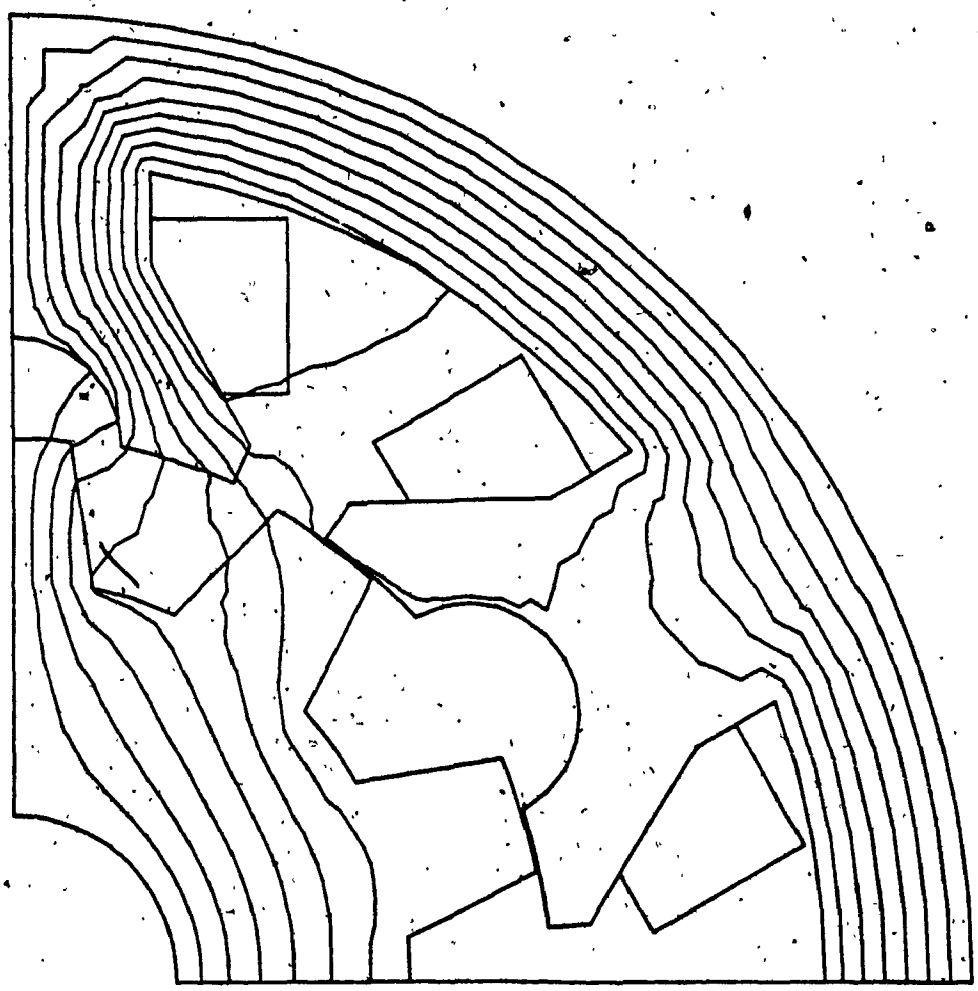

Fig. 3.18 Flux plot. Unaligned position

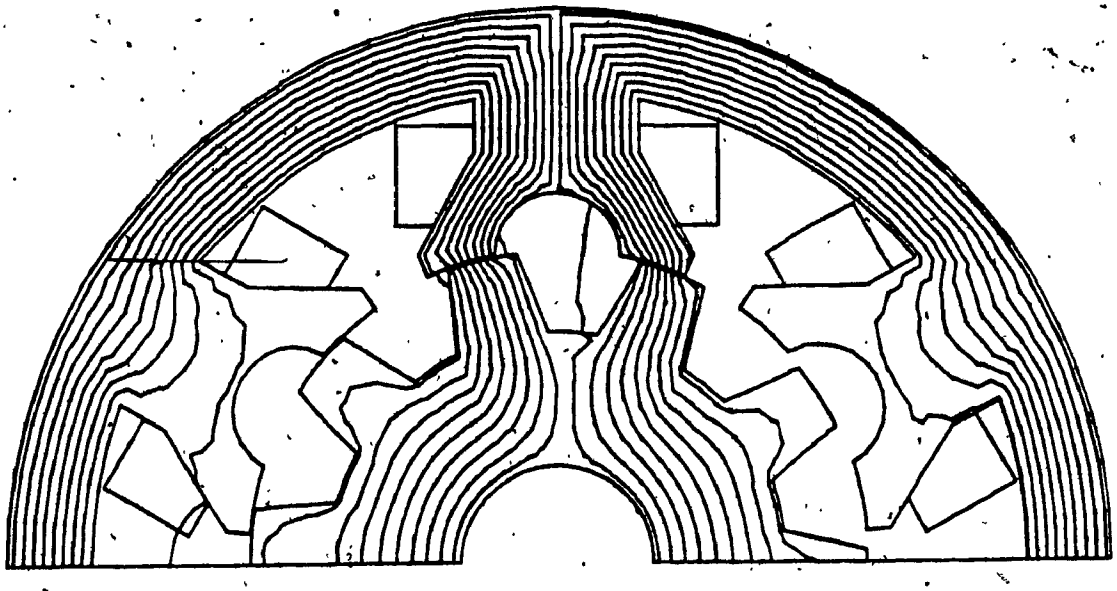

Fig. 3.19 Flux plot. Rotor pole axis at 4 degrees from the aligned position

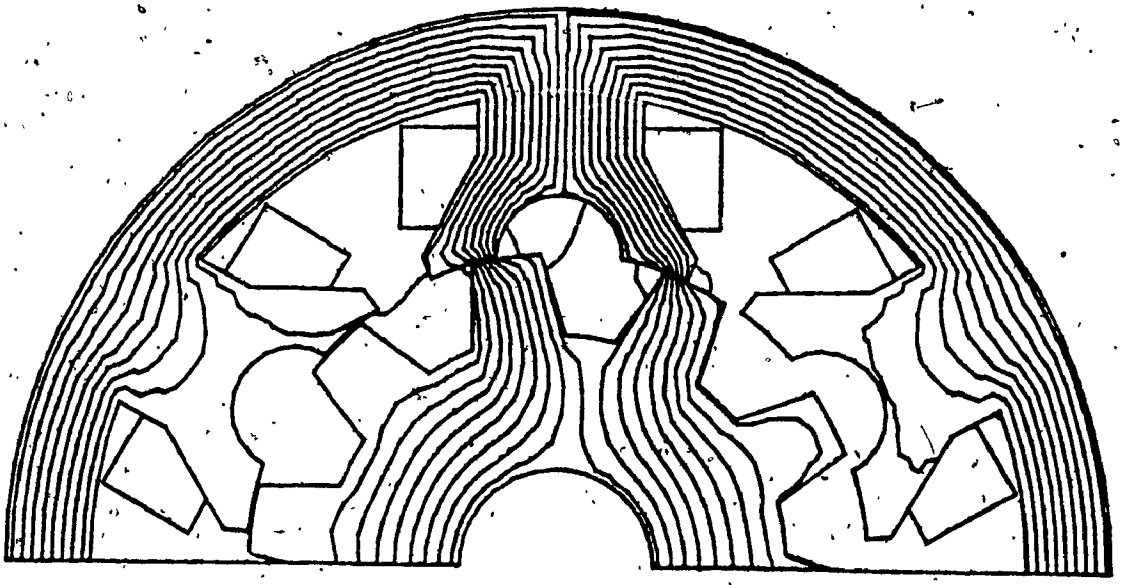

Fig. 3.20 Flux plot. Rotor pole axis at 8 degrees from the aligned position

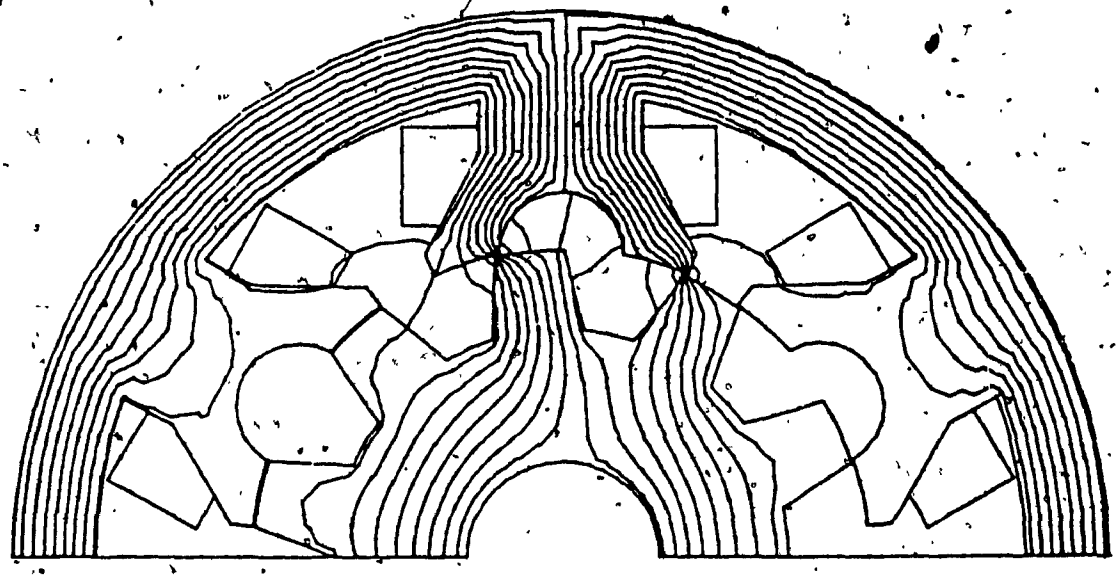

Fig. 3.21 Flux plot. Rotor pole axis at 12 degrees from the aligned position

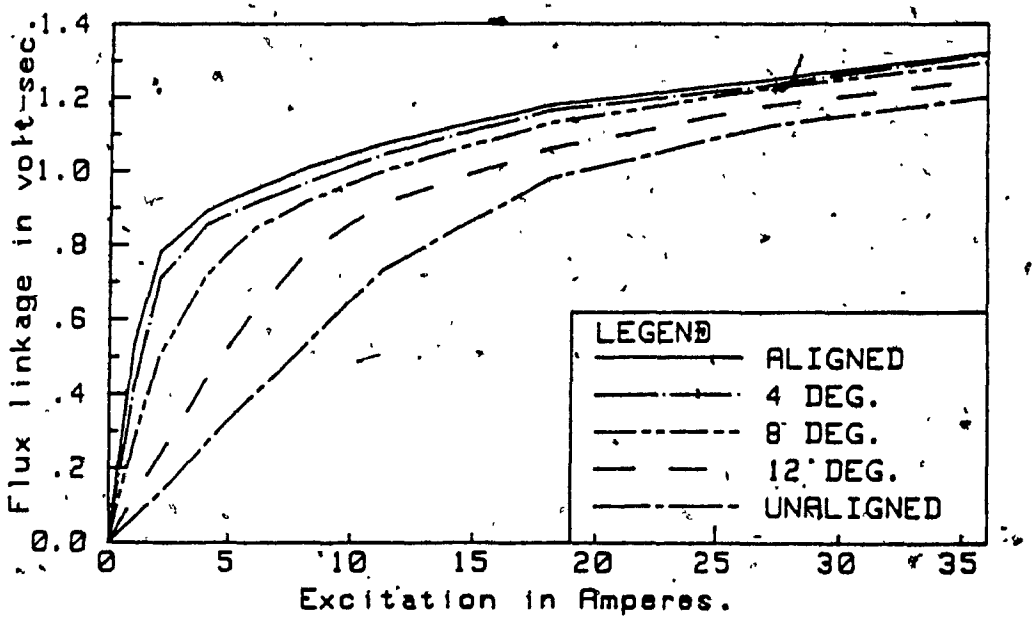

Fig. 3.22 Total flux linkages vs excitation of one pole winding

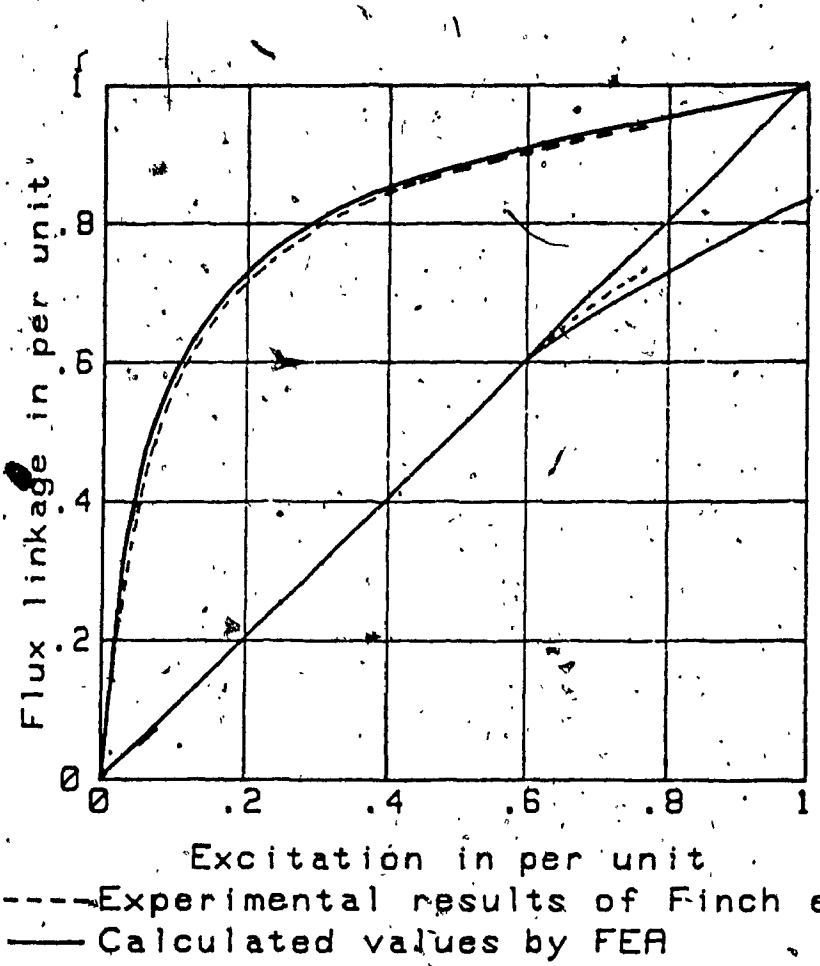

Fig. 3.23 Comparison of flux linkages

ment analysis shows smaller values. However, the difference is very small. In spite of the same physical dimensions of the motor, differences are inevitable due to measurement errors in the experiment and the tolerances in the numerical computation.

Inductance is defined as the ratio of flux linkages to the excitation current. Values based on this definition are presented in Figs. 3.24 - 3.26 although the nonlinear characteristic of the magnetic circuit limits their use. It should be noted that it is the flux linkages that are determined and used in all inductance calculations.

Fig. 3.24 shows the terminal inductance variation for different rotor positions and excitation currents. In the aligned position, the inductance is the greatest at low excitations and decreases rapidly as the excitation is increased due to saturation. For other positions of the rotor, it decreases as the rotor moves away from the aligned position. At higher excitations the inductance is relatively insensitive to rotor position change.

The leakage inductance due to the leakage flux that passes through the interpolar gap and the yoke is shown in Fig. 3.25. The leakage inductance due to the flux linking the adjacent pole windings of the excited poles is shown in Fig. 3.26. Compared with the aligned values the change in leakage inductances at different rotor positions is not appreciable for a given excitation.

The average torque developed between the rotor positions at which the finite element analysis was performed, namely, 0, 4, 8, 12 and 18 degrees from the aligned position, has been calculated. A typical torque variation curve is shown in Fig. 3.27 for a steady excitation of 6 amperes. This shows the nature of torque pulsation that is present in SR motors even though the excitation is held constant.

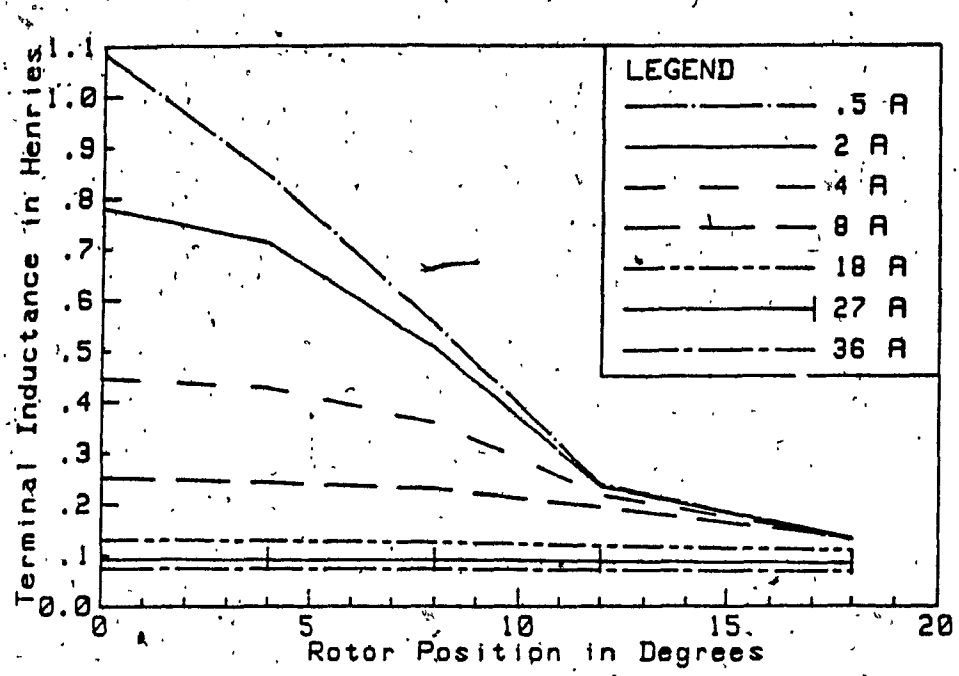

Fig. 3.24 Terminal inductance vs rotor position

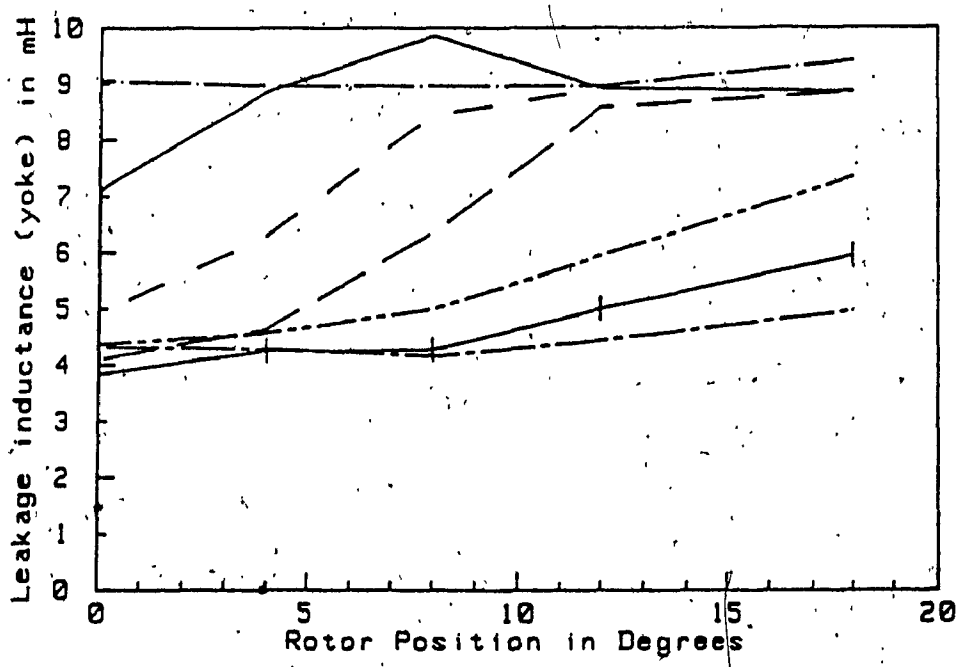

Fig. 3.25. Leakage inductance vs rotor position, due to leakage flux to yoke of one phase

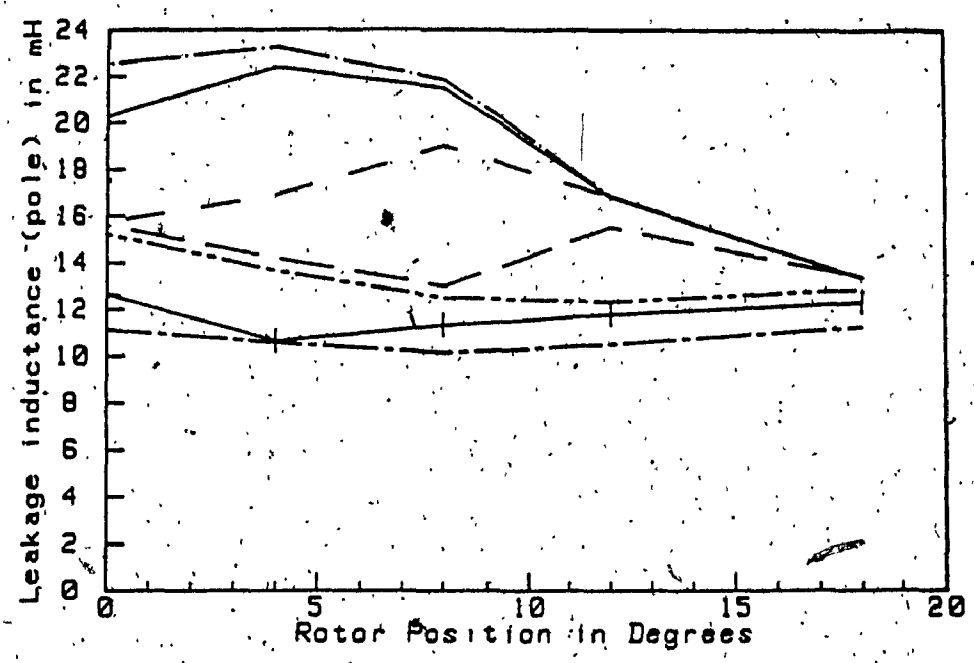

Fig. 3.26 Leakage inductance vs rotor position, due to leakage flux to adjacent pole winding of one phase

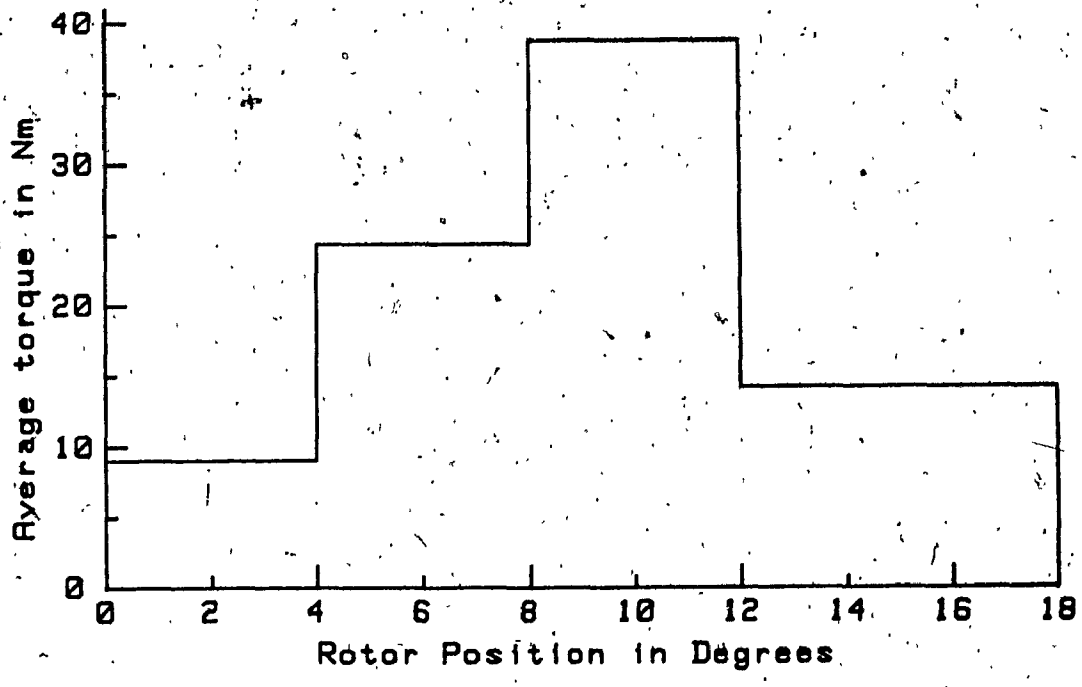

Fig. 3.27 Average torque vs rotor position for 6 A excitation

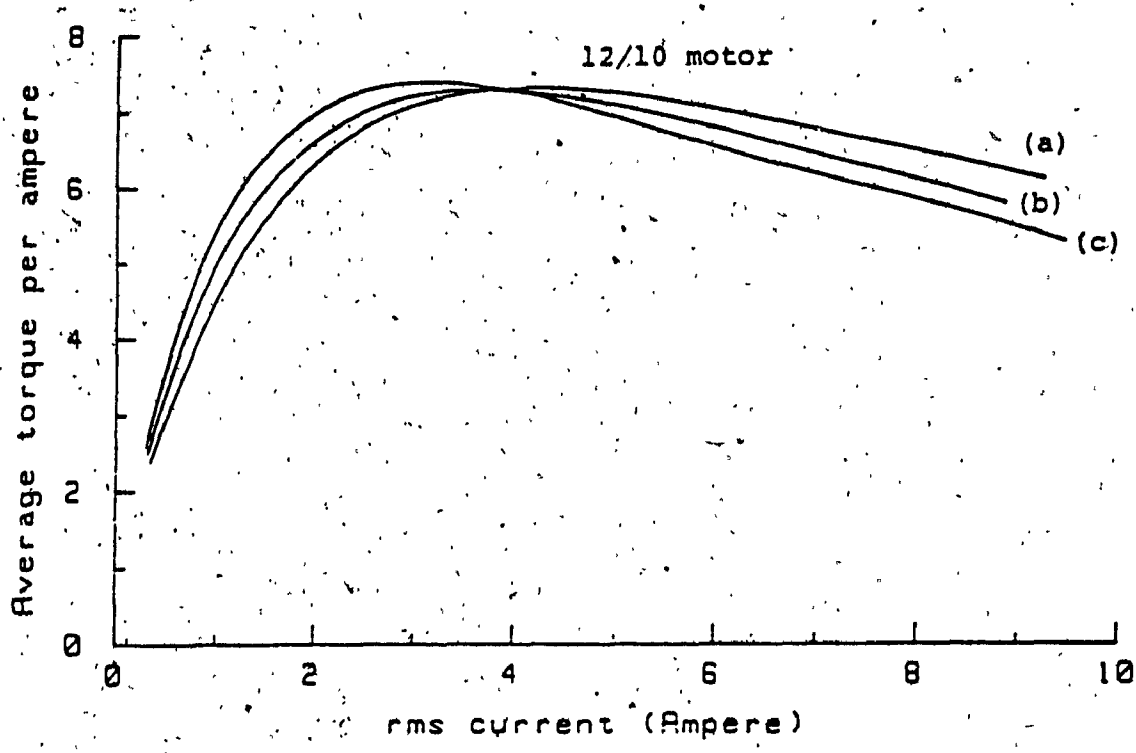

Fig. 3.28 Average torque per ampere characteristic

(a) 33% excitation (b) 40% excitation (c) 50% excitation

The average torque developed per rms ampere excitation having durations of 33, 40 and 50 percent duty cycle are shown in Fig. 3.28. As in the 6/4 motor, the average torque increases with a longer period of excitation, but the maximum values of torque per ampere decrease. Thus, for a particular application if the torque per ampere is a more important criterion than the torque per unit volume, the duration of excitation can be chosen accordingly, taking due account of the likely increase in pulsating torque. The average torque also varies with the angle of switching. The general pattern of the torque per ampere characteristics shows substantial agreement with the experimental values reported by Finch et al. Differences are inevitable due to the assumption of rectangular blocks of current and a possibly different magnetic material characteristic used in the computation.

3.5 Comparison of 6/4 and 12/10 Motor Performances

In this section, some of the performance parameters such as the flux linkages, terminal inductances, leakage inductances and torque per ampere, which are obtained using the finite element analysis are compared.

The flux linkages of a pole winding are shown in Fig. 3.29 for both 6/4 and 12/10 motors. The values are expressed in per unit. The variation of flux linkages with excitation when the rotor is in the unaligned position is almost the same for both the motors. For the aligned position, the 6/4 motor has more flux linkages than the 12/10 motor. Due to the two teeth per pole construction of the 12/10 motor, its core saturates at relatively lower excitation.

The terminal inductance variations for both 6/4 and 12/10 motors are shown in Figs. 3.11 and 3.24, respectively. The inductance decreases rapidly as the rotor moves away from the aligned position at lower excitations. The change is not very much at higher currents. In the 6/4 motor the unaligned

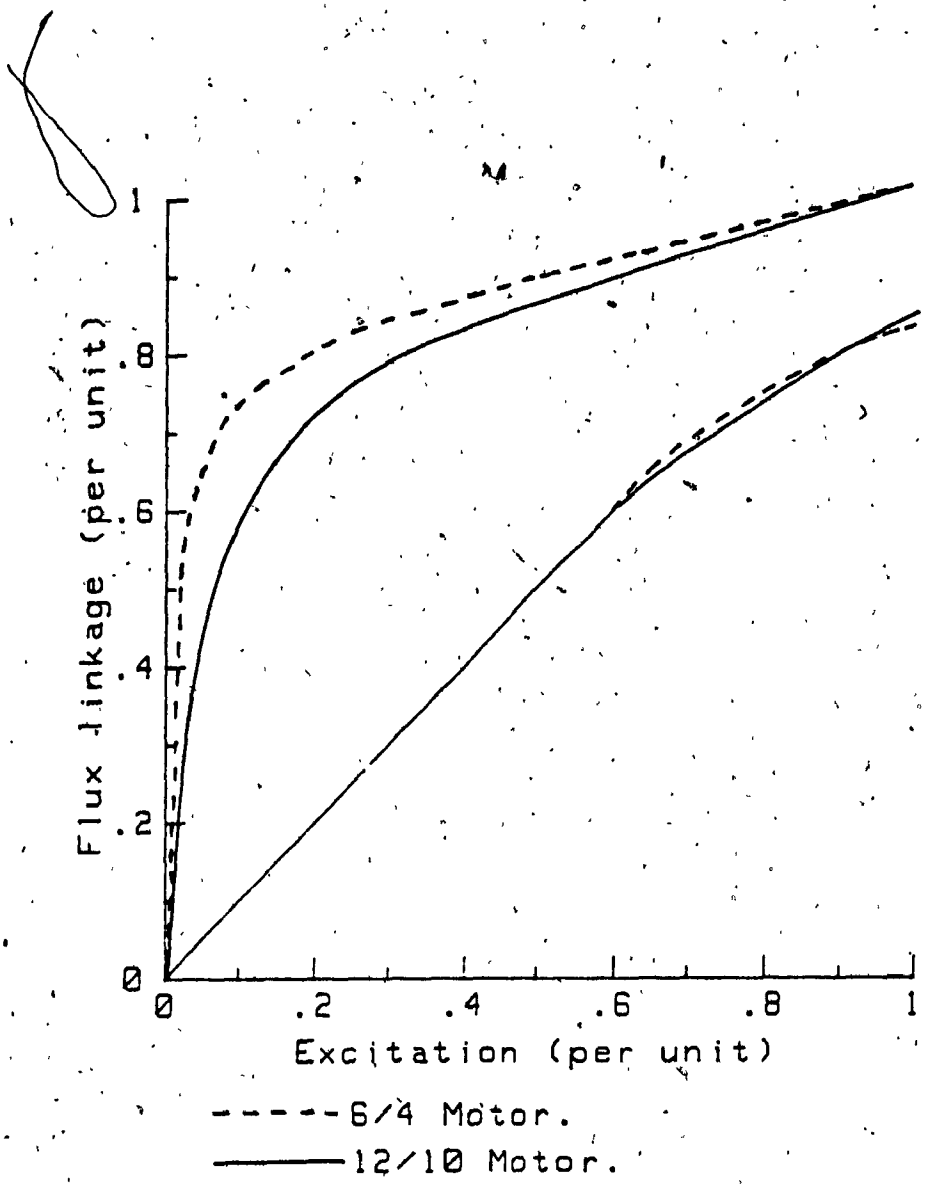

Fig. 3.29 Comparison of flux linkages of 6/4 and 12/10 motors

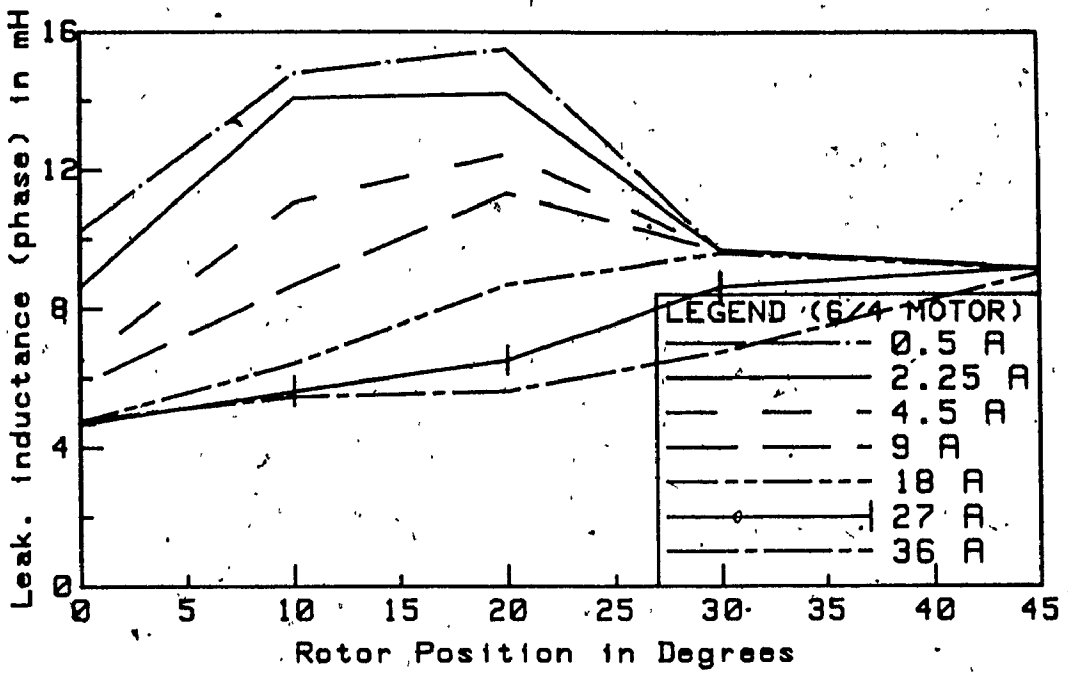

(a)

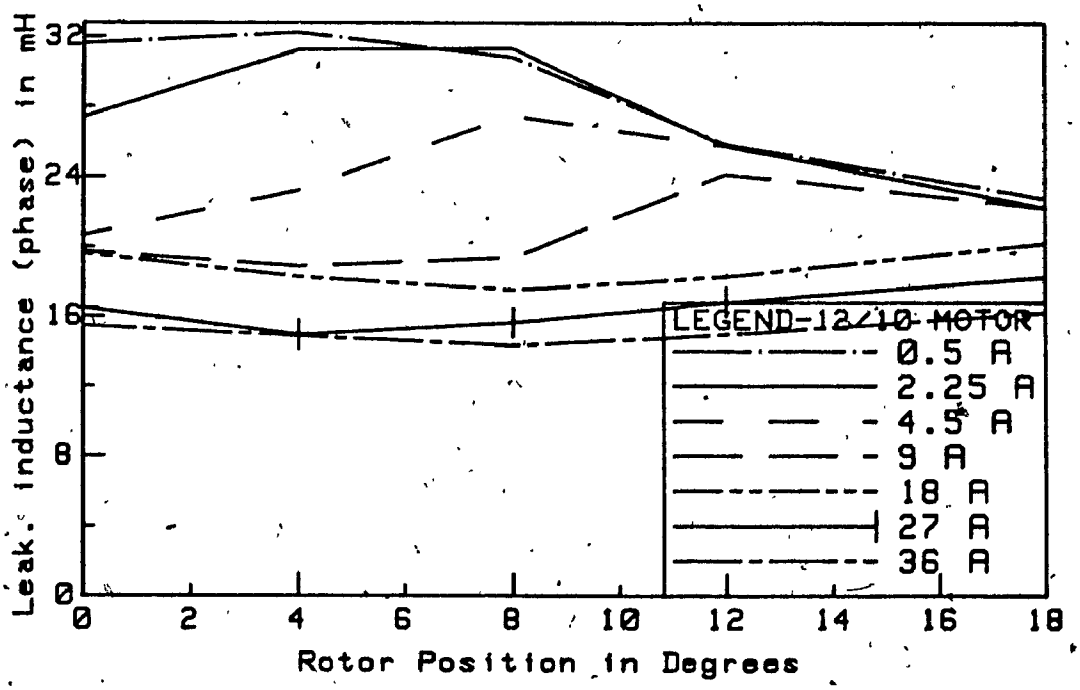

(b)

Fig. 3.30 Total leakage inductance vs rotor position per phase

(a) 6/4 motor. (b) 12/10 motor.

position inductance is less than that in the 12/10 motor. This may permit faster rise of currents in the phase windings of the 6/4 motor during switching. In the 12/10 motor the rate of rise of inductance with rotor position is greater, which results in higher torque developed for a given excitation.

The total leakage inductance which is due to the leakages to the yoke and the adjacent pole windings in the interpolar gap is shown in Fig. 3.30. Although the leakage flux increases with increasing excitation for a given rotor position the leakage inductance decreases slightly. The amount of leakage inductance for the 12/10 motor is more, which is due to the stator pole configuration and the location of the winding. In the unaligned position, the leakage inductance is about 20 percent of the unsaturated inductance. In the aligned position, the leakage is only about 2 to 5 percent of the unsaturated inductance. In both motors, the leakage inductance is relatively insensitive to rotor position when the excitation remains constant.

The average torque per ampere characteristics are shown in Figs. 3.15 and 3.28 for 33, 40 and 50 percent duty cycle excitations. The average torque developed by the motors depends on the instant of switching and the duration of excitation applied to the phase windings. The higher rate of change in coenergy with rotor position which occurs in 12/10 motor causes a higher torque per ampere compared with that in the 6/4 motor.

3.6 Conclusion

This chapter has presented a method of performance prediction for the doubly salient SR motors by directly computing the coenergy in the motors at different rotor positions and excitations. A two dimensional finite element analysis is used to predict the performance of two different SR motors. One of the motors has a single tooth on the stator pole and the other has two teeth

per stator pole. In order to examine the effect of the motor configuration on the performance, these motor structures were considered. The main dimensions of both the motors are taken to be the same for analysis and comparison.

The field pattern obtained gives a better understanding of the flux distribution in the motors. The dependence of terminal and leakage inductances on rotor position and excitation has been demonstrated. The nature and amount of leakages in SR motors are clearly identified and calculated. In general, there does not seem to be any simple relationship to relate these parameters with rotor position and excitation. The one exception is that the total leakage inductance which remains almost constant independent of rotor position for a given excitation. The terminal inductance does not have a linear dependence on rotor position with the result that the ratio of change of inductance to the change in rotor angular position is not constant.

The flux linkages increase monotonically with excitation. When plotted for different rotor positions, it can be noted that the changes in coenergy when the rotor is nearer to the aligned position is relatively small. Hence, the excitation to the phase windings may be switched off before the rotor reaches the aligned position. Increasing excitation beyond the saturation value results in reduced coenergy changes but may increase the iron losses.

The value of inductance for the 12/10 motor seems somewhat high compared with that for the 6/4 motor. This may inhibit the growth of current in the phase windings. With the increased losses due to higher switching frequency of the two teeth per stator pole construction of the 12/10 motor, this motor may not be suitable for high speed operations.

Even with constant excitation, the torque developed by the SR motors is inevitably a function of rotor position and thus the motors produce a pulsating

torque. A pulsating torque is also present with standard excitation arrangements. As in all variable reluctance motors the developed torque maximizes before full alignment is reached.

The torque developed by the motor with two teeth per stator pole is greater than that of a motor with a single tooth per stator pole. This is due to saturation at a relatively lower excitations and the higher rate of change of coenergy for a smaller angular movement of the rotor.

CHAPTER 4

SENSITIVITY OF POLE ARC/POLE PITCH RATIO ON SR MOTOR PERFORMANCE

In this chapter, the sensitivity of the pole arc/pole pitch ratio of the stator and rotor on the performance of a SR motor is investigated. An analytical method based on 'magnetic flux path' and a two dimensional finite element analysis are used for the study. The method of sensitivity study is performed by comparing the average torque developed for different stator as well as rotor pole arc/pole pitch ratios and choosing the ratio combination that produces the greatest value of average torque.

4.1 Introduction

In recent years, a number of papers, on SR motors, has been published in the literature [1],[40]-[62]. Only a few of them address the design aspects [1],[49],[57],[58]. The design philosophy published so far, is based on the knowledge of variable reluctance stepper motor designs. In those papers, the pole arc/pole pitch ratio has been either derived from the permeance values assuming parallel sided teeth and slots or taken to be slightly less than that used for variable reluctance stepper motors. Unlike these variable reluctance stepper motors SR motors have smaller, unequal but even numbers of poles on the stator and rotor. Moreover, SR motors can be used for higher power applications requiring larger sizes. Hence, the change in motor performance due to variations of the stator and rotor pole arc/pole pitch ratios will be of interest to the SR motor designer. With the above considerations the present study, described in this chapter, is undertaken.

An analytical method based on the lumped magnetic circuit model at

different judiciously selected sections of the magnetic circuit has been proposed by Corda and Stephenson [38]. This method is used, as a first approximation, to determine the suitable pole arc/ pole pitch ratio that enables the SR motor to develop the greatest value of the average torque.

The advantage of using finite element analysis for electromagnetic field analysis and particularly for the SR motor, in which high levels of saturation are encountered, has already been discussed in Chapter 2. A two dimensional finite element analysis is used, in this study, to calculate the energy stored in the motor when its rotor is in the aligned and unaligned positions. The coenergy change between the above two positions of the rotor is computed from which the average torque developed is determined. As in the analytical method, the best choice for the pole arc/pole pitch ratio is determined by considering the average torques for different pole arc/pole pitch ratio combination.

4.2 Basis of Sensitivity Study

In SR motors the airgap geometry plays a vital role on their performance. A suitable choice of the airgap length, pole width and pole height is necessary for a better design of the motor. Therefore, attention has been directed to optimize the airgap geometry so that a SR motor with a greater value of torque is designed. The length of the airgap is made as small as mechanically possible so that the torque developed is maximum when all other airgap parameters are held constant. In this study, it is assumed that the height of the pole is fixed. The pole arcs on the stator and rotor are changed in steps of about 0.05 pole pitch, starting from a pole arc/pole pitch ratio of 0.25 upto 0.55. A study, below 0.25 and above 0.55 pole pitch arc length is not required, which will become evident from the trend of the results of this study.

Due to the nonlinear nature of the fields in the SR motor under operating conditions, the virtual displacement principle can be used to calculate the average torque. The flux linkages are calculated for different excitation currents when the rotor is in the aligned and unaligned positions. The coenergy change is obtained from which the average torque is calculated. The range of pole arc/pole pitch ratios which produces a greater average torque is chosen as the preferred values for a better design.

4.3 Methods of torque calculation

In this study, two methods have been used for torque prediction. One is an analytical method which is used to calculate the aligned and unaligned flux linkages for various pole arc/pole pitch ratios. The other is the finite element analysis. The forthcoming paragraphs give a brief description of these methods.

4.3.1 Analytical method

The analytical method describes the determination of the minimum and maximum inductances when the configuration of the motor is known. The minimum inductance is calculated using the assumption that the magnetic fields in the interpolar and airgap regions consist of straight line segments and circular arcs. Unlike the earlier methods, this method takes into account the actual distribution of the winding on the stator poles. The flux linkages when the rotor is in the unaligned position are obtained assuming that the minimum inductance remains constant for the range of excitation considered for analysis. When the rotor is in the aligned position there is considerable mmf drop in the stator and rotor cores compared with that in the airgap. Hence, the conventional magnetic circuit analysis is used to determine the flux linkages.

The application of the technique proposed by Corda et al. may lead to large errors in the minimum inductance calculation unless care is exercised. The formulae derived for permeance components are based on the assumption that the ratio of pole arc/pole pitch is 0.5 for both the stator and rotor. Also, the windings are taken to be extented upto the middle of the stator interpolar regions. Hence, a suitable modification of the formulae is required when this technique is used for a particular motor configuration and winding arrangement.

In the maximum inductance position the cores are saturated even at lower excitations due to the shorter airgap length. Hence, the mmf drops in various sections of the core and the nonlinear characteristic of the core are taken into account when the flux linkages vs current characteristic is computed.

The data for the magnetization characteristic of the iron (M-19 steel) is taken from the manufacturer's data sheets. The characteristic is divided into 20 line segments and each segment is represented using cubic spline polynomials. For flux densities beyond the range of available values, a linear extrapolation is used.

In order to determine the flux linkages vs current characteristic in the aligned position, the flux linkages are assumed and the excitations required to establish the assumed flux linkages are calculated. From the known number of turns, the flux and flux densities in various sections of the magnetic circuit are computed. Using the magnetization curve and the flux densities, the mmf drops in different sections of the core are determined. The excitation current is obtained as the ratio of the ampere turns expended in the core and the airgap and the number of turns.

The flux linkages vs current characteristic for the aligned and unaligned

positions are stored in a data file. The area between these curves is obtained using numerical integration. Having obtained the coenergy change for the chosen ratios of pole arc/pole pitch in the stator and rotor, the average torque developed is calculated.

The procedure used to determine the optimum pole arc/pole pitch ratio is as follows:

1. Set the pole arc/pole pitch ratio of the stator to 0.25.

2. Set the pole arc/pole pitch ratio of the rotor to 0.25.

3. Determine the flux linkages vs current characteristics for the aligned and unaligned positions.

4. Calculate the change in coenergy and hence the average torque developed.

5. Increment the pole arc/pole pitch ratio of the rotor by 0.05.

6. If the rotor pole arc/pole pitch ratio is greater than 0.55, then go to step 7. Otherwise, go to step 3.

7. Increment the stator pole arc/pole pitch ratio by 0.05.

8. If the stator pole arc/pole pitch ratio is greater than 0.55, then go to step 9. Otherwise, go to step 2.

9. Tabulate the average torque developed as a function of the stator and rotor pole enclosures for different excitations.

10. Choose the pole arc/pole pitch ratios corresponding to the greatest average torque for a given current.

It can be realized that there are 49 combinations of pole arc/pole pitch ratio when both the stator and rotor pole arcs are varied. For each combination, one flux linkages vs current characteristic is obtained for both aligned

and unaligned positions. When five excitation currents are considered for each combination, there are 245 average torque values computed. It is presumed that this will give sufficient information on the nature of torque development for the changes in stator and rotor pole widths. Any number of average torque values can be calculated if a suitable number of excitations is considered. On the other hand, when finite element analysis is used, separate problems are to be set up and solved for each excitation and pole arc/pole pitch ratio combination in the aligned and unaligned positions. Thus, for the chosen five excitation currents 490 problems are solved and postprocessed to obtain the coenergy for both aligned and unaligned positions. The coenergy is directly computed in finite element analysis and hence the flux linkages vs current characteristic need not be plotted to determine the average torque.

4.3.2 Finite Element Analysis

The finite element formulation used for field analysis has already been described in Chapter 2. The configuration of the SR motor considered for investigation is shown in Fig. 5.1.

For each stator pole arc/pole pitch ratio, the rotor pole arc/pole pitch ratio is changed from 0.25 to 0.55 in steps of 0.05. Thus, seven finite element analysis models are developed for the aligned position, each model having provision to change the rotor pole arc/pole pitch ratio. Since, the field solutions are obtained for five chosen excitations, 35 problems are set up for each stator pole arc/pole pitch ratio. Similarly, for the unaligned position, seven different models have been used, each time solving and postprocessing 35 problems.

The coenergy for each pole arc/pole pitch ratio combination and current, when the rotor is in a given position, is directly computed as described earlier. The change in coenergy and the average torque are determined.

4.4 Results

The average torque values calculated by the analytical method is given in Table 4.1. To illustrate the nature of results that lead to these values, a typical flux linkages vs current characteristic for a pole arc/pole pitch ratio of 0.4 on the stator and 0.35 on the rotor is shown in Fig.4.1. The variation of the average torque with changes in stator pole arc/pole pitch ratio is plotted for different rotor pole arc/pole pitch ratios and is shown in Fig.4.2. Keeping the pole arc/pole pitch ratios for the stator and rotor the same, average torque values are calculated for various excitation currents. The resulting average torque variation for different pole arc/pole pitch ratios is shown in Fig. 4.3.

The average torque is proportional to the change in coenergy values when the rotor moves from the unaligned to the aligned position. Hence, the results obtained by the finite element method are presented in terms of coenergy itself. Excitation currents of 1,2,4,8 and 12 amperes are used for the investigation. The results of 1 ampere excitation are not presented as they are very similar to 2 ampere results. Fig. 4.4 shows the variation of coenergy change with varying stator and rotor pole arc/pole pitch ratios when the excitation is 2 amperes. The results of 4,8 and 12 ampere excitation are shown in Figs. 4.5, 4.6 and 4.7, respectively.

4.5 Conclusion

The changes in stator pole arc greatly influence the average torque compared with the changes in rotor pole arc. At lower excitation currents, when the saturation in the core is not appreciable, the developed torque increases invariably with increase in stator pole arc for a given rotor pole enclosure. Instead, at higher excitations, the increase in average torque with stator pole enclosure is less and at at higher stator pole arcs the average torque decreases.

TABLE 4.1
Average Torque Calculated Using Analytical Method

Stator pole enclosure	Rotor pole enclosure						
	0.25	0.30	0.35	0.40	0.45	0.50	0.55
			Excitation = 1 ampere				
0.25	0.3527	0.3540	0.3552	0.3565	0.3571	0.3574	0.3572
0.30	0.4113	0.4150	0.4163	0.4176	0.4181	0.4182	0.4178
0.35	0.4649	0.4721	0.4745	0.4758	0.4763	0.4761	0.4752
0.40	0.4656	0.5244	0.5284	0.5299	0.5303	0.5298	0.5282
0.45	0.4119	0.5615	0.6294	0.6860	0.7318	0.7693	0.7992
0.50	0.4812	0.5610	0.6289	0.6850	0.7308	0.7676	0.7962
0.55	0.4802	0.5600	0.6276	0.6830	0.7280	0.7641	0.7904
			Excitation = 2 amperes				
0.25	1.2503	1.2541	1.2561	1.2567	1.2573	1.2567	1.2541
0.30	1.4286	1.4337	1.4362	1.4374	1.4371	1.4354	1.4318
0.35	1.5956	1.6073	1.6100	1.6105	1.6093	1.6061	1.6000
0.40	1.6154	1.7184	1.7230	1.7230	1.7203	1.7150	1.7065
0.45	1.5058	1.7819	1.8761	1.9450	1.9970	2.0340	2.0580
0.50	1.6482	1.7790	1.8723	1.9401	1.9895	2.0240	2.0420
0.55	1.6440	1.7740	1.8654	1.9314	1.9780	2.0070	2.0160
			Excitation = 4 amperes				
0.25	3.1576	3.1576	3.1487	3.1411	3.1330	3.1233	3.1067
0.30	3.8732	3.8719	3.8681	3.8620	3.8530	3.8400	3.8210
0.35	4.1178	4.1230	4.1180	4.1088	4.0960	4.0773	4.0492
0.40	4.2307	4.3424	4.3380	4.3260	4.3080	4.2820	4.2420
0.45	4.1056	4.4240	4.5218	4.5880	4.6290	4.6450	4.6330
0.50	4.2649	4.4064	4.5006	4.5610	4.5930	4.5960	4.5613
0.55	4.2420	4.3800	4.4690	4.5214	4.5420	4.5260	4.4530
			Excitation = 8 amperes				
0.25	6.0733	6.0097	5.9640	5.9193	5.8747	5.8240	5.7590
0.30	8.3843	7.2550	8.3117	8.2730	8.2260	8.1660	8.0810
0.35	9.3810	9.3530	9.3130	9.2656	9.2055	9.1240	9.0060
0.40	9.6302	9.7220	9.6750	9.6140	9.5330	9.4220	9.2590
0.45	9.4844	9.8099	9.8726	9.8880	9.8550	9.7640	9.5860
0.50	9.6206	9.7320	9.7787	9.7710	9.7040	9.5590	9.2900
0.55	9.5230	9.6190	9.6450	9.6060	9.4930	9.2730	8.8520
			Excitation = 12 amperes				
0.25	8.276	8.136	8.019	7.915	7.810	7.690	7.540
0.30	12.906	12.816	12.727	12.635	12.528	12.391	12.197
0.35	14.599	14.514	14.414	14.301	14.162	13.975	13.706
0.40	14.991	15.030	14.913	14.770	14.585	14.331	13.960
0.45	14.814	15.102	15.090	15.009	14.846	14.568	14.110
0.50	14.885	14.922	14.874	14.740	14.500	14.102	13.436
0.55	14.662	14.666	14.570	14.367	14.023	13.454	12.449

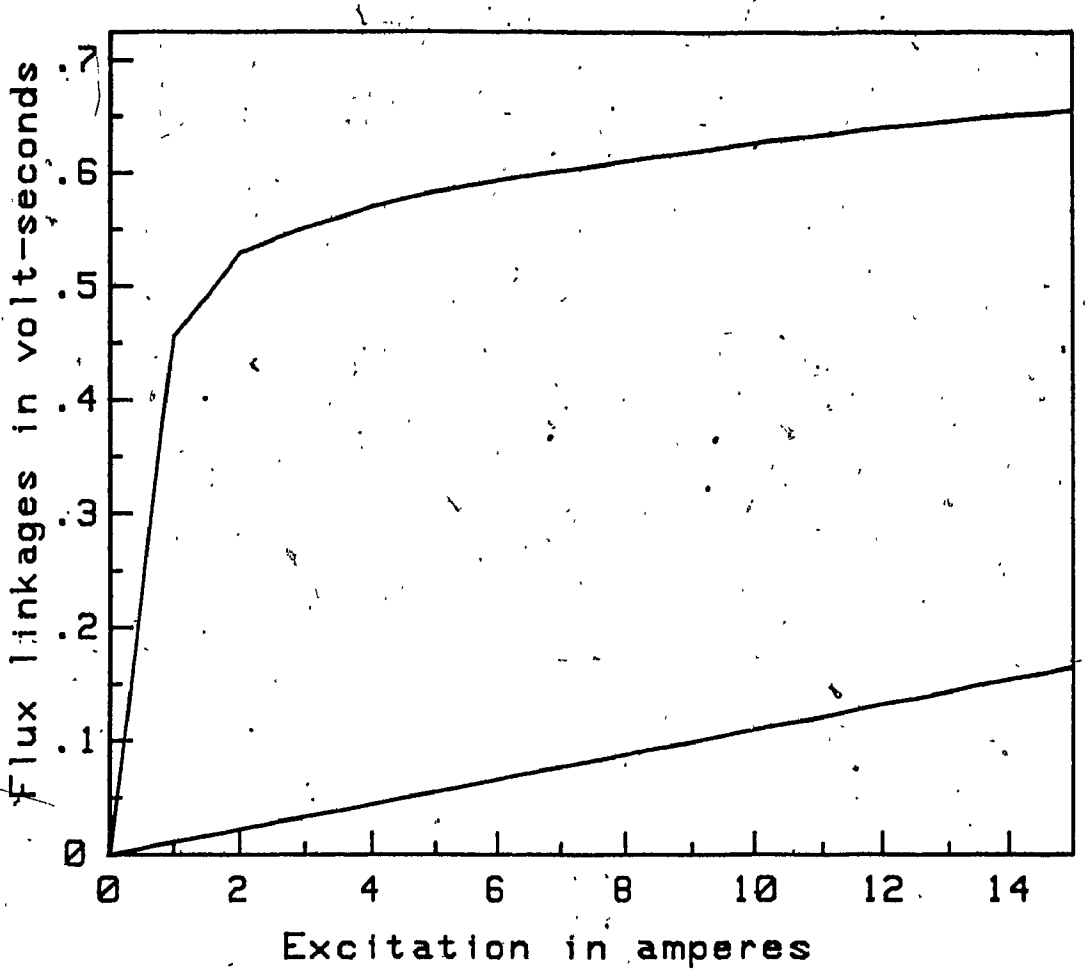

Fig. 4.1 Flux linkages vs excitation characteristic (Analytical Method)

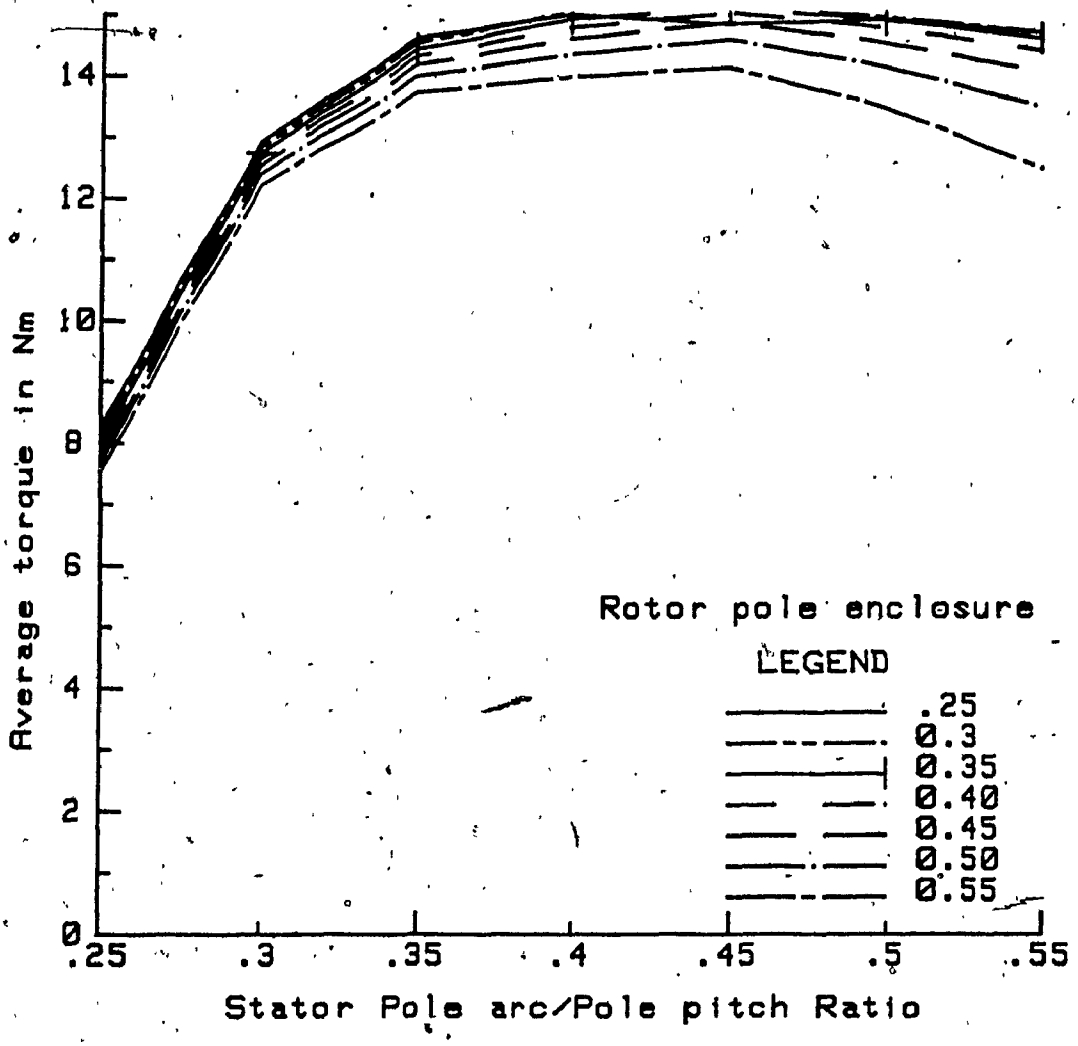

Fig. 4.2 Average torue vs stator pole arc/pole pitch ratio

(Excitation at 12 ampere)

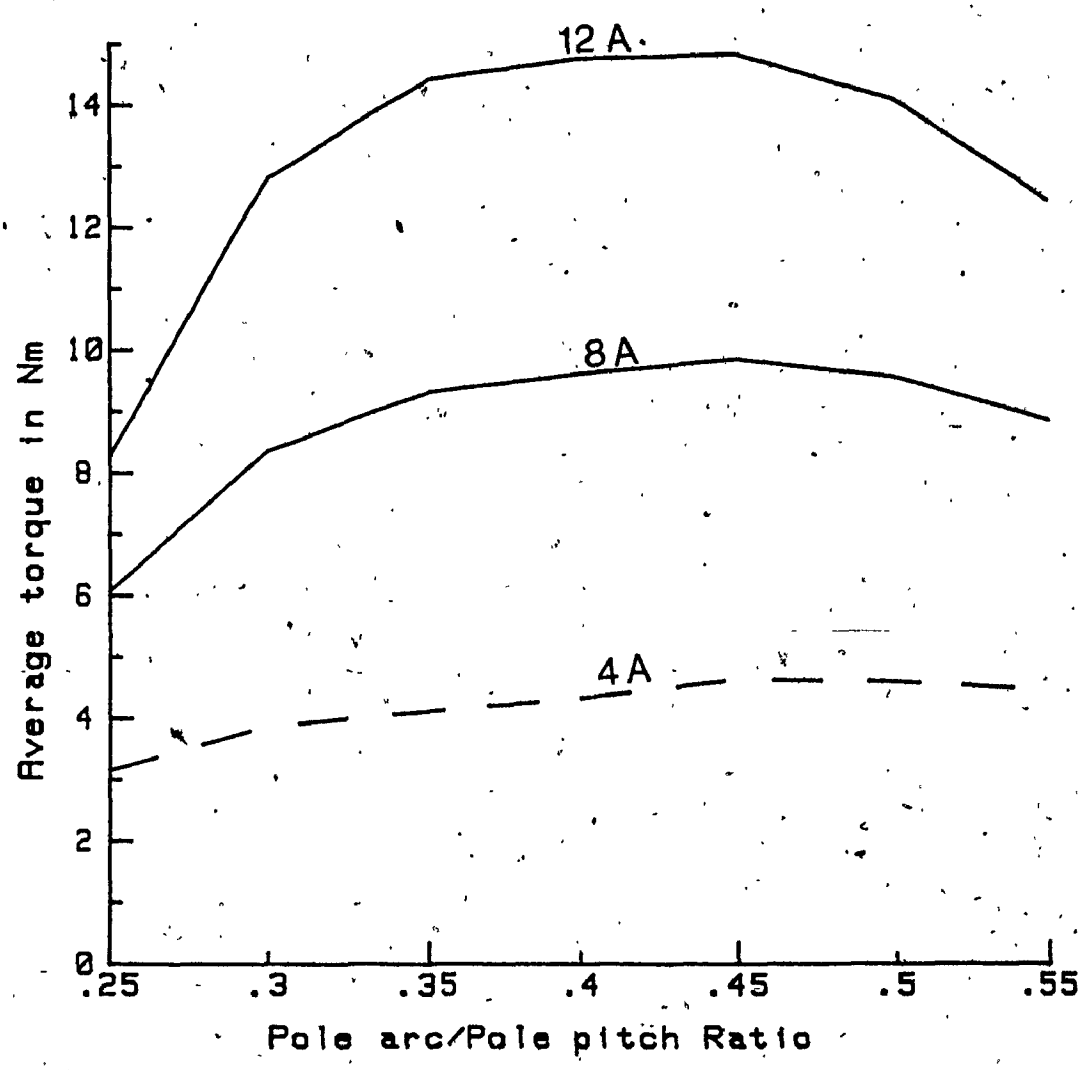

Fig. 4.3 Average torque vs pole arc/pole pitch ratio (stator and rotor ratios are equal)

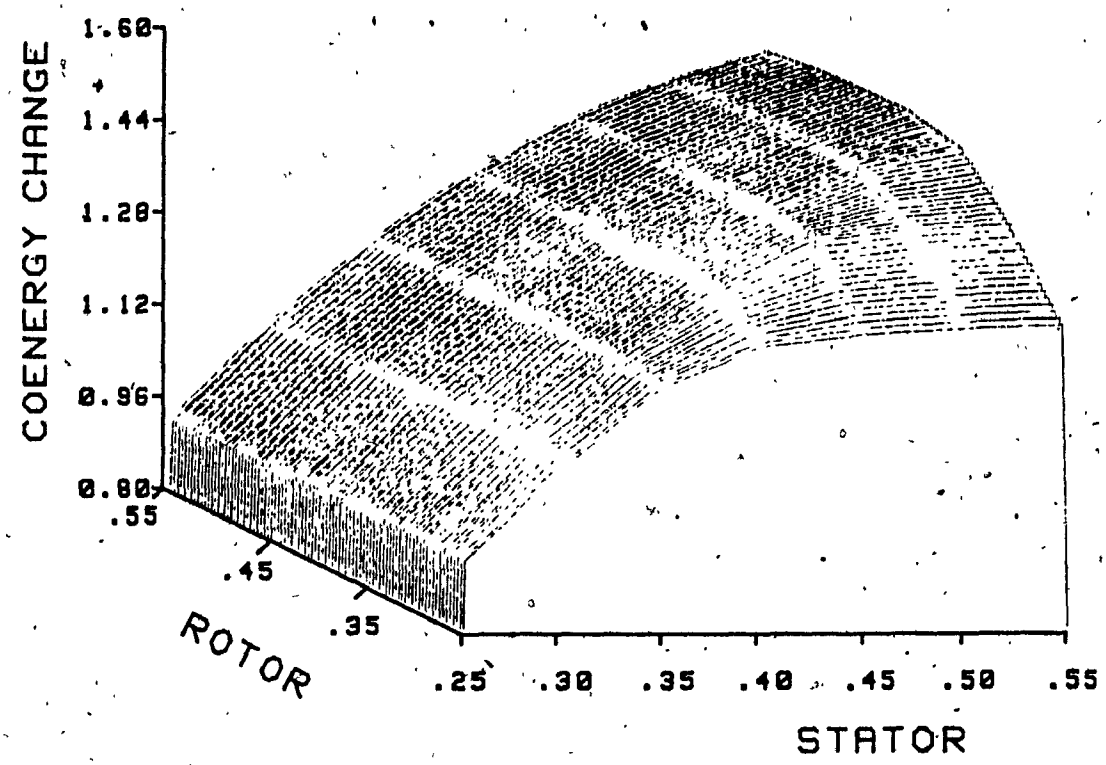

Fig. 4.4 Average torque vs pole arc/pole pitch ratios of stator and rotor (Excitation at 2 amperes)

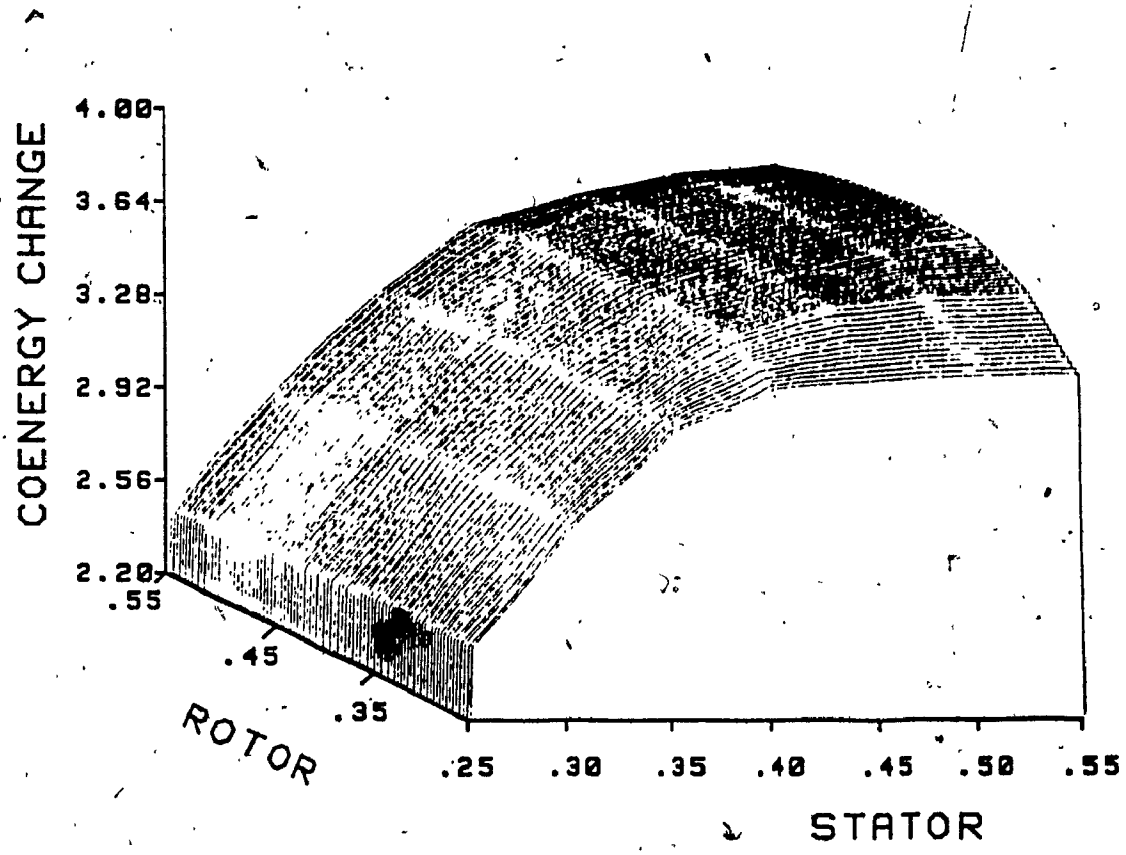

Fig. 4.5 Average torque vs pole arc/pole pitch ratios of stator and rotor (Excitation at 4 amperes)

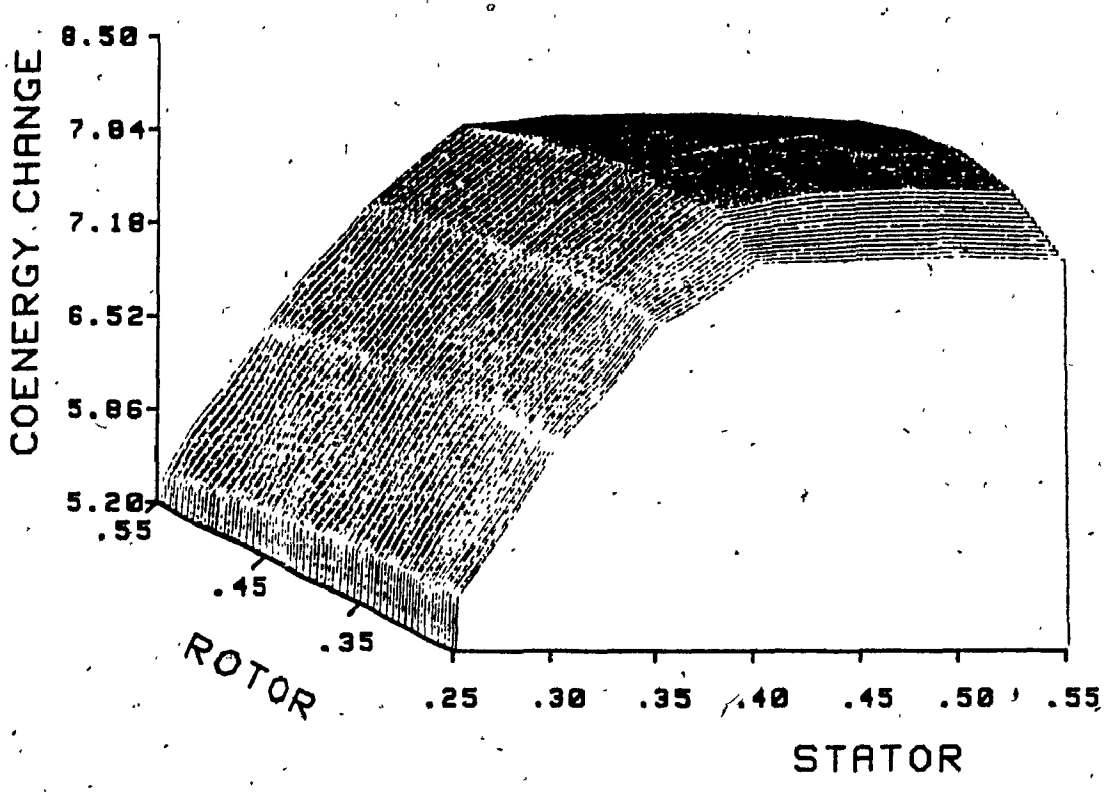

Fig. 4.6 Average torque vs pole arc/pole pitch ratios of stator and rotor (Excitation at 8 amperes)

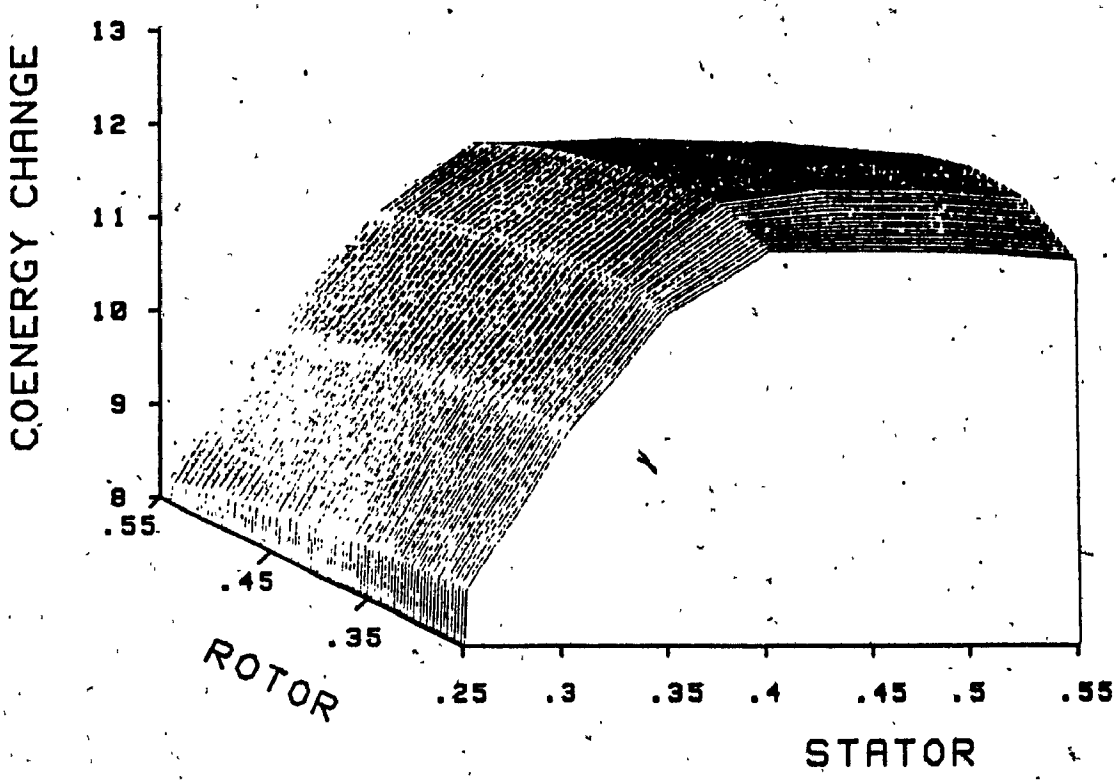

Fig. 4.7 Average torque vs pole arc/pole pitch ratios of stator and rotor (Excitation at 12 amperes)

It is particularly evident at a steady excitation of 12 amperes where the average torque is less for a stator pole arc/pole pitch ratio of 0.55 compared with that for 0.5. When the stator pole arc/pole pitch ratio is less than 0.35, there is distinctly less developed torque at all excitations. Hence, it may be recommended that the stator pole arc/pole pitch ratio be chosen in the range of 0.35 to 0.5. Higher pole arc/pole pitch ratios for the stator may be limited by considerations of winding space and the necessary clearance between the windings.

At all excitation currents, the average torque value increases with increase in rotor pole arc, reaches a peak value and then decreases when the stator pole arc is held constant. It is observed that there is no increase in torque developed when the rotor pole arc/pole pitch is increased beyond 0.45. Higher excitation currents produce maximum values of average torques when the ratio is slightly less than 0.4, whereas, at lower currents the average torque values reach peaks when the ratio is slightly above 0.4. Considering the nature of currents, normally encountered in SR motors, choosing the rotor pole arc/pole pitch ratio around 0.4 may produce the highest torques. The average torque is less for a rotor pole arc/pole pitch ratio of 0.25 compared with that for higher ratios when the stator pole arc/pole pitch ratio is in the range of 0.35 to 0.5.

It can be concluded that the pole arc/pole pitch ratio on the stator and rotor of a SR motor need not be the same. The range of values that may be used for the pole arc/pole pitch ratio of the rotor can be 0.3 to 0.45 and that of the stator 0.35 to 0.5.

CHAPTER 5

DESIGN PROCEDURE FOR SR MOTORS

Switched reluctance motors have gained the attention in variable speed drive market. The savings in manufacturing cost of the motor due to its simplicity of construction, minimum maintenance and the use of minimum number of switching devices in the drive circuit are the important factors in its favour compared to other motor drives. This chapter is concerned with some of the design aspects of the SR motor. A step by step procedure is developed for the design of the SR motor from the basic principles of electromagnetics.

5.1 Introduction

Switched reluctance motors have been developed for electric propulsion, fan, pump and other commercial applications. Variable speed drives comprising SR motors have been investigated and built during this decade. They have simple and rugged construction and provide high overall efficiency. Due to unidirectional current requirement, their controllers use a minimum number of power switches and therefore have significant advantages over the conventional three phase inverters used for induction or synchronous motor control.

In spite of its growing popularity, very few papers have dealt with the design aspects of the SR motor itself [1],[49],[57],[58]. The parer by Lawrenson et al. [1] gives some of the design aspects that are to be considered for the SR motor. In another paper by Fulton et al. [49] they discuss some more options to design a cost effective SR motor. The design philosophy described by Finch et al. [57],[58] extents the design method developed for variable reluctance stepping motors [22],[23], the validity of which depends on the accurate

determination of permeance values in the aligned and unaligned positions. While a finite element analysis of a SR motor has brought to light the complexity of the motor [72], it has not given way to a simple design procedure that could be used with minimum computational effort.

This chapter attempts to fill the void in the design procedure for the SR motor. The output equation is developed in a manner very similar to that used for conventional rotating machines, thereby bringing the design engineer's experience to bear on this new machine. The main dimensions are obtained using an output equation. While the existing procedures are used for the computation of inductances, the sensitivity of their prediction on the performance calculation is given. A criterion to find the upper limit of the stator excitation is introduced relating the incremental ratio of mechanical energy and stator current.

The study of SR motor reveals that there are a number of parameters such as the number of poles, ratio of length to diameter, winding, losses, etc. affect the motor performance. Hence, the sensitivity of these parameters has to be considered in the design of the SR motor. In order to design a motor which satisfies the given requirements, it is essential that a method of performance prediction be developed. For preliminary design purposes a computer programme, based on the method proposed by Corda et al. [38] for the determination of aligned and unaligned inductances, has been developed and used to calculate the SR motor performance.

5.2 Output Equation

In general, conventional machines are designed starting from the output equation. A similar development of the output equation for the SR motor will make its design process a systematic one. Moreover, the experience of the

machine designers can be effectively used in the design of these new machines as they can use the commonality between these and conventional machines, at least to start with. The output equation of a SR motor will be significantly different from those of conventional machines. In this thesis , the emphasis is placed mainly on the similarities in the design process.

The output equation of any machine relates the power output to its main dimensions such as the bore diameter and length, the speed of operation and the electric and magnetic loadings at the operating conditions of the machine. Normally, the output power and the operating speed of the machine are specified. From experience, depending on the method of cooling and the characteristic of the core material the specific electric and magnetic loadings will be chosen. Depending on the type of application the relation between the length and bore diameter is fixed. By making use of the output equation, the main dimensions of the motor will be determined.

The output equation for the SR motor has been developed based on the following assumptions.

1. The motor operates with a flat topped current, i.e., the back emf generated is equal to the voltage applied to the phase windings.

2. The inductance changes only during the interval when the stator and rotor poles overlap. This occurs for an angular rotor movement equal to the stator pole arc, β_s.

The configuration of a typical SR motor with six stator poles and four rotor poles is shown in Fig. 5.1. When voltage, V is applied to a phase winding, it is related to the flux linkages, Ψ, at any instant by

$$V = Ri + \frac{d_o \Psi(\theta, i)}{dt} \qquad (5.1).$$

where R is the resistance of the winding and i is the phase current. If the

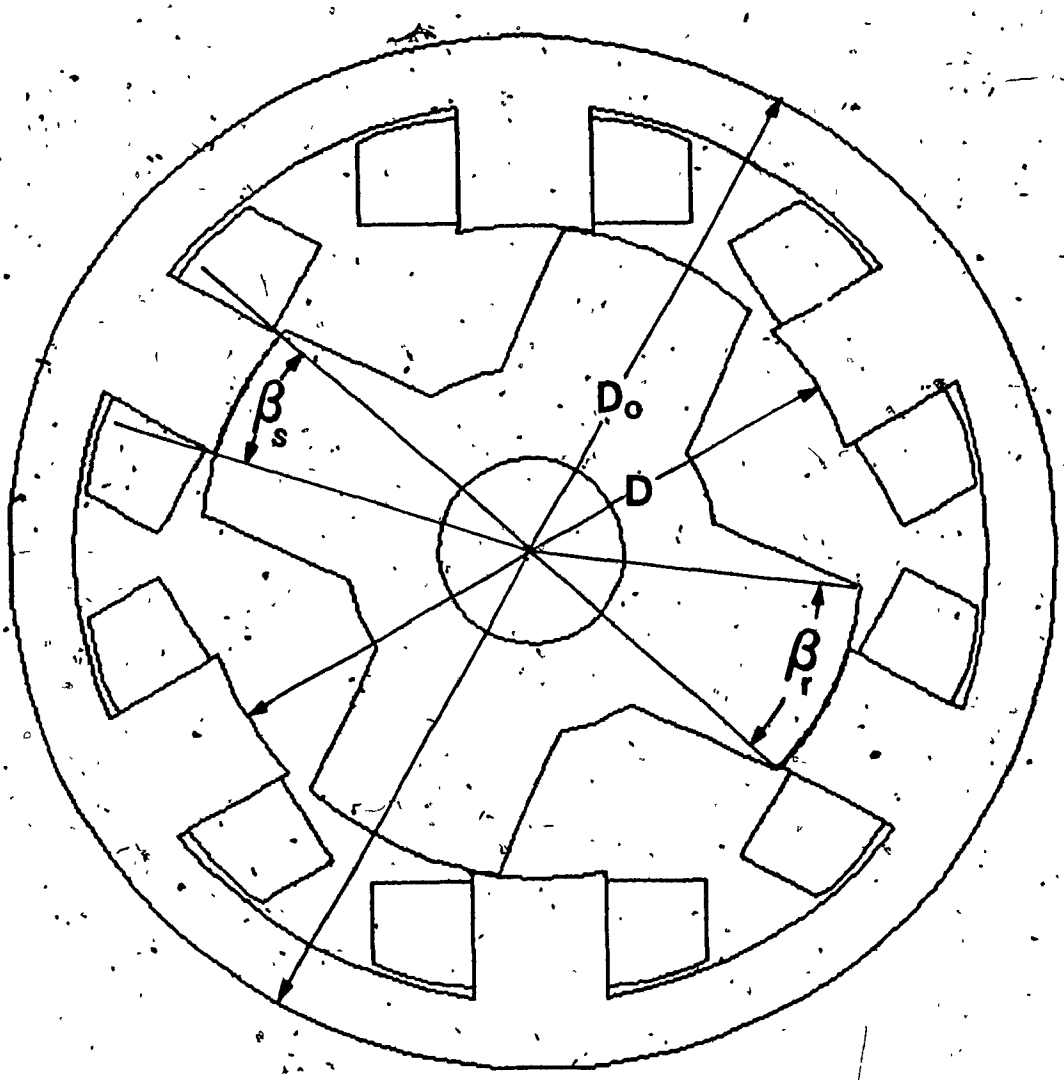

Fig. 5.1 Typical SR motor configuration (6/4 motor)

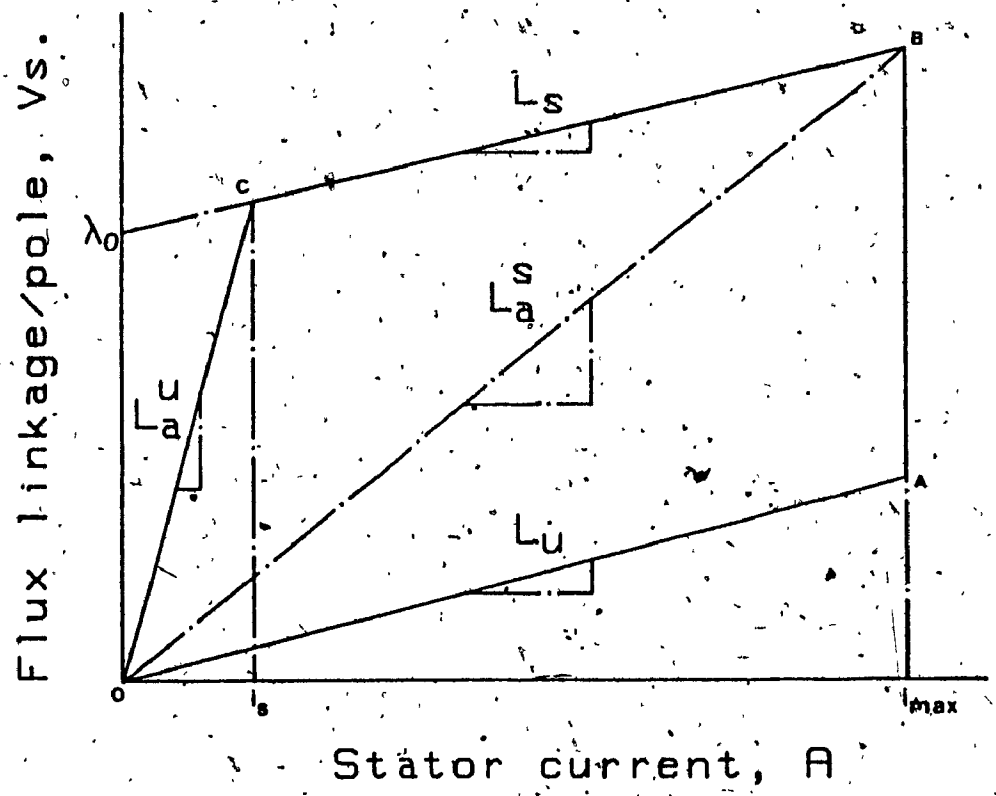

Fig. 5.2 Approximate flux linkages vs current characteristic

resistance R is neglected, to simplify the analysis, the special case of a flat topped current condition will be obtained.

Typical flux linkages vs current characteristics for SR motors, obtained using finite element analysis, are shown in Figs. 3.10 ans 3.22. For the purpose of simplified analysis, the aligned and unaligned flux linkages can be approximated as those shown in Fig. 5.2, similar to those used by Miller [59], with the following assumptions.

1. The unaligned inductance, L_u, remains constant until the stator and rotor poles just begin to overlap.

2. The aligned flux linkages curve is approximated by two straight line segments, one, from the origin to the point C associated with the unsaturated aligned inductance, L_a^u, and the other line segment CB, roughly parallel to L_u, with a slope $L_s \approx L_u$. The area enclosed by OABCO represents the electromagnetic energy that is converted to mechanical output of the motor in each working stroke.

The back emf developed in the winding during the rotor movement for a flat topped current, i, is

$$V = \frac{d\,\Psi(\theta)}{dt} \qquad (5.2)$$

The flux linkages change from $L_u i$ to $L_a^s i$, during the interval, t, when the rotor moves from the unaligned position to the aligned position. Hence,

$$(L_a^s - L_u)i = Vt \qquad (5.3)$$

where L_a^s - aligned saturated inductance per phase.

L_u - unaligned inductance per phase

V - applied voltage

and t - the time taken by the rotor pole to move through an angular distance of β_s radians, i.e., from the instant it just begins to overlap the stator pole until it reaches the aligned position.

When the rotor speed is ω_m rad/sec, the time

$$t = \frac{\beta_s}{\omega_m} \tag{5.4}$$

Defining

$$\sigma = \frac{L_a^s}{L_a^u} \tag{5.5}$$

$$\lambda_u = \frac{L_a^u}{L_u} \tag{5.6}$$

and substituting equations (5.4),(5.5) and (5.6) in equation (5.3)

$$V = \frac{\omega_m}{\beta_s} L_a^s i \left(1 - \frac{1}{\sigma \lambda_u}\right) \tag{5.7}$$

The flux linkages in the aligned position are

$$L_a^s i = BAT_{ph} \tag{5.8}$$

and

$$A = \frac{D}{2} L \beta_s \tag{5.9}$$

where B - flux density in the airgap when the poles are aligned

A- area of the stator pole.

D - bore diameter

L - length of the stator pole

β_s - stator pole arc

and T_{ph} - number of turns per phase.

The stator current may be obtained from the specific electric loading A_{sp}

which is defined as,

$$A_{sp} = \frac{m\,2T_{ph}\,i}{\pi D} \tag{5.10}$$

where m is the number of phases that conduct simultaneously.

The power developed is

$$P_d = mk_d\,k_e\,Vi. \tag{5.11}$$

where V and i are the peak values of the voltage and current respectively

k_d is the duty cycle defined in equation (5.12).

and k_e is the efficiency.

The duty cycle can be expressed as,

$$k_d = \frac{\theta_i\,qP_r}{360} \tag{5.12}$$

where θ_i - current conduction angle for each rising inductance profile

q - number of phases $= \frac{P_s}{2}$

and P_r - number of rotor poles.

Combining equations (5.7) to (5.11)

$$P_d = k_d\,k_e\,(\frac{\pi^2}{120})(1 - \frac{1}{\sigma\lambda_u})BA_{sp}\,D^2LN_r \tag{5.13}$$

where N_r is the rotor speed in rpm.

Equation (5.13) can be rearranged to resemble that of the conventional output equation of ac machines. Thus,

$$P_d = k_d\,k_e\,k_1k_2BA_{sp}\,D^2LN_r \tag{5.14}$$

where

$$k_1 = \frac{\pi^2}{120} \tag{5.15}$$

and

$$k_2 = (1 - \frac{1}{\sigma\lambda_d}) \tag{5.16}$$

The equation for the torque can be expressed as

$$T = k_d k_c k_2 k_3 B A_{sp} D^2 L \tag{5.17}$$

where

$$k_3 = \frac{\pi}{4} \tag{5.18}$$

Note that the torque and power output are proportional to the product of specific electric and magnetic loadings and bore volume. The variable k_2 is dependent on the operating current of the motor and is determined by the stator phase current, magnetic characteristic of the core material and dimensions of the motor. For a given operating current k_2 is a constant. Hence, to asses the maximum power output of the SR motor, k_2 needs to be calculated at the maximum stator current. In order to determine the value of k_2, the flux linkages vs current characteristic for the aligned and unaligned positions are to be estimated for various values of stator currents.

For k_d equal to one, the power developed is maximum for a given stator current. It is usual to find that the maximum possible duty cycle is less than unity. Torque and power controls are exercised by the variation of duty cycle similar to a chopper controlled dc motor. The speed is controlled by the frequency of switching of the phases resembling the control of a synchronous motor.

5.3 Design considerations

There are a number of parameters that determine the SR motor performance. These parameters, their effect on the motor performance and the conflicting requirements that arise in parameter selection are to be considered

during the design process. The SR motor, unlike a conventional ac motor, has to be operated only with power controllers. Hence, the SR motor design is to be done in conjunction with the power controller design.

5.3.1 Number of Poles

The number of poles is selected based on the following considerations.

1. Minimum mutual inductance to maximize power output.

2. Higher ratio between the inductances in the aligned and unaligned positions.

3. The capability to start from any rotor position and to run in either direction.

4. A suitable pole combination of the stator and rotor such that the switching frequency is minimum.

In a single phase SR motor with a single pair of coils, positive torque is developed only over a limited range of rotor positions. A two phase motor, such as the one described by Byrne and Lacy [4] can start and run from any rotor position, but it can only be unidirectional. In order to have self starting capability and bidirectional rotation it is necessary that a SR motor have a minimum of three phases.

A suitable pole combination for a three phase motor will be, six poles on the stator and four poles on the rotor. Similarly, for a four phase motor the pole combinations are, eight poles on the stator and six poles on the rotor.

In order to satisfy the above considerations, the number of poles on the stator and rotor are to be even numbers. When the windings on the diametrically opposite poles are excited, the mutual inductance between the excited windings will be zero and these two windings can form a phase of the motor.

The choice of more poles on the stator requires that the stator pole arc be less than that of the rotor in order to accommodate the windings.

5.3.2 Pole Arcs on the Stator and Rotor

The effect of the pole arc/pole pitch ratio changes on the motor performance has been dealt with in Chapter 4. From the analysis it was concluded that the design with unequal pole arc/pole pitch ratios for the stator and rotor are favoured. In practical designs, unequal pole arcs at the airgap are used which has the effect of reducing the ratio of maximum to minimum reluctances in the magnetic circuit and thus reducing the static mean torque. This is done so that the best possible combinations of efficiency and specific output for a particular speed range is achieved.

5.3.3 Starting Torque

It has been seen in Chapter 3 that the torque developed by a SR motor is a function of rotor position even though the excitation is maintained constant. The choice of the number of phases and pole arcs must be such that there is enough starting torque at all rotor angles. It is achieved by having adequate overlap between the inductance variations of adjacent phases.

5.3.4 Windings

The windings on a SR motor are very simple. They are normally wound on a former and later transferred to the stator poles. For large motors, the conductors may be stranded to reduce the skin effect. The windings are compact having least overhang which enables the SR motor to have greater core volume within the same volume of space occupied by an equivalent induction motor.

5.3.5 Airgap

In the SR motor, the developed torque decreases as the length of the airgap is increased [23]. Hence, the airgap length is made as small as mechanically possible in terms of manufacturing technique and tolerance for shaft deflection. A compromise has to be made between the electromagnetic and mechanical requirements.

5.3.6 Losses

The selection of current density and conductor size must be such that there is less I^2R loss. The number of turns, excitation current and the iron area have to be increased suitably to have sufficient flux in the airgap to produce the required torque. The increase in iron area to reduce flux density in the core and thus the core loss may impose restrictions on the winding space. A compromise has to be made keeping copper loss in mind. The core loss will increase due to higher switching frequency if the number of poles is increased.

5.4 Selection of Design Parameters

5.4.1 Speed

Since the SR motor is normally used as a variable speed drive, it is appropriate to have a base speed specification. At base speed, the motor is expected to deliver the rated torque and hence rated power output.

5.4.2 Diameter and Length

From the output equation (5.14) it is evident that the rated power output is proportional to the bore volume and can be expressed as

$$P_d \propto D^2L \qquad (5.19)$$

Depending on the nature of application and space limitations, the stack length

of a motor is chosen as a multiple or submultiple of bore diameter. Thus,

$$L = kD \qquad (5.20)$$

where k is the ratio between the length and bore diameter. The value of k need not be chosen arbitrarily. For non-servo applications, the range of k can be

$$0.25 \leq k \leq 0.7 \qquad (5.21)$$

and for servo applications

$$1 \leq k \leq 3 \qquad (5.22)$$

The bore diameter D is evaluated from the output equation (5.14) if the rated speed N_r, B, A_{sp}, k_2, k_d and k are known. It is possible to start the iterative process for design with reasonable values.

In general, at rated condition the range of k_2 will be

$$0.6 \leq k_2 \leq 0.75 \qquad (5.23)$$

The magnetic loading B for the aligned position can be taken as the allowable maximum for the core material. The specific electric loading, A_{sp}, in ampere conductors per meter is in the range of

$$25000 \leq A_{sp} \leq 60000 \qquad (5.24)$$

The duty cycle k_d can be taken to be unity to start with. Using the above starting values, the bore diameter D is computed.

5.4.3 Airgap Length

In order to achieve better performance from a variable reluctance motor, it is necessary that the inductance of the phase winding vary to the largest possible extent with rotor position. Therefore, it is essential to keep the airgap length as small as possible. The airgap length, as mentioned in the previous section, is determined by the machining tolerance and assembly techniques. Small machines may have airgaps of about 0.25mm.

5.4.4 Number of Turns

Using equation (5.10) the number of turns per phase is calculated for a given current. The current is obtained from the consideration of power output, efficiency and the converter voltage supply at the motor input terminals. Depending on the nature of cooling employed in the motor, the maximum permissible current density is chosen. The conductor size is determined from the winding current and the chosen current density. The volume of space required to accommodate the winding is calculated and checked against the available space for the winding taking due consideration of insulation thickness and the clearance required between the adjacent pole windings. Instead of choosing the current density, the conductor size can be chosen such that the available space is filled. The resulting current density can be checked against the maximum permissible value. The height of the stator pole is then derived from the winding space requirement.

From equation (5.10) for a given specific electric loading and bore diameter it can be seen that the product of T_{ph} and i is a constant. The best values are those which would satisfy the following mutually contradictory demands:

1. Small current and inductance.

2. Small value of resistance implying a smaller number of turns.

An engineering trade off has to be made with thermal considerations in perspective. It is emphasized here that the selection of i and T_{ph} depends on the ac supply available for rectification and subsequent input to the converter to control the SR motor.

5.4.5 Thermal Considerations

The thermal capacity of the motor is one of the important characteristics in motor design. It is determined by the copper loss and core loss in the motor, the temperature rise, the available surface area for cooling and additional cooling arrangements such as fan etc.

If R is the phase resistance of the winding, the total copper loss for non-overlapping currents in the stator is given by

$$P_{cu} = qI^2R \tag{5.25}$$

where the rms value of phase current

$$I = i/\sqrt{(q)} \tag{5.26}$$

and q is the number of phases of the SR motor.

Hence,

$$P_{cu} = i^2R \tag{5.27}$$

The resistance of each phase winding is

$$R = \frac{\rho l}{a_c} \tag{5.28}$$

This can be rewritten in terms of the number of turns etc. as

$$R = \frac{k_r T_{ph}}{a_c} \tag{5.29}$$

where a_c is the area of cross section of the conductor

l is the total length of winding conductors per phase

ρ is the resistivity of the conductor

and k_r is the product of resistivity and the mean length of turn.

Substituting equation (5.29) in equation (5.27)

$$P_{cu} = k_r \frac{i}{a_c} T_{ph}\, i \qquad (5.30)$$

$$J_c = \frac{i}{a_c} \qquad (5.31)$$

$$P_{cu} \propto J_c\, T_{ph}\, i \qquad (5.32)$$

Since, the maximum $T_{ph}\, i$ is a constant, the copper loss is proportional to the current density. Thus, to decrease the copper loss the current density has to be decreased.

The core loss is influenced by the characteristics of core laminations, their thickness, the peak value of flux density and the frequency of flux reversals due to switching. The fundamental frequency of flux reversal depends on the speed and the number of poles of the motor. The harmonics in the flux waveforms due to the nature of winding currents increase the core loss. The stator poles have flux density excursions from zero to B only, but the back iron regions experience flux reversals in segments for each switching of the phase. The rotor poles experience one flux reversal per revolution while the flux in the rotor core has a complex waveform and contains higher order harmonics. In contrast with ac machines, the procedure for predicting core losses in a SR motor and their distribution demands a considerable sophistication of approach.

5.5 Design Verification

As seen in the previous section the design of the SR motor involves a number of variables and often requires a judicious selection of the variables meeting conflicting requirements. In order to design a motor to meet the given specification it is essential to develop a method of accurately determining the performance from design details. Due to high levels of saturation usually

encountered in SR motors, the finite element analysis has been used to estimate the performance. It may involve more computational effort and time for a chosen motor configuration. In order to get a quick feel for the problem at hand, the analytical method described in Chapter 4 can be used for performance prediction.

While the evaluation of aligned flux linkages can be accurate, the same cannot be said for the unaligned values, when the analytical method is used. The leakage fluxes and the path of mutual flux complicate the accurate estimation of unaligned flux linkages and inductances. The inaccurate value of the unaligned inductance introduces an error in the computation of k_2 and hence in the output equation. It can be recalled that

$$k_2 = 1 - \frac{L_u}{L_a^s} \tag{5.33}$$

Great accuracy in the calculated unaligned inductance is not necessary. It can be proved, using equation (5.33), that an error of 50 to 100 percent compared to the actual value introduces only 10 to 15 percent deviation in the predicted motor output.

An experimental motor has been designed with the same bore diameter and length as that of an existing induction motor to enable performance comparisons between these two types of motors. The main dimensions of the experimental SR motor are given in Table 5.1.

The configuration of the motor core laminations is shown in Fig. 5.1. The core is made up of M-19 silicon steel laminations. The flux linkages vs current characteristic, calculated using finite element analysis, is shown in Fig. 5.3. The inductance variation when the rotor is in the aligned position is shown in Fig. 5.4 as a function of stator current. The value of k_2 and the ratio of the aligned to unaligned inductance vs stator current are shown in Fig. 5.5. Such a

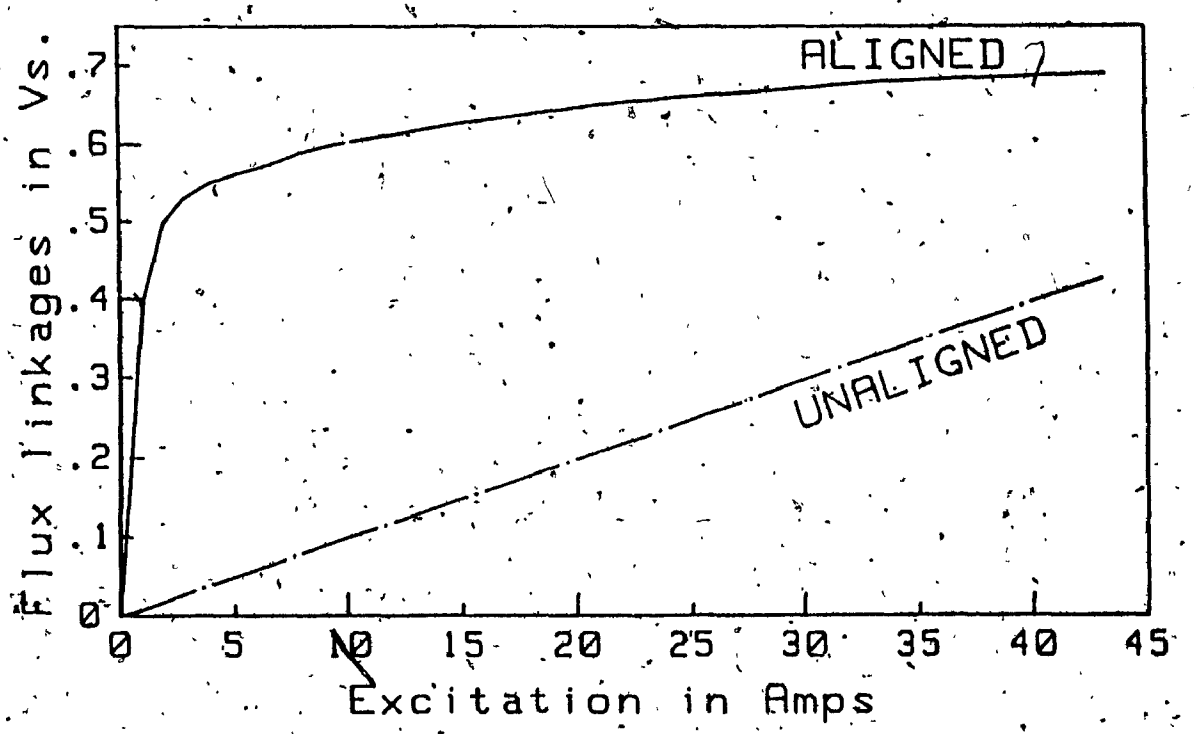

Fig. 5.3 Flux linkages vs excitation characteristic of the designed motor obtained using finite element analysis

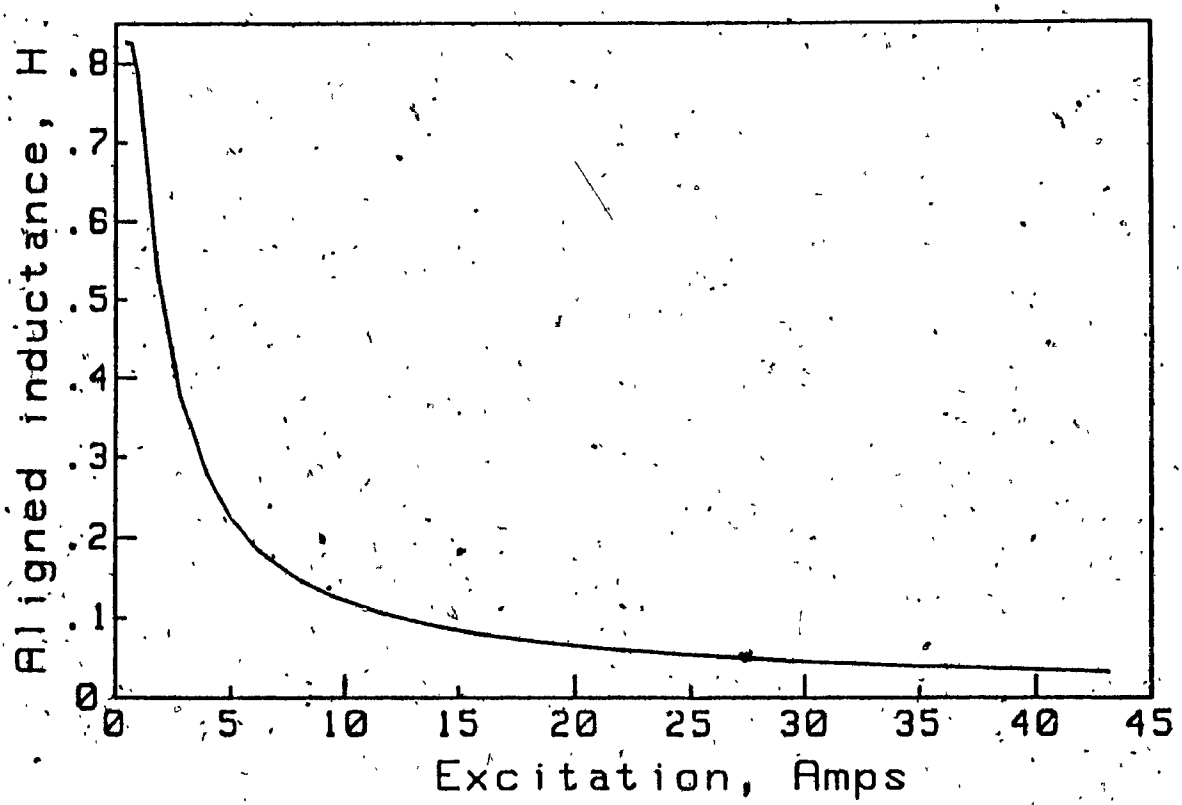

Fig. 5.4 Terminal inductance vs excitation

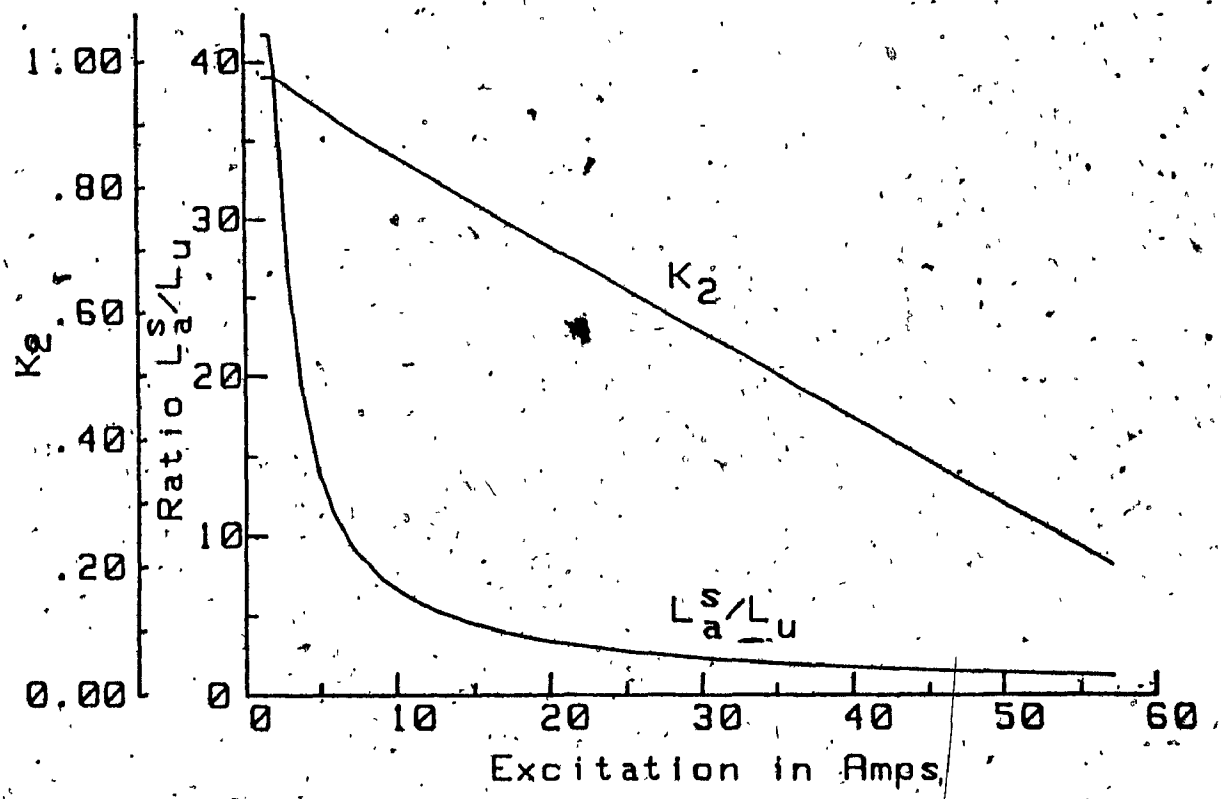

Fig. 5.5 k_2 and $\frac{L_a^s}{L_u}$ vs excitation

wide variation of k_2 affects the power developed per ampere input when all other machine variables are constant. This is shown in Fig. 5.6 relating the product of flux density and k_2 vs stator current. From the output equation, it can be realized that the power developed per ampere is proportional to the product of flux density and k_2.

TABLE 5.1

Motor Main Dimensions

Number of stator poles	= 6
Number of rotor poles	= 4
Stator outside diameter	= 19.4 cm
Rotor bore diameter	= 12.2 cm
Core length	= 5.09 cm
Airgap length	= 0.025 cm
Back iron width	= 1.25 cm
Number of turns per phase	= 536
Stator pole arc	= 0.418 rad.
Rotor pole arc	= 0.628 rad.

Based on a maximum current of 20 amperes and base speed of 1800 rpm the design calculation yields an output power of 2866 watts. This calculation is on the basis of 85 percent efficiency.

5.6 Operational Limit

An increase in the stator current results in enhanced mechanical power output of the SR motor. But, the enhancement of mechanical energy is not uniform for all operating points, particularly in the saturated region. At those

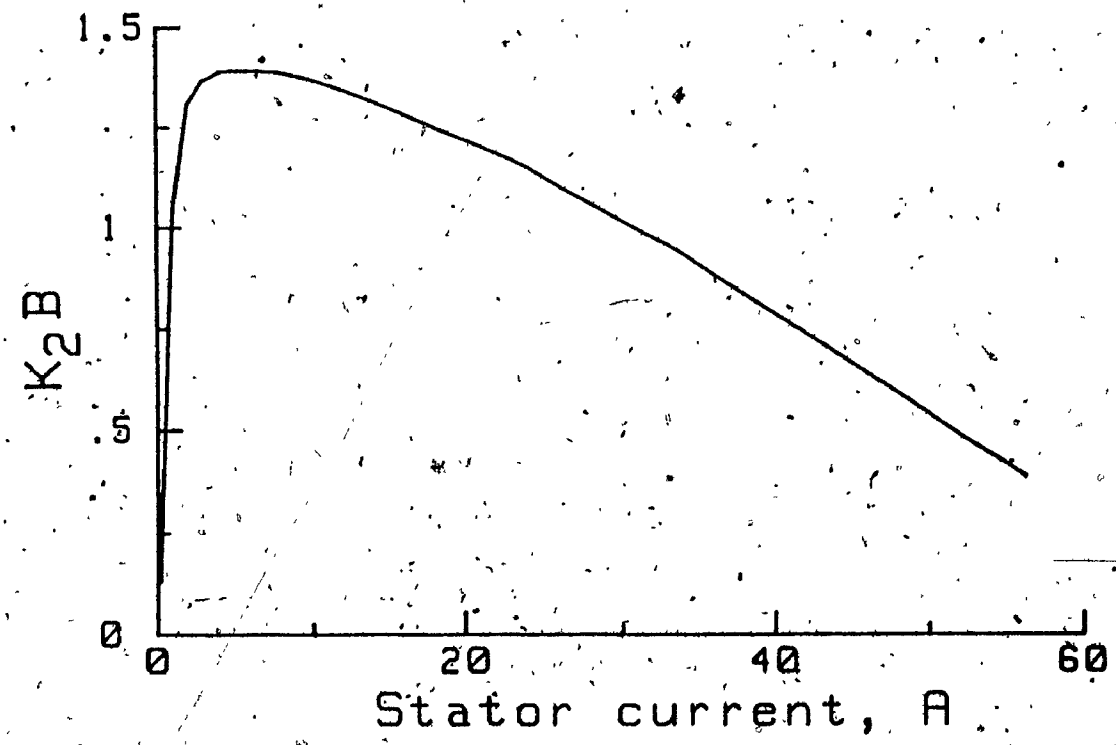

Fig. 5.6 k_2B vs excitation

operating points the return diminishes necessitating an operational limit on the maximum excitation current. The incremental mechanical energy per input current can be written as

$$g_{mi} = \frac{\Delta\omega_m}{\Delta i}$$
$$\doteq \lambda_o + i_{so}(L_s - L_u) + \frac{\Delta i}{2}(L_s - L_u) \qquad (5.34)$$

where λ_o is the intercept on the flux linkages axis from the saturated portion of the aligned flux linkages curve, shown in Fig. 5.2. The incremental values are calculated at the operating stator current i_{so}. Δi denotes the incremental stator current. $\Delta\omega_m$ is the resulting mechanical energy per stroke and the inductances are given as the slopes of the characteristic shown in Fig. 5.2.

It can be seen that $L_u > L_s$ in the present design example and hence the incremental gain g_{mi} decreases with decreasing stator current. It is shown, in Appendix I, that the maximum value of g_{mi} occurs when $L_s = L_u$ and is given by

$$g_{mi}(max) = \lambda_o \qquad (5.35)$$

5.7 Conclusion

A step by step design procedure has been developed for SR motors. An output equation is derived which is similar to that used for conventional ac machines. The influence of certain design parameters such as the number of poles, pole arc/pole pitch ratio, winding arrangement, airgap length, starting torque, losses, etc. on SR motor performance are discussed. In order to design a SR motor that can start from any rotor position and run on either direction the number of poles must be chosen such that there is sufficient overlap of static mean torques when the windings are energized in sequence. An increase in the number of poles will increase the switching frequency and hence the

core loss. The length of the airgap and the pole arc/pole pitch ratio must be such that the motor develops greater torque and also provides enough space to house the windings. A compromise has to be made between the mechanical, electromagnetic and thermal considerations. The selection of design parameters such as the ratio of length to bore diameter, airgap length, number of turns and the specific electric and magnetic loadings are also discussed.

To verify the design procedure developed the finite element analysis which provides a more accurate performance prediction, has been used. The flux linkages in the aligned and unaligned positions are determined from which the constant k_2 is computed. The range of variation of k_2 plotted in Fig. 5.5 can be used as a guideline to choose k_2. The sensitivity of the unaligned inductance on the output equation has shown that a certain amount of error in its prediction can be tolerated for preliminary designs.

Increasing excitation beyond saturation may result in increased developed torque. But there is an optimum operating limit of excitation beyond which the mechanical output decreases with increasing excitation causing increased losses. This limit occurs when the incremental aligned inductance is equal to the value of the unaligned inductance.

CHAPTER 6

COMPARISON OF 2D AND 3D FINITE ELEMENT ANALYSIS OF A SR MOTOR

6.1 Introduction

A two dimensional (2D) finite element analysis approximates a three dimensional (3D) device by assuming that the device has a constant cross section and infinite depth. Consequently, it has been assumed that two dimensional analysis yields good results for motors with constant cross sections and in which end effects do not significantly affect the performance. The doubly salient SR motors, on the other hand, may have significant end effects particularly when the stator and rotor poles are not fully aligned. Hence, a three dimensional finite element modeling may be necessary for a better performance prediction during the design stage.

The finite element analysis using a 3D software packages is significantly more expensive than the 2D finite element analysis packages. Moreover, a 3D analysis requires more computational effort and time. In order to determine whether a 3D analysis yields a better result than a 2D analysis when the SR motor is analyzed, the study presented in this chapter is undertaken. The 12/10 motor, already described in Chapter 3, is analyzed using 2D and 3D finite element analyses.

Owing to the higher computational cost and effort, a global parameter such as the inductance and a local parameter such as the flux density are evaluated using 3D finite element analysis and compared with the results of the 2D analysis. The study shows significant end effects when the rotor is in the unaligned position.

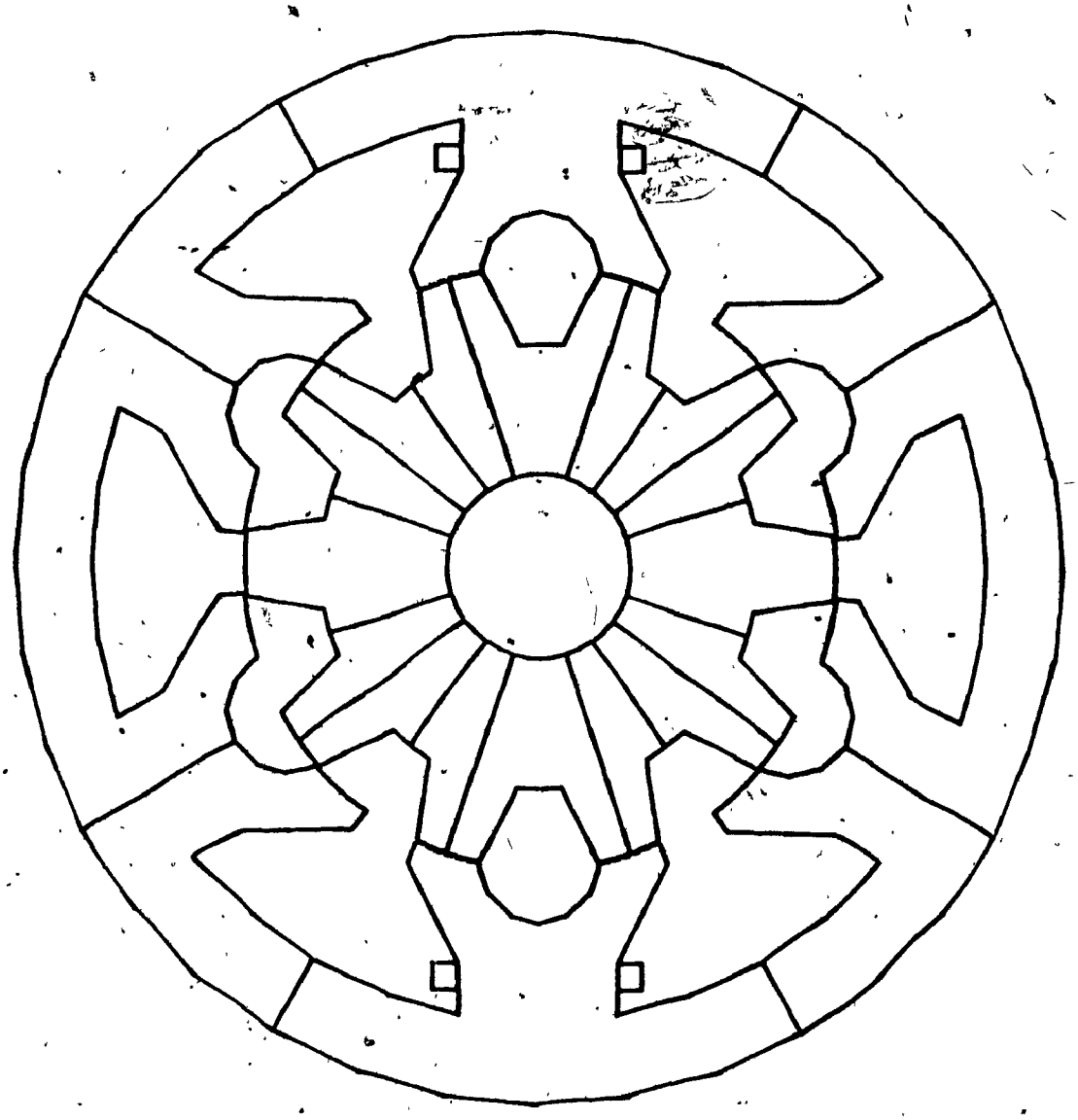

Fig. 6.1 Motor configuration used for 2D analysis

Aligned position

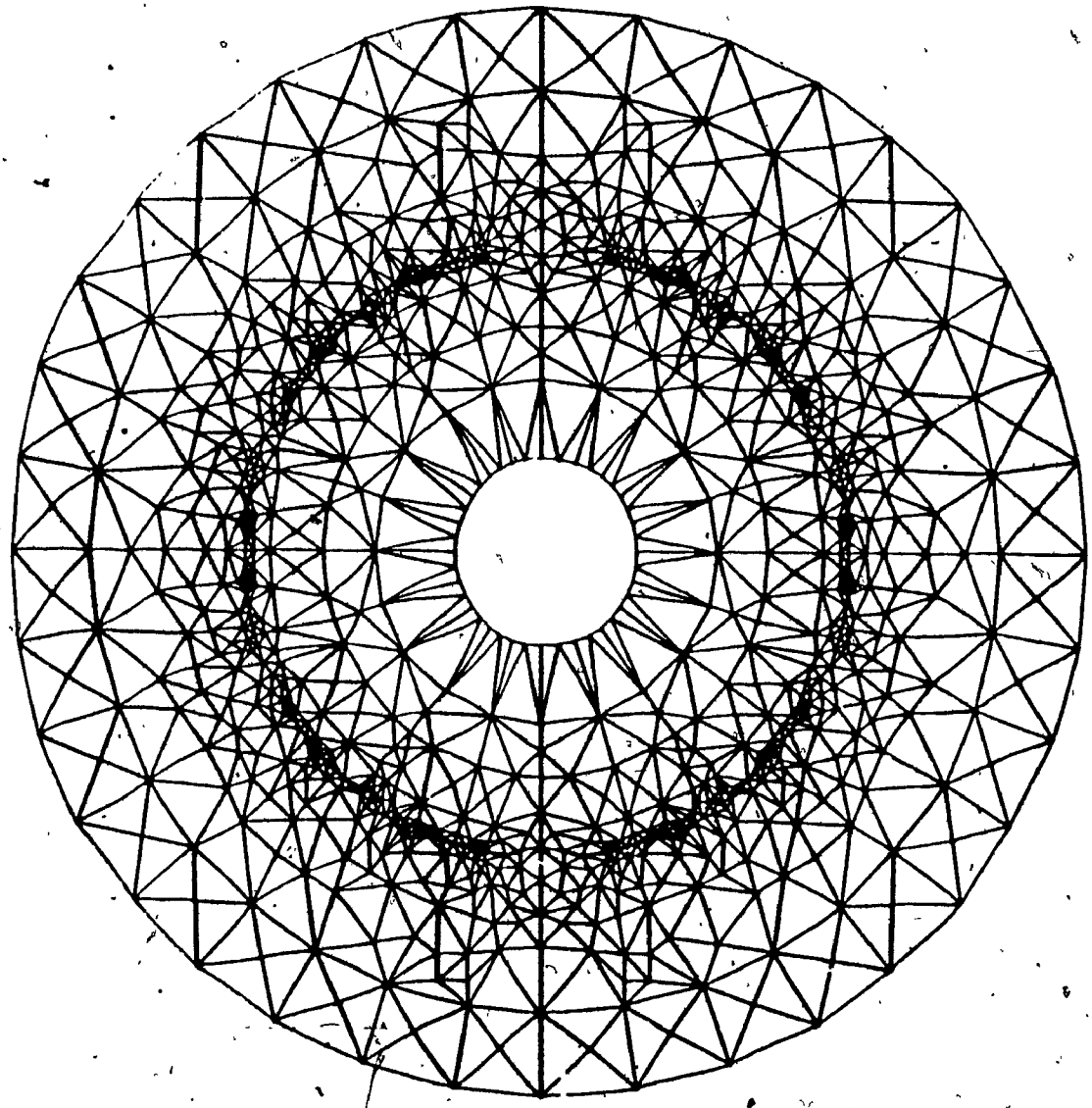

Fig. 6.2 2D Finite element mesh for aligned position

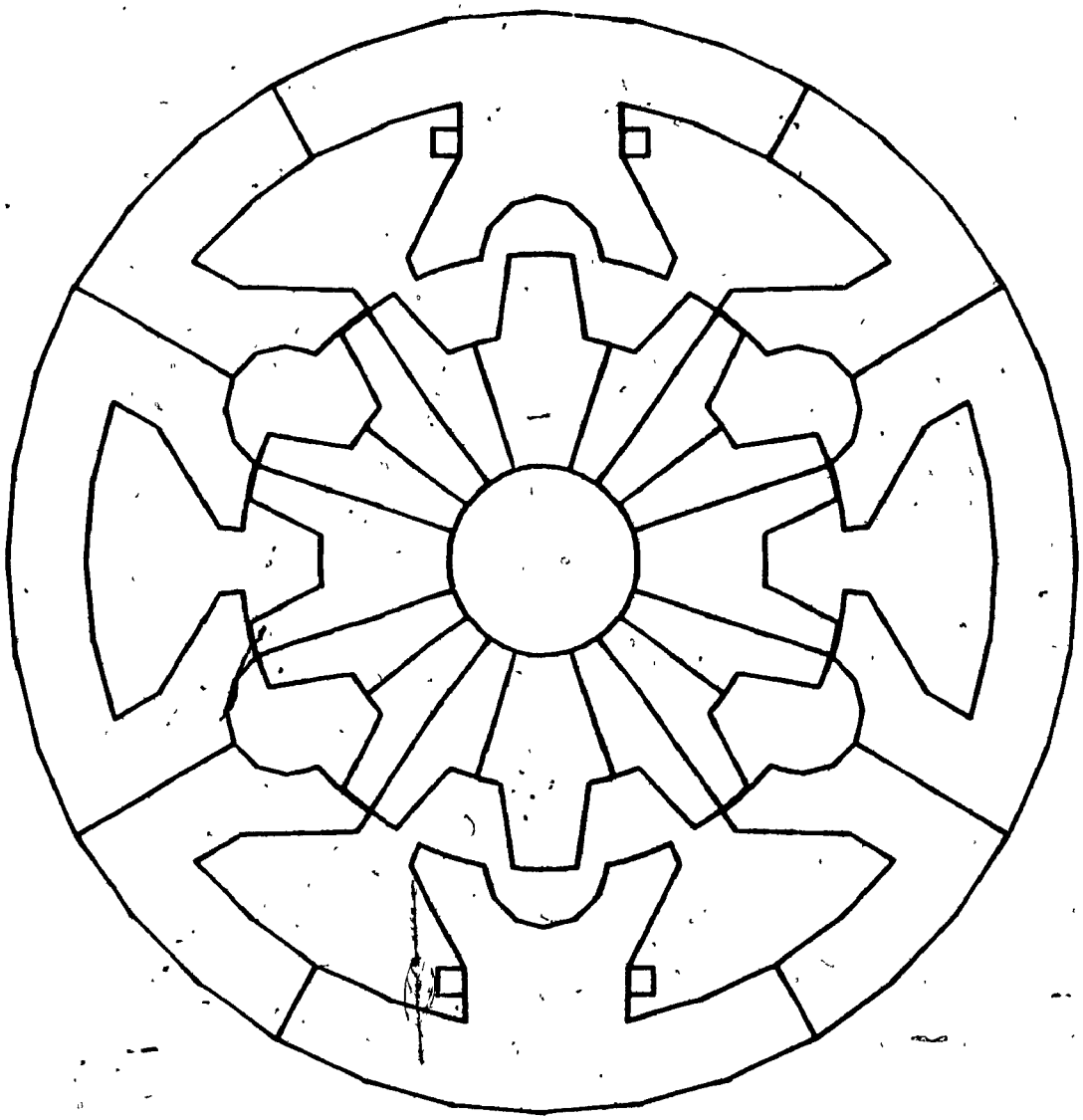

Fig. 6.3 Motor confoguration used for 2D analysis

Unaligned position

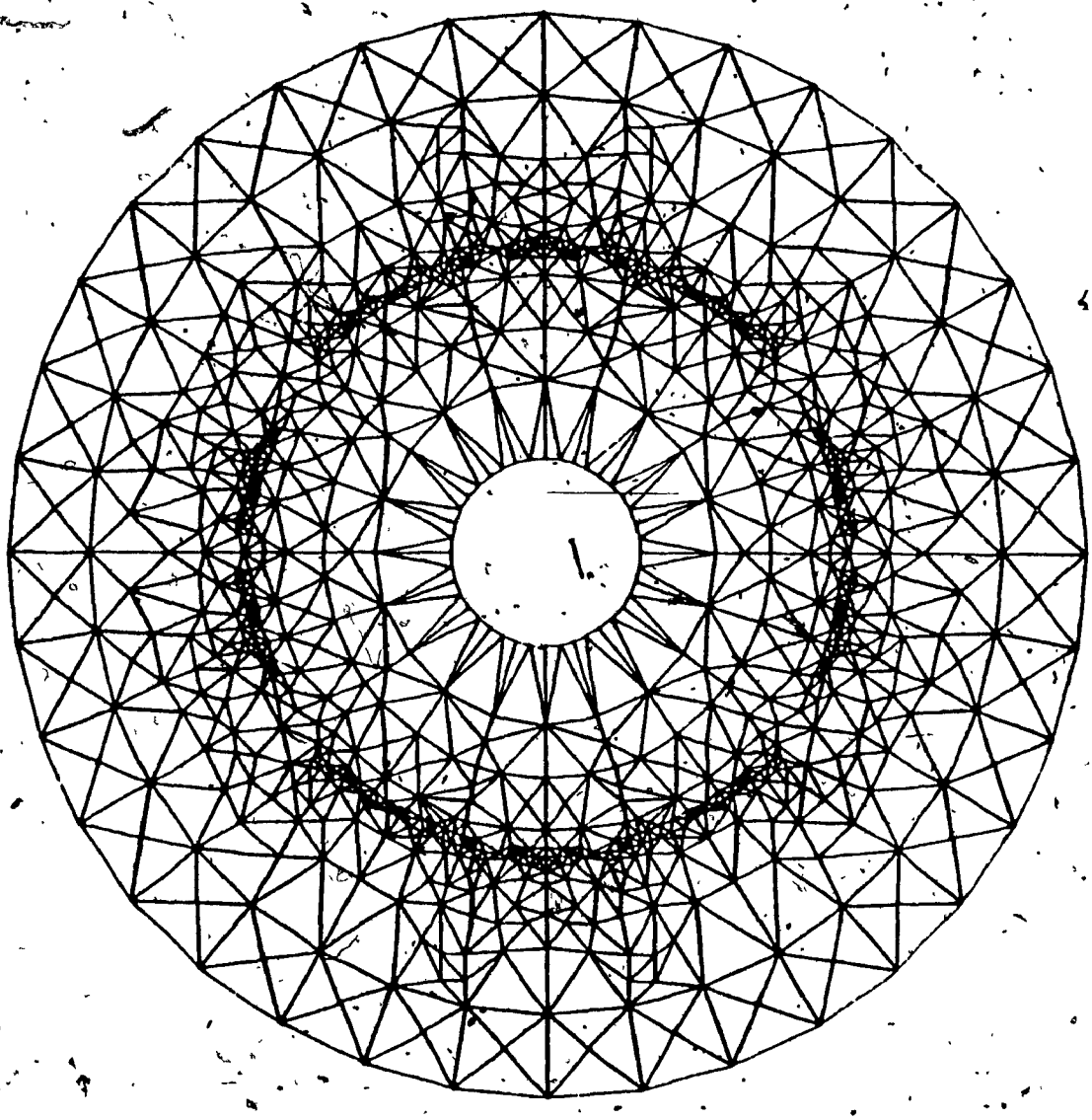

Fig. 6.4 2D Finite element mesh for unaligned position

6.2 Problem Specification

For the purpose of comparison, both 2D and 3D models were set up at two rotor positions, one with the rotor fully aligned and the other with the rotor pole completely unaligned. The motor model used in the 2D and 3D analyses are shown in Fig. 6.1 for the aligned position and in Fig. 6.3 for the unaligned position. Solutions were obtained at one current level of 8 amperes that caused saturation for the aligned case but not for the unaligned case. It is to be noted that the 2D analysis presented in earlier Chapters was performed for five rotor positions and ten excitation currents for a complete analysis.

6.2.1 Two Dimensional Model

For the 2D analysis, two relatively coarse finite element meshes of approximately 950 meshes and 1800 elements were defined for the aligned and unaligned positions. The finite element meshes are shown in Fig. 6.2 for the aligned position and in Fig. 6.4 for the unaligned position. Although only one quarter of the motor geometry is sufficient to be modeled due to the magnetic and geometric symmetries, the full cross section was modeled so as to have exactly the same model for both the 2D and 3D analyses.

6.2.2 Three Dimensional Model

To define the 3D finite element meshes, the 2D meshes were imported into MagNet 3D's mesh generator and extruded along the motor axis to generate a 3D mesh. Fig. 6.6 shows a view of the resulting model and Fig. 6.5 shows where the planes were defined along the z-axis during modeling process. The resulting 3D finite element meshes are about 6600 meshes and 10850 elements. In order to evaluate the leakage flux at the end of the motor, a 5.4cm air was modeled past the end of the motor (Fig. 6.5). The windings were not shown

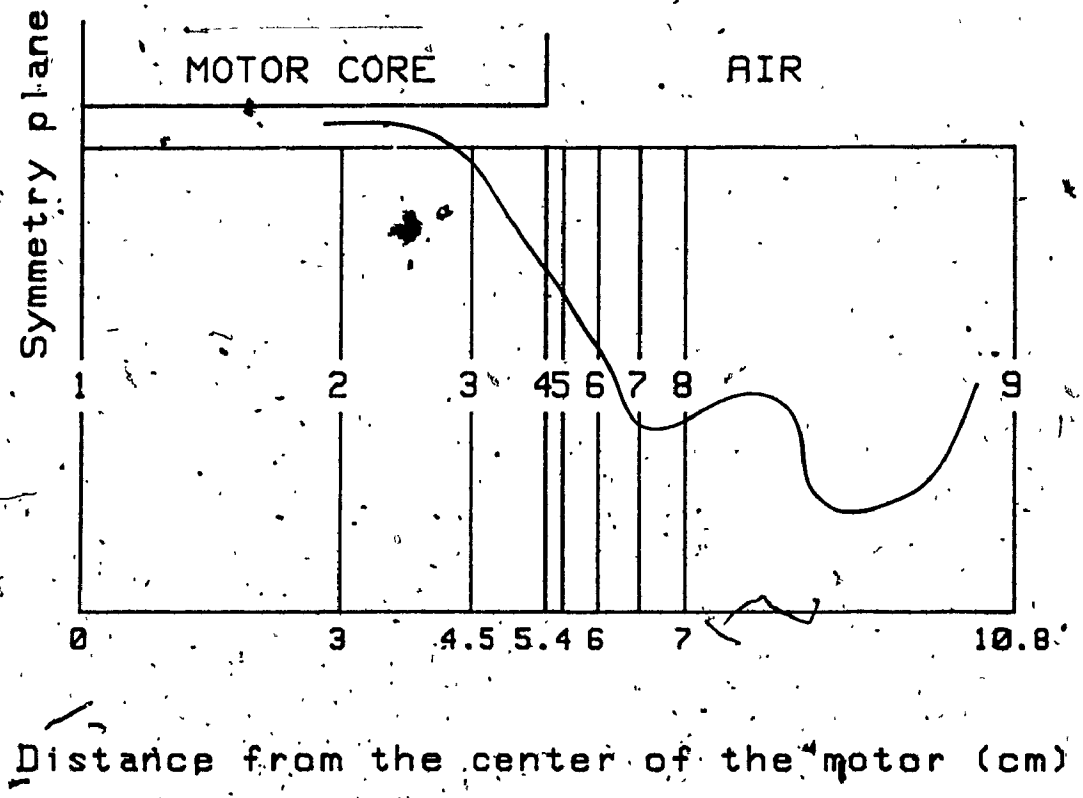

Fig. 6.5 Side view of the motor model used for 3D analysis

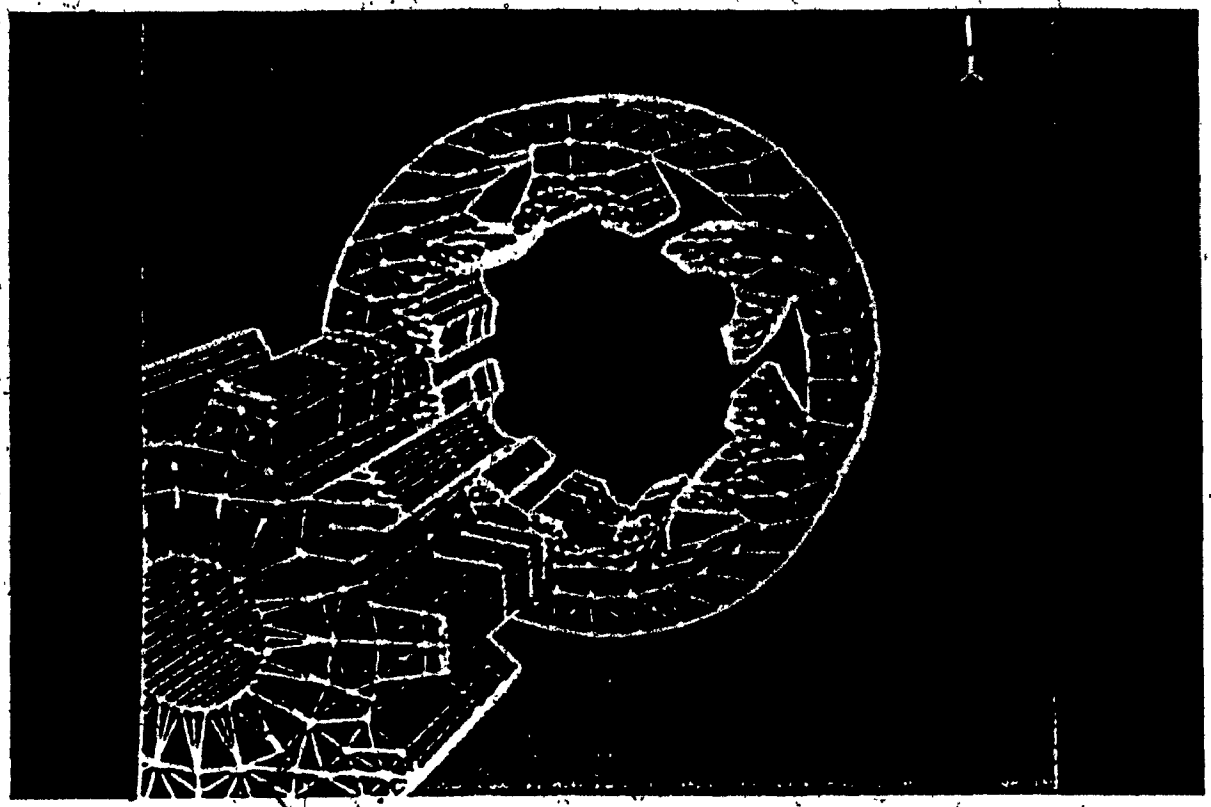

Fig. 6.6 3D finite element model for unaligned position

since they were defined during problem specification process. The B-H curve used for the analysis is shown in Fig. 6.8.

6.3 Results

As noted above, only two parameters have been calculated to provide the comparison, namely inductance and flux density. These may clearly illustrate the differences in the results obtained using a 2D and 3D finite element analysis of the SR motor, with any other parameters of interest having comparable differences.

6.3.1 Inductance

For the purpose of analysis, the inductance has been defined as the flux linkages per unit current excitation. The total flux passing through the line shown in Fig. 6.7 in the airgap underneath the excited stator pole has been used in the calculations. Due to periodicity, only the flux coming into the pole has been calculated since both the excited coils see the same flux. The inductances calculated are given in Table. 6.1.

For the aligned position, the results of 2D and 3D analyses are more or less the same. The difference in the inductance value is about 3 percent. When the 3D result is broken up into contributions from each block (i.e planes 1-2, planes 2-3,etc.) the ends of the motor contribute relatively less than the inner segments. If we observe the inductance per unit axial length of the motor, the contributions between the planes 1 and 3 are almost constant. The contribution in the last 0.9cm axial length segment of the core is slightly less. This may be due to the flux leaking beyond the edges of the motor. The inductance contributions from the end region is calculated by adding the inductance contributions of the segments considered in the air beyond the end of the

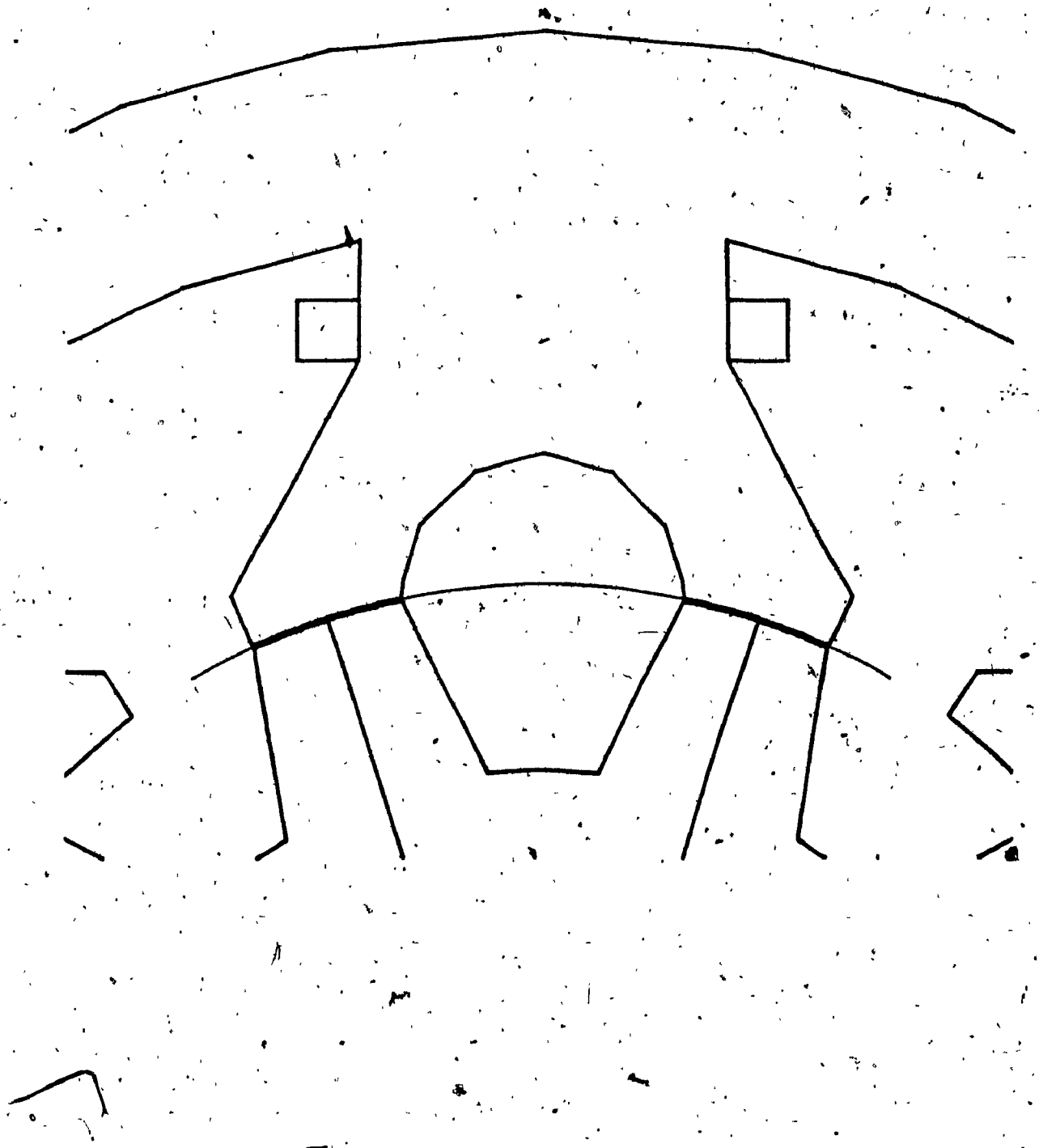

Fig. 6.7 Contour used for flux calculation

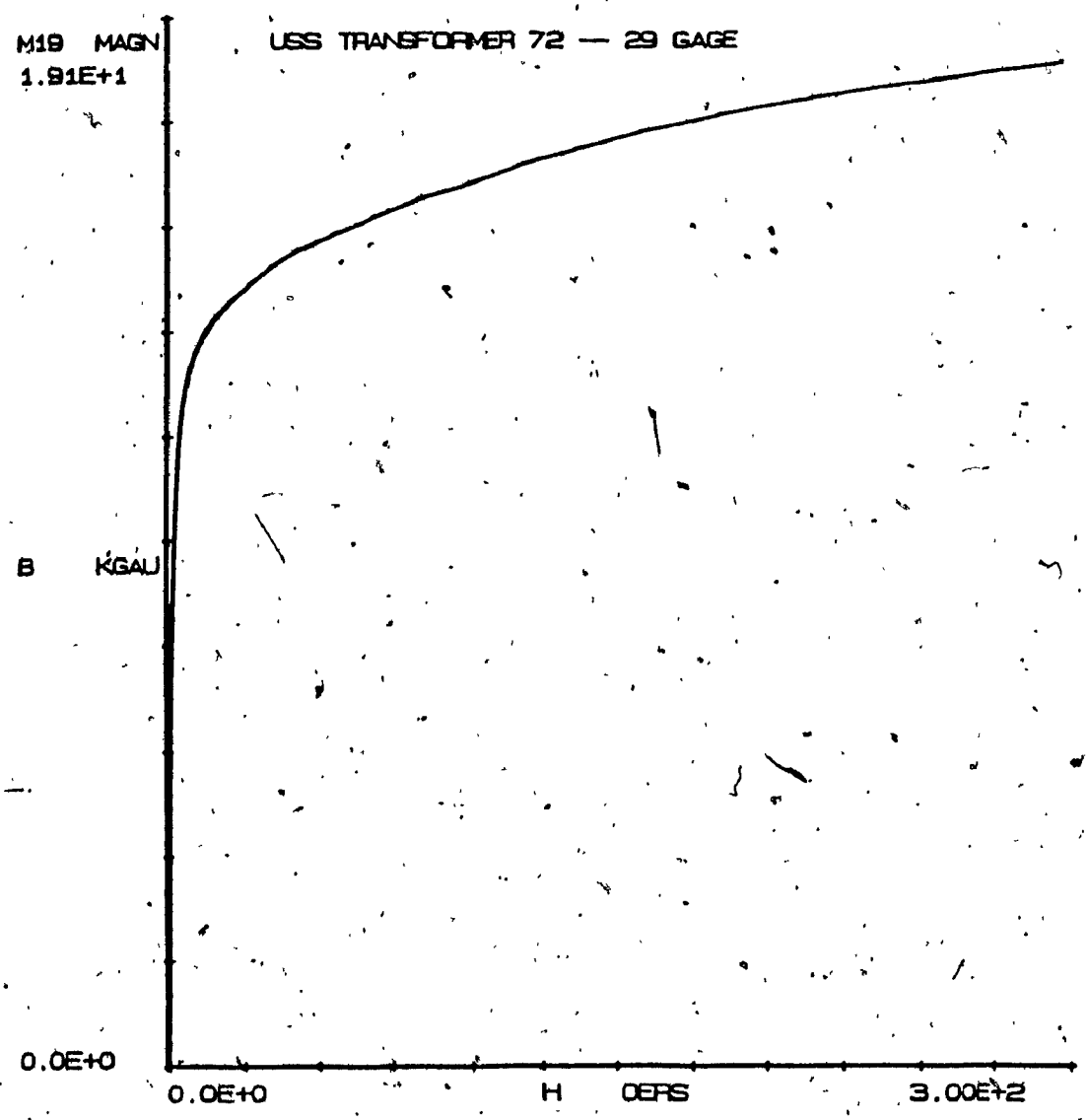

Fig. 6.8 B-H Curve used for 2D and 3D analysis

motor (i.e., planes 4-5, planes 5-6, planes 6-7 and plane 7-8). It is seen that the end region contribution is about 7.4 percent of the total aligned inductance.

TABLE 6.1

Inductance Values

	Aligned mH	Unaligned mH
2D	232.7	117.3
3D	226.0	80.4
3D Contributions		
Planes 1-2	118.9	44.1
Planes 2-3	59.3	19.9
Planes 3-4	31.0	10.3
Planes 4-5	6.1	2.2
Planes 5-6	7.4	2.8
Planes 6-7	2.2	0.8
Planes 7-8	1.1	0.3

For the unaligned inductance values, there is about 32 percent difference between the results of the 2D and 3D analyses, when the end region contribution is taken into account. When we consider the contributions due to each segment along the axial direction, the inductance per unit length decreases when the plane segments are away from the center of the motor. The rate of decrease is more than that in the aligned case. It is observed that the end region contributes about 7.6 percent of the total unaligned inductance even when the motor is unsaturated. It suggests that there may be considerable end effects in SR motors when operated under saturated condition.

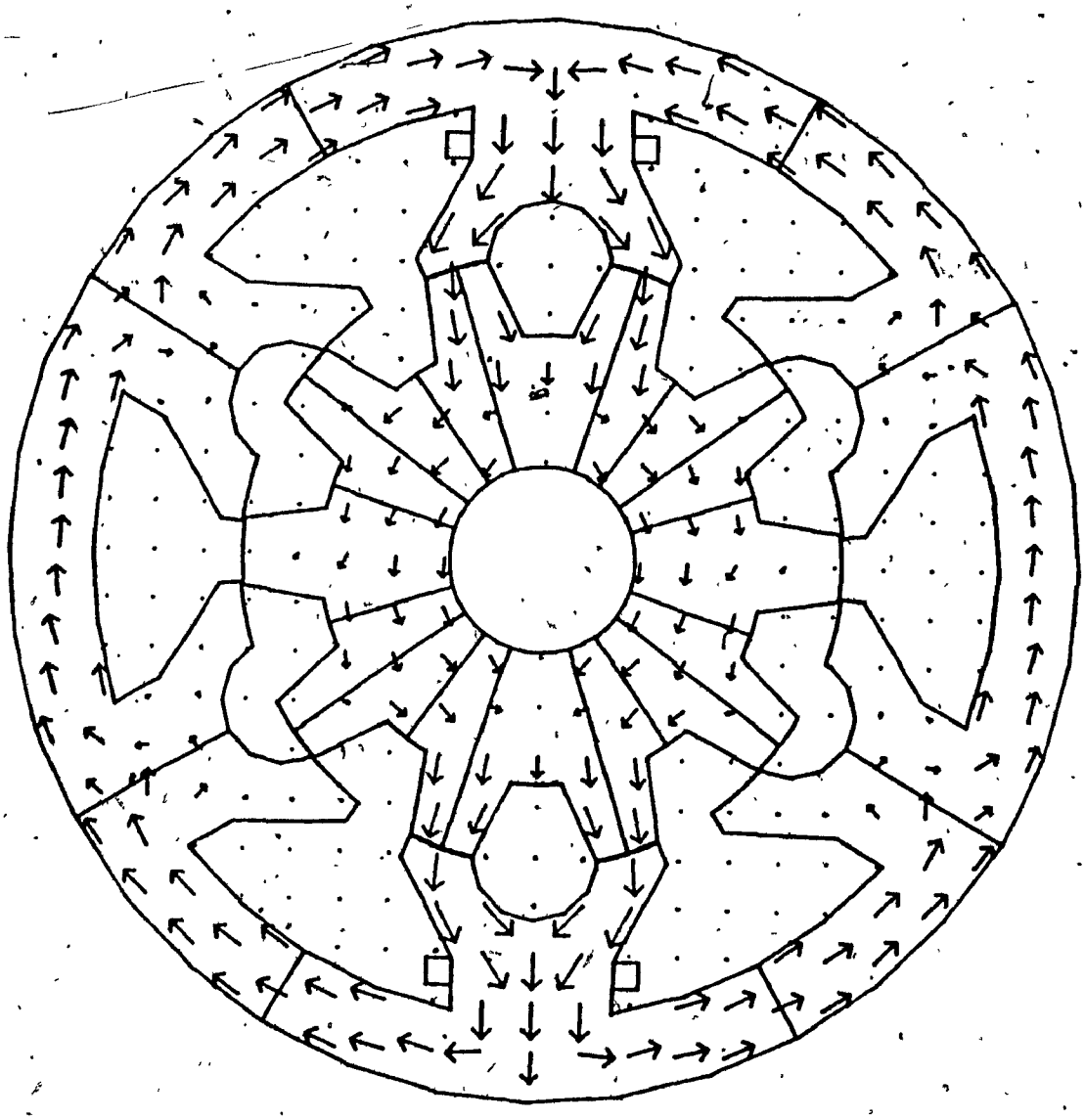

Fig. 6.9 Flux density plot for 2D solution

Aligned position

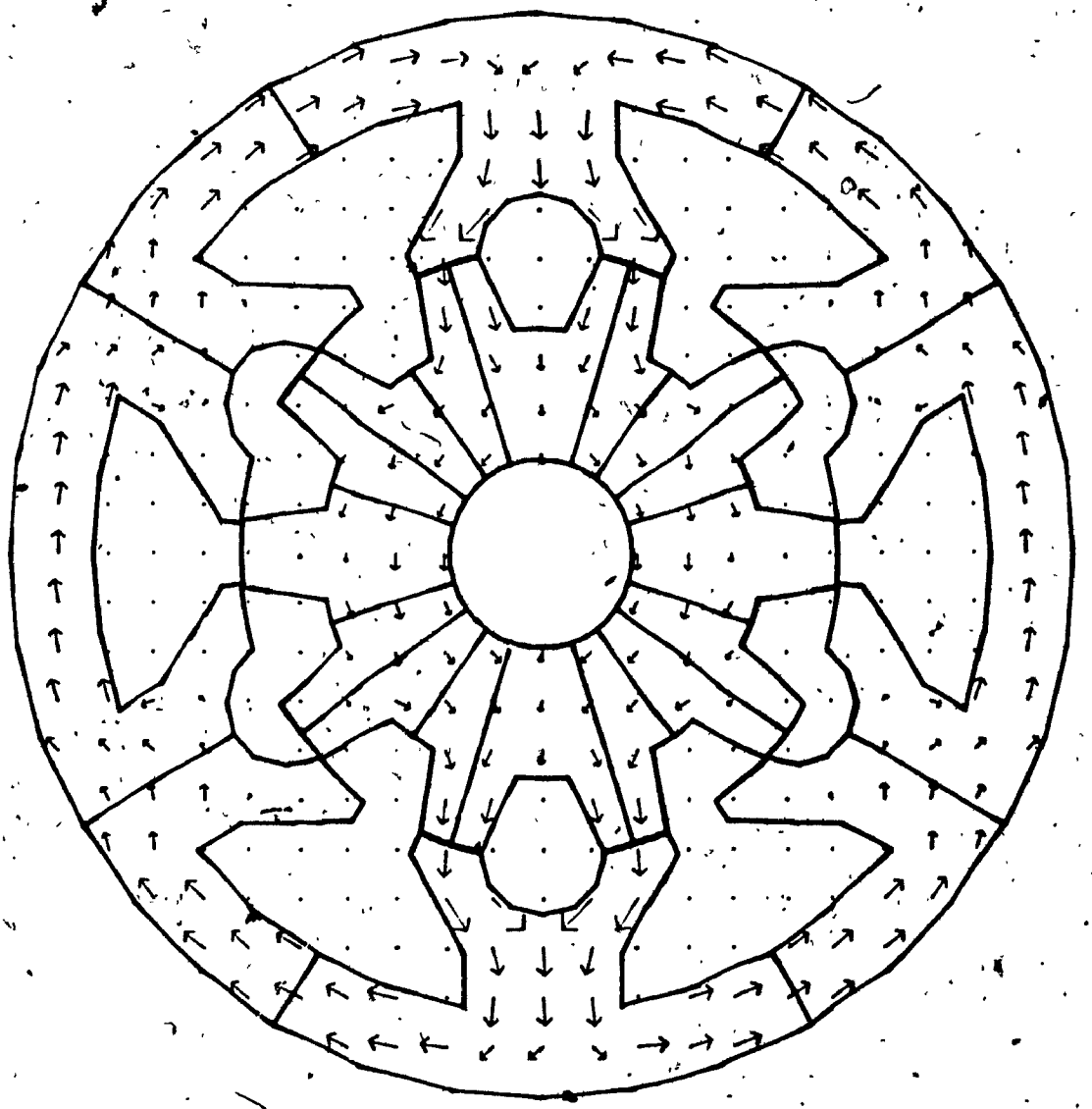

Fig. 6.10 Flux density plot for 3D solution

Plane at z=0 cm, aligned position

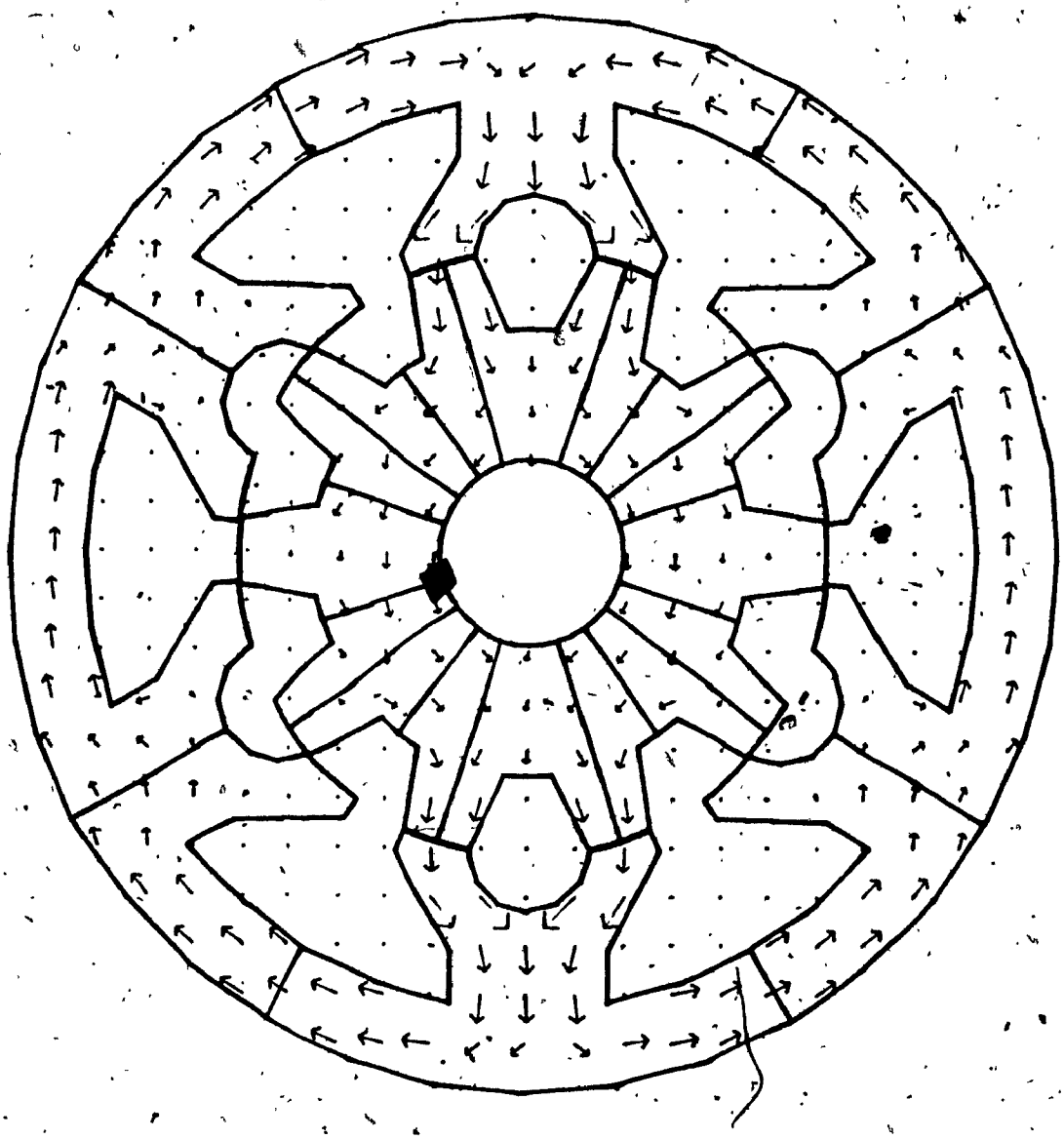

Fig. 6.11 Flux density plot for 3D-solution

Plane at z=4.5 cm, aligned position

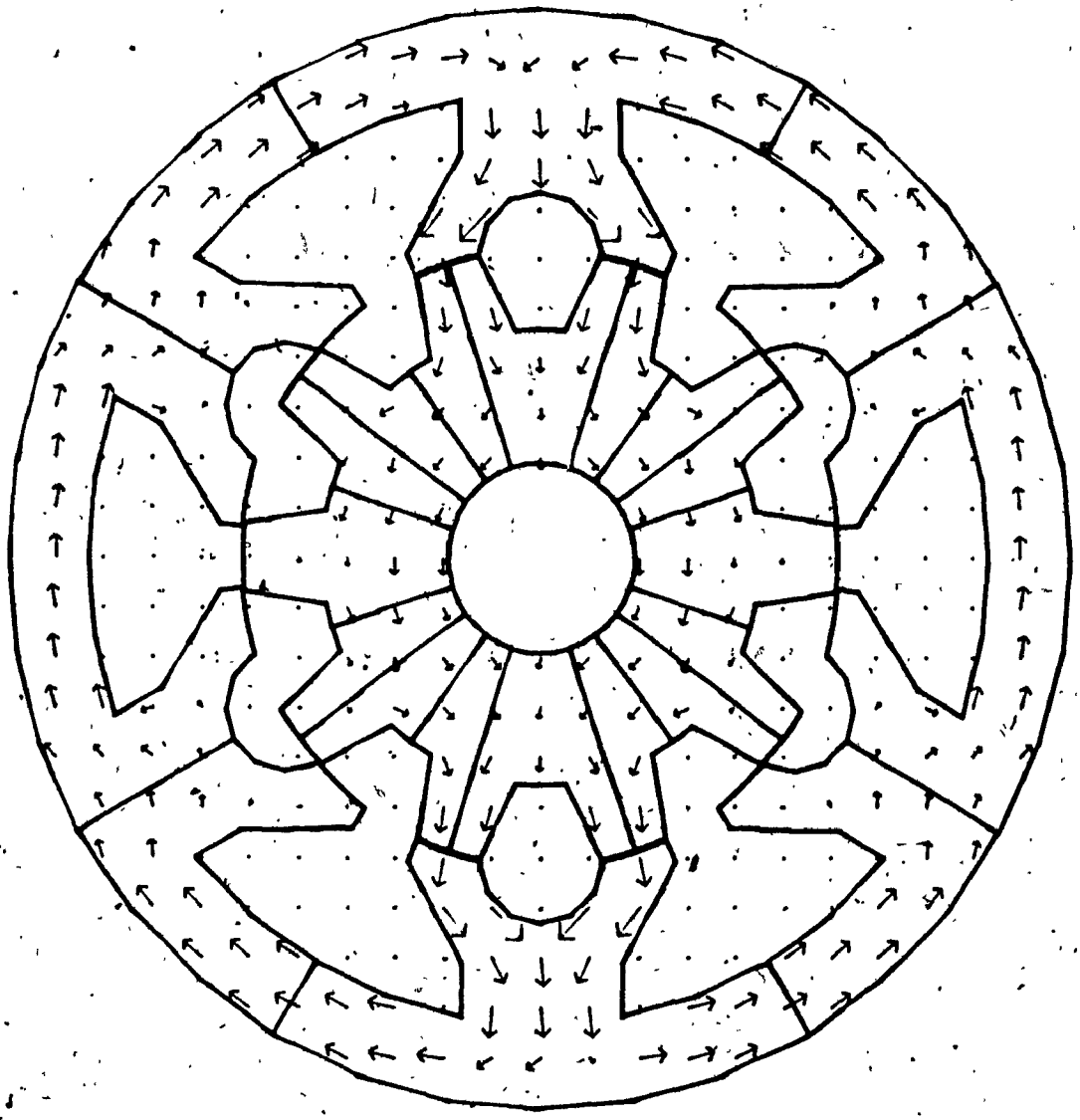

Fig. 6.12 Flux density plot for 3D solution

Plane at z=5.4 cm, aligned position

6.3.2 Flux Density

To compare the flux densities predicted by the 2D and 3D analysis an arrow plot showing magnitude and direction for the x and y components of flux density are plotted. The 2D case should give approximately the same result as the center plane (plane 1 in Fig. 6.5) value for the 3D analysis.

For the aligned position the flux density plot obtained using the 2D analysis is shown in Fig. 6.9. The flux density plots obtained by the 3D analysis at the planes 1,2 and 3 are shown in Figs. 6.10-6.12, respectively. As in the case of the aligned inductance value, the flux density plots in the aligned position show very good agreement between the values predicted by the 2D analysis and those obtained by the 3D analysis. The plots look essentially the same, allowing for numerical and sampling errors.

The flux density plots obtained using the 2D analysis for the unaligned position is shown in Fig. 6.13. The three dimensional flux density plots at the planes 1,2 and 3 are shown in Fig. 6.14-6.16, respectively. The unaligned position results, in contrast, show significant differences between flux densities obtained by 2D analysis and those by 3D analysis. Even allowing for numerical and sampling errors, the flux density plots shown in Figs. 6.14 - 6.16 show a significant drop compared to those shown in Fig. 6.13.

The variation of flux underneath an excited stator pole in the axial direction of the motor, is shown in Fig. 6.17 for the aligned position. The flux variation for the unaligned position is shown in Fig. 6.18. In both the cases, it is seen that the flux magnitude at the outer edge of the stator pole is small compared with that at the center of the motor. Also, there is a slight increase in flux nearer to the edge of the pole. The magnitude variation for the unaligned position is greater than the variation in the aligned position.

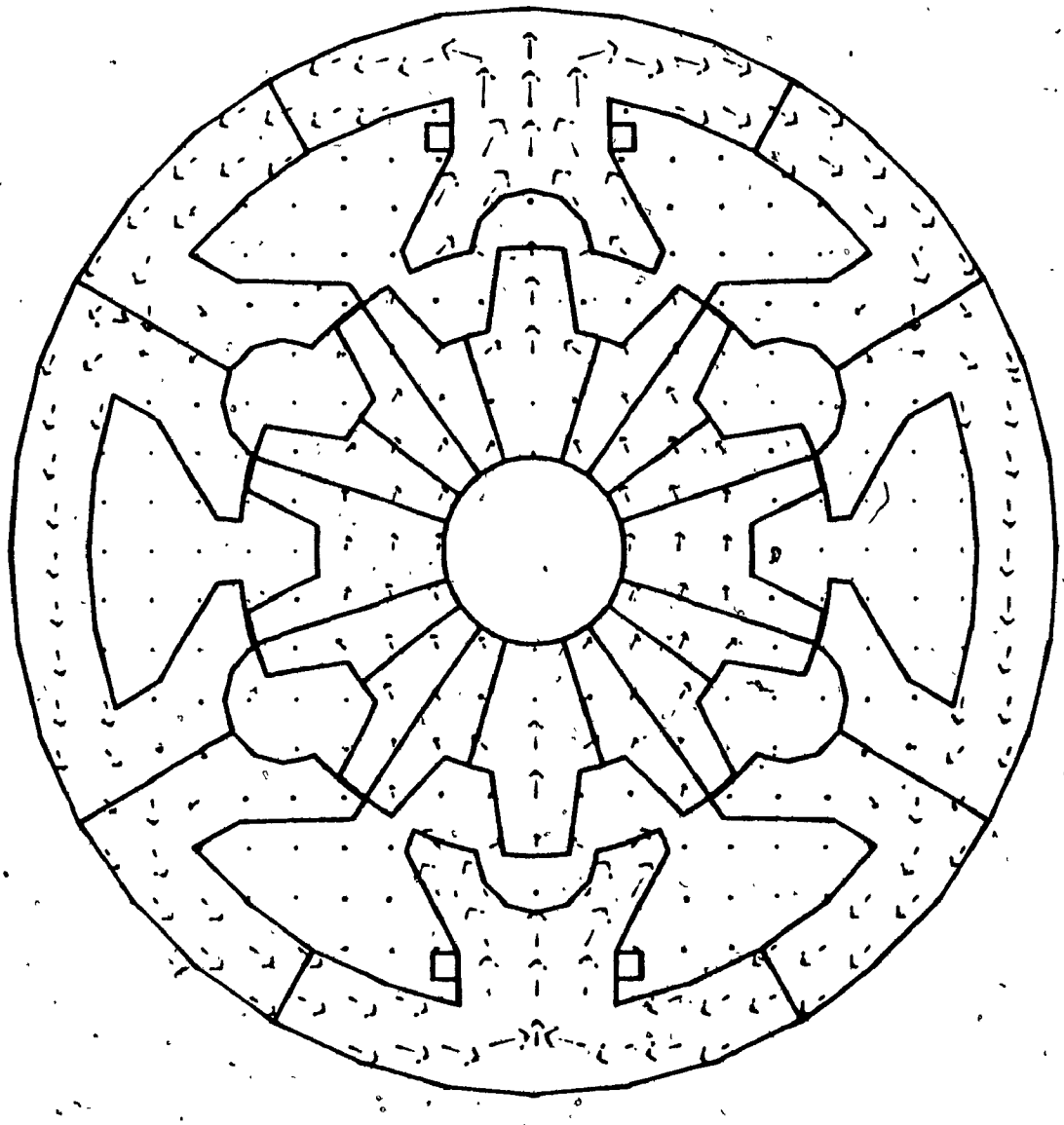

Fig. 6.13 Flux density plot for 2D solution

Unaligned position

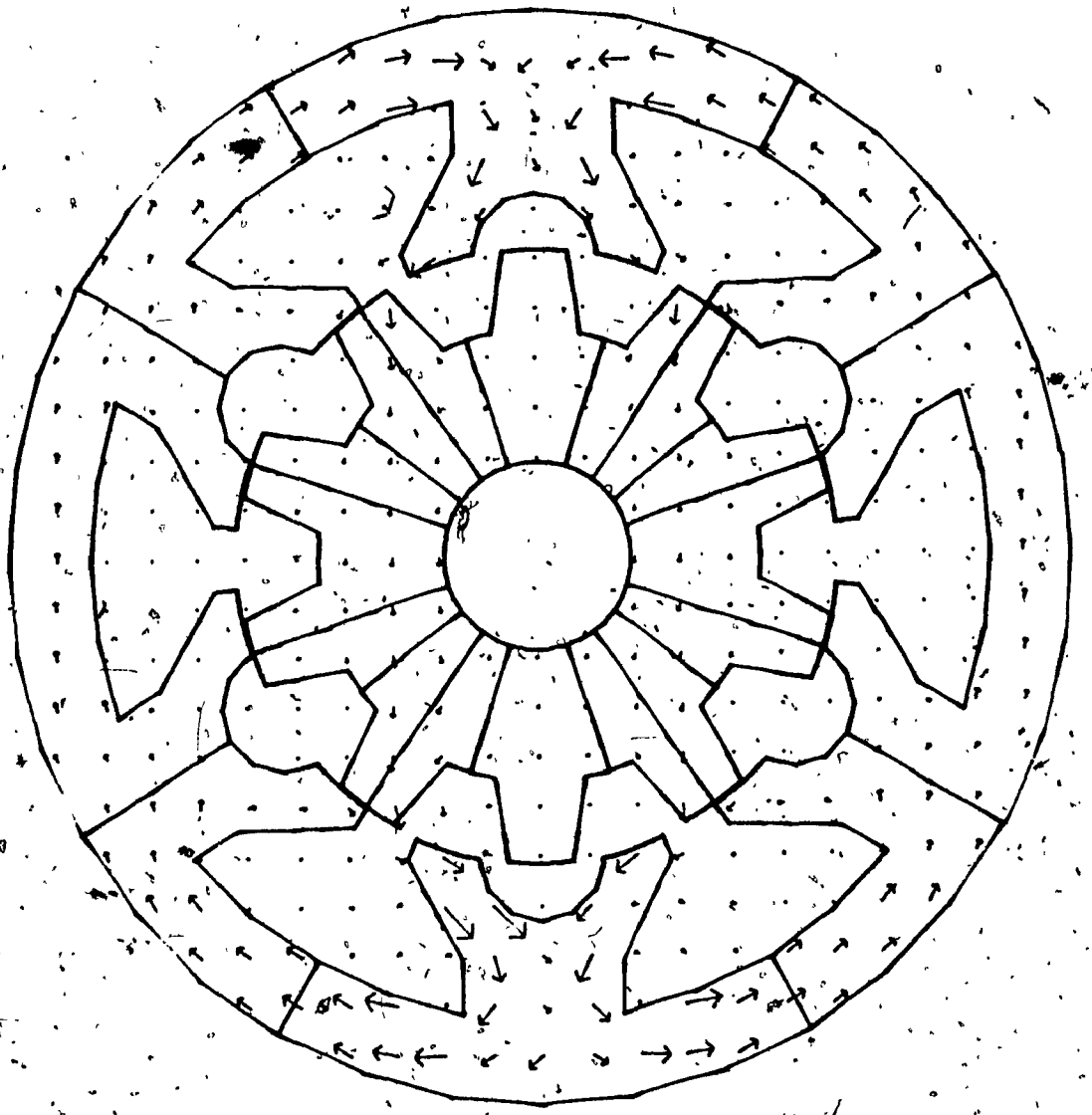

Fig. 6.14 Flux density plot for 3D solution

Plane at z=0, unaligned position

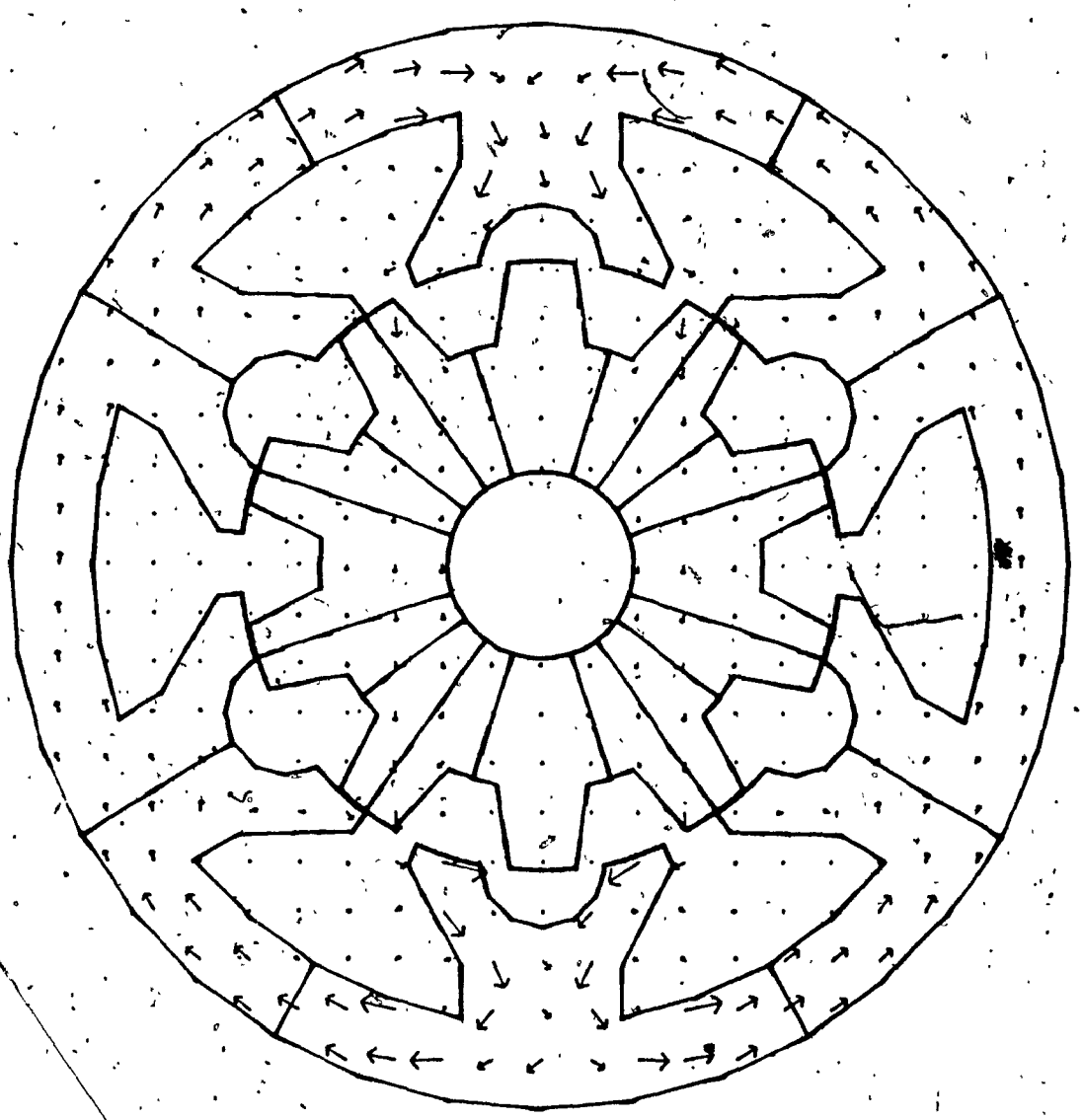

Fig. 6.15 Flux density plot for 3D solution

Plane at z=4.5 cm, unaligned position

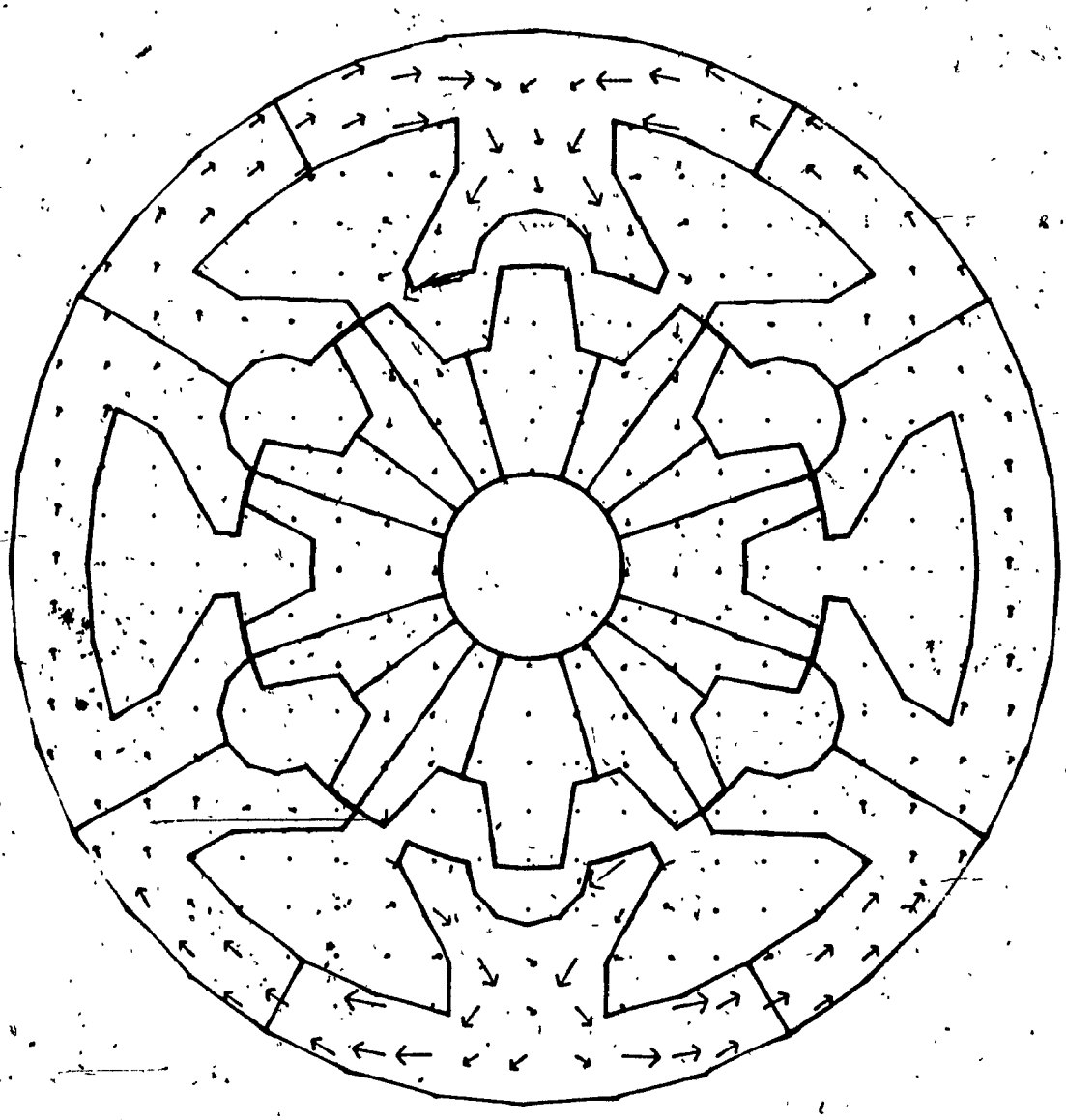

Fig. 6.16 Flux density plot for 3D soultion

Plane at z=5.4 cm, unaligned position

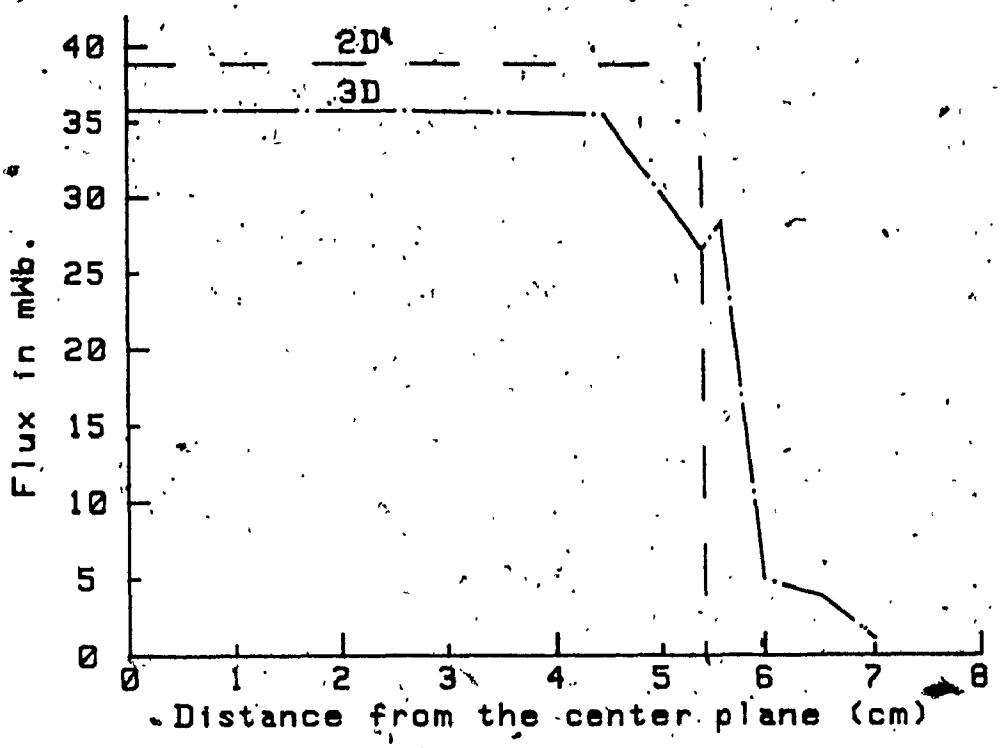

Fig. 6.17 Flux under a stator pole in the axial direction

Aligned position

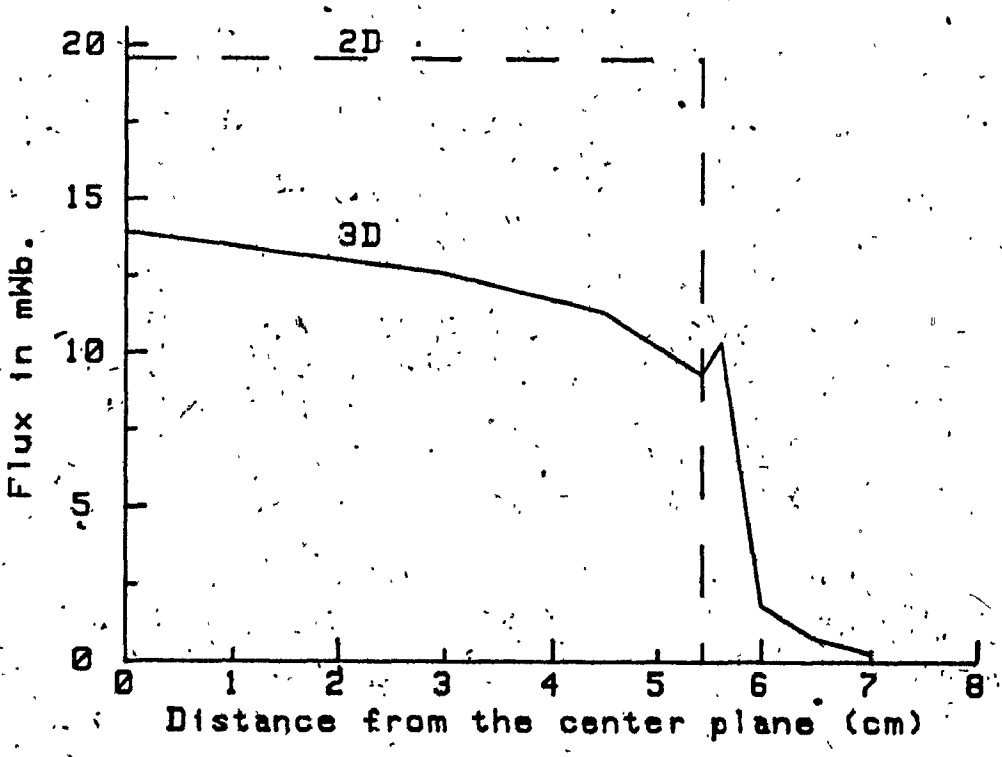

Fig. 6.18 Flux under a stator pole in the axial direction

Unaligned position

In order to obtain an experimental verification of these trends, measurements of flux density were made for a SR motor having single tooth per stator pole. These were taken underneath an excited stator pole along the axial length. They show that the general trend of the flux density variation along the axial length is the same, but the magnitudes of variation are not the same as that obtained using 3D analysis. This may be due to the following reasons:

(a) The 3D analysis was performed for a SR motor with two teeth per stator pole.

(b) The axial length of the motor used in 3D analysis was much less than that of the motor on which the flux density measurements were made.

In 3D analysis, it has been pointed out by Simkin and Trowbridge [73] that the measured and computed magnitudes of flux and inductance may disagree due to longer airgaps and coarser problem discretization. Hence, a refined mesh in the region of airgap and pole edges of the motor had to be used to achieve an accurate solution.

6.3.3 End Effects

In order to determine the end effects, planar slices are taken along the axis of the motor so as to plot the flux densities in the end region. For the aligned position, Fig. 6.19 shows the location of the slice at 75 degrees through the airgap between the rotor tip and the stator pole face in the motor model. Fig. 6.20 shows the slice cut across the motor geometry consisting of the motor core and the end air region. The flux density plot in the air region beyond the end of the motor core is shown in Fig. 6.21. In order to have a close look at the plot, a zoomed view of the motor core end region is shown in Fig. 6.22. It is evident that there is a small amount of flux indicating some but not overly significant end effects in the aligned position.

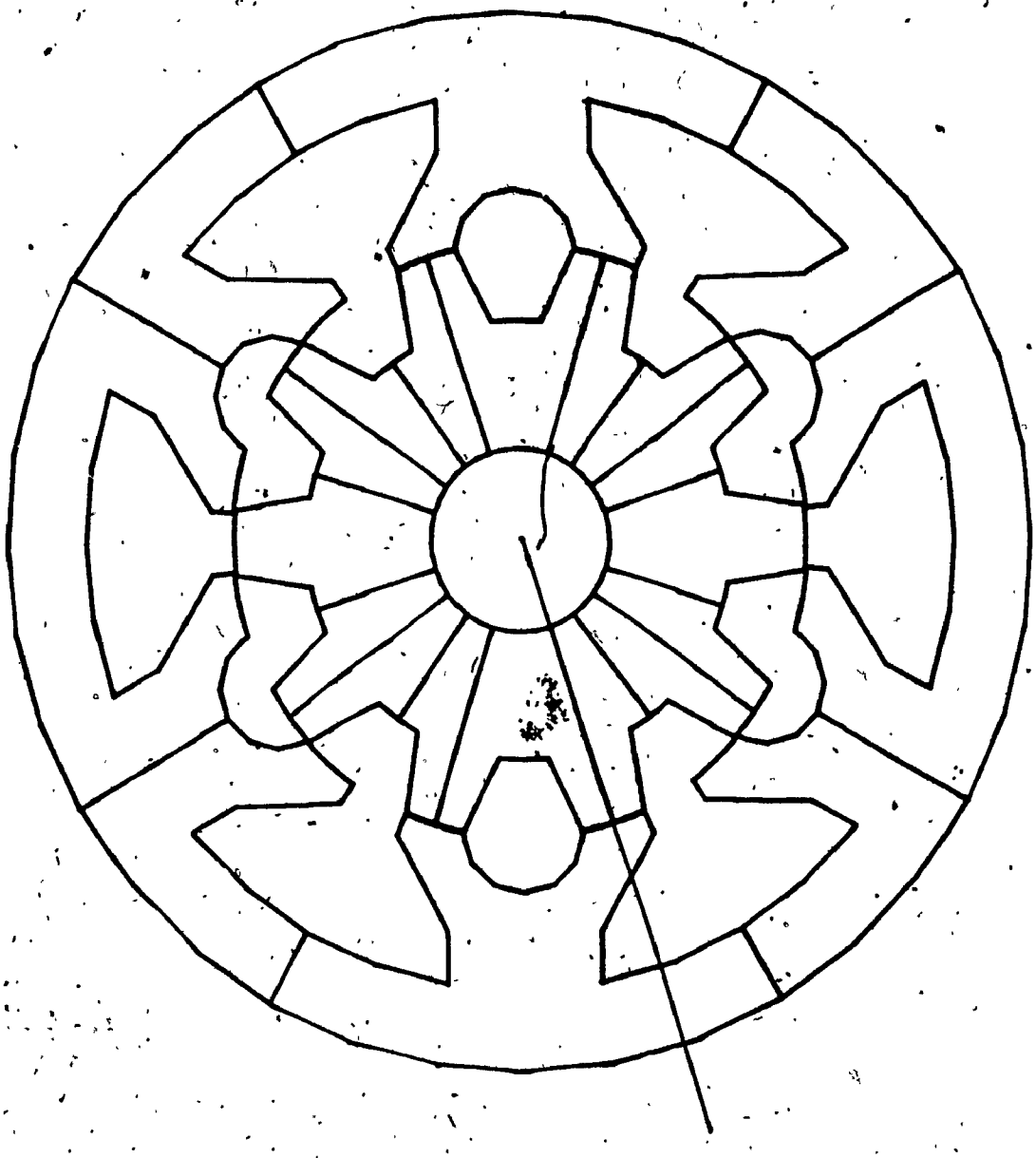

Fig. 6.19 Line showing longitudinal slice at 75 degrees

Aligned position

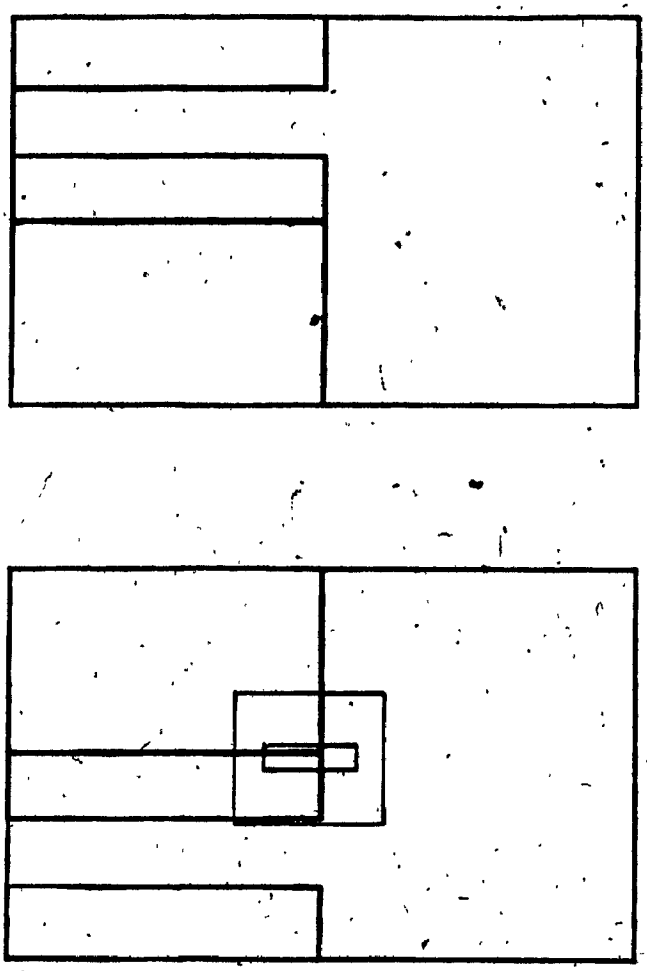

Fig. 6.20 Outline of longitudinal slice, showing zoom area
Aligned position

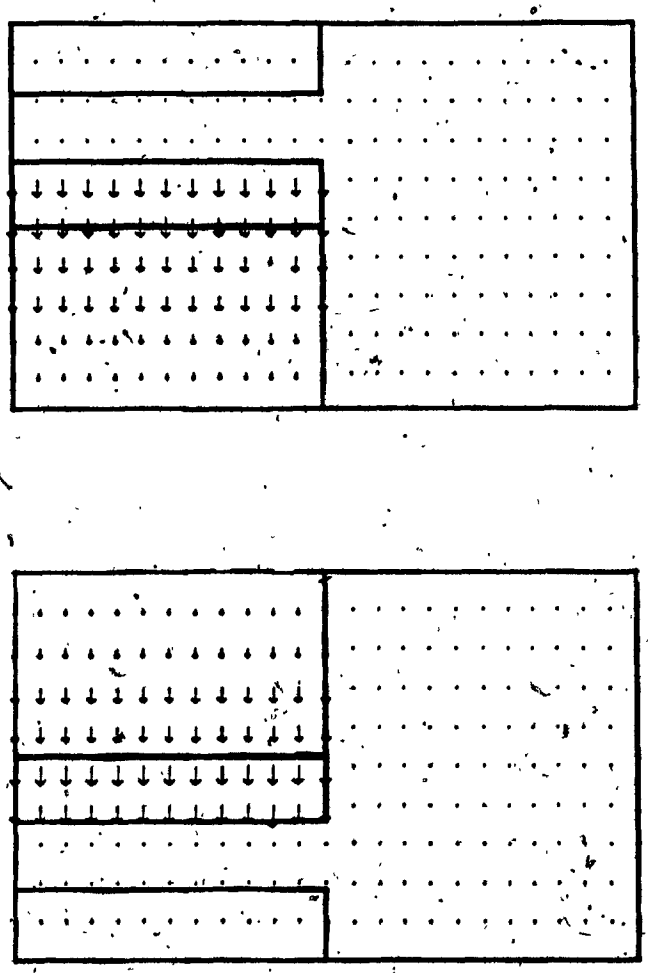

Fig. 6.21 Flux density plot along longitudinal slice

Aligned position

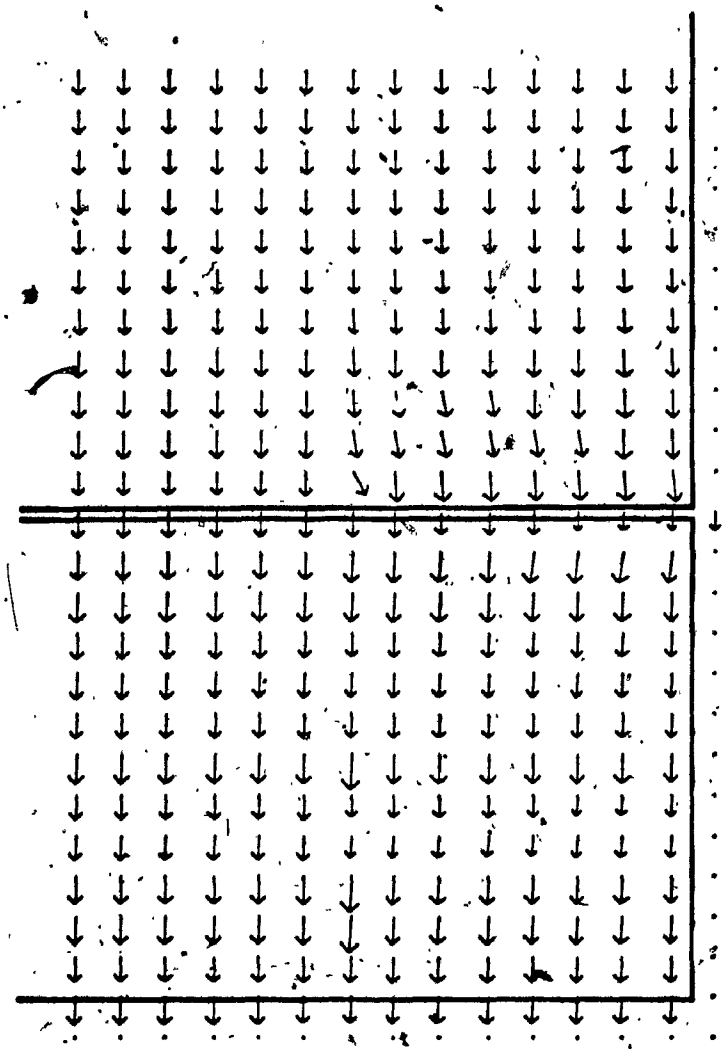

Fig. 6.22 Flux density plot over zoomed area

Aligned position

For the unaligned position, a slice is shown at 63 degrees, halfway between the unaligned rotor tip and the nearest stator pole face. The location of the slice when viewed from the end of the motor is shown in Fig. 6.23. The slice showing the motor core end region and the air is shown in Fig. 6.24. The flux density plot at the end region is shown in Fig. 6.25 and a zoomed view around the airgap region is shown in Fig. 6.26. From Figs. 6.25 and 6.26, it is seen that there is a large disturbance around the end region of the motor core. This indicates far greater end effects in the unaligned position than those in the aligned position.

6.4 Conclusion

The field analysis of a SR motor has been re-examined using a 3D finite element analysis CAD package. The results obtained indicate differences when the 2D and 3D analyses having the same degree of fineness in the finite element mesh are used. A comparison of the results such as the inductance and flux density, shows that the 2D analysis is adequate when the rotor is in the aligned position. On the other hand, a 3D analysis may be necessary if an accurate determination of the unaligned values is required. This is mainly due to the end effects which are significant when the rotor is not in the fully aligned position.

A comparison of the computational cost and time shows that a 3D finite element CAD package is more expensive and time consuming than the 2D analysis package. We have already seen in Chapter 5 that an error in the unaligned inductance values does not affect the predicted motor performance very much. Considering the above factors, the choice of using either the more expensive 3D or the less accurate 2D finite element analysis CAD package for SR motor is left to the motor designer.

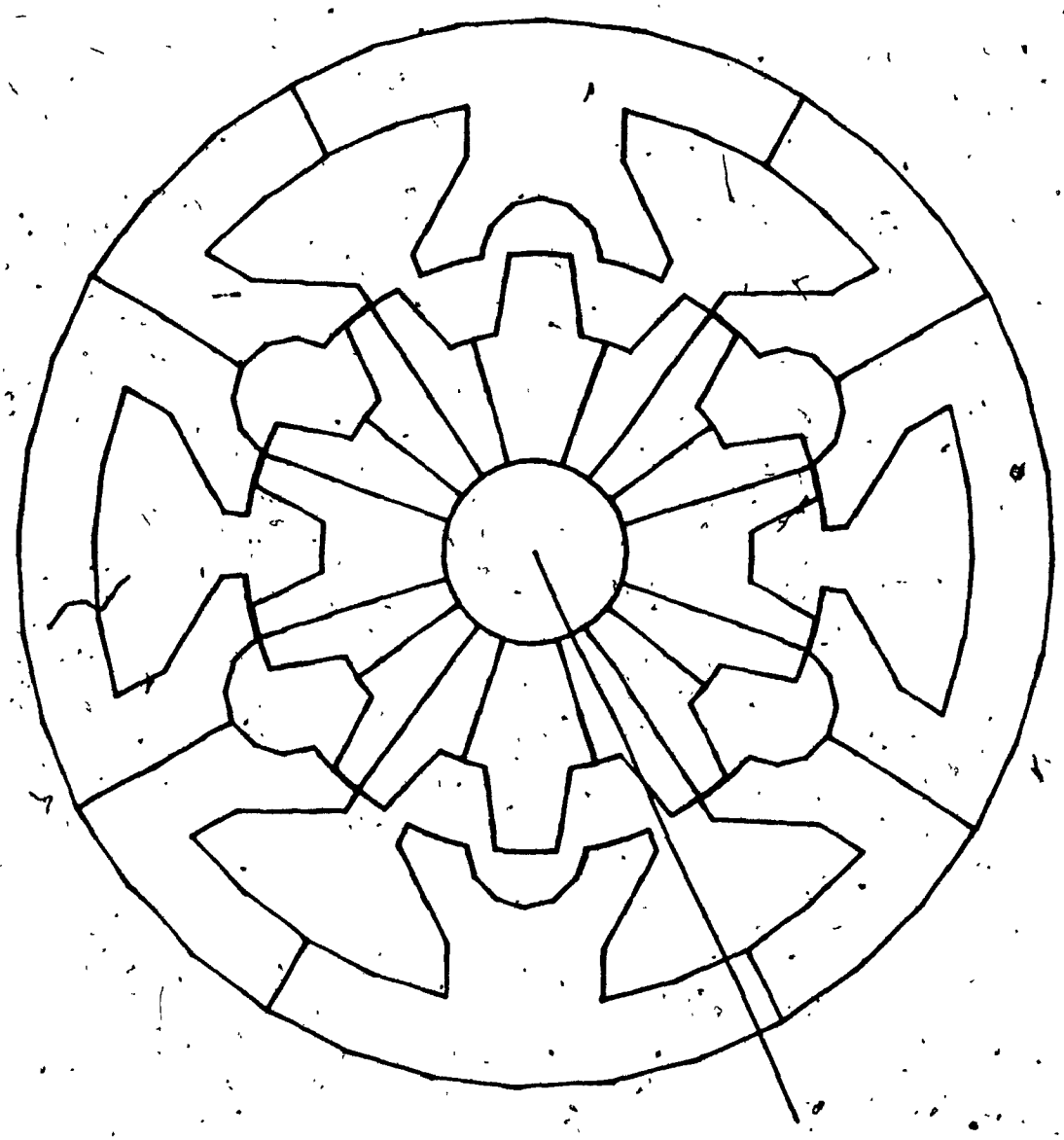

Fig. 6.23 Line showing longitudinal slice at 63 degrees

Unaligned position

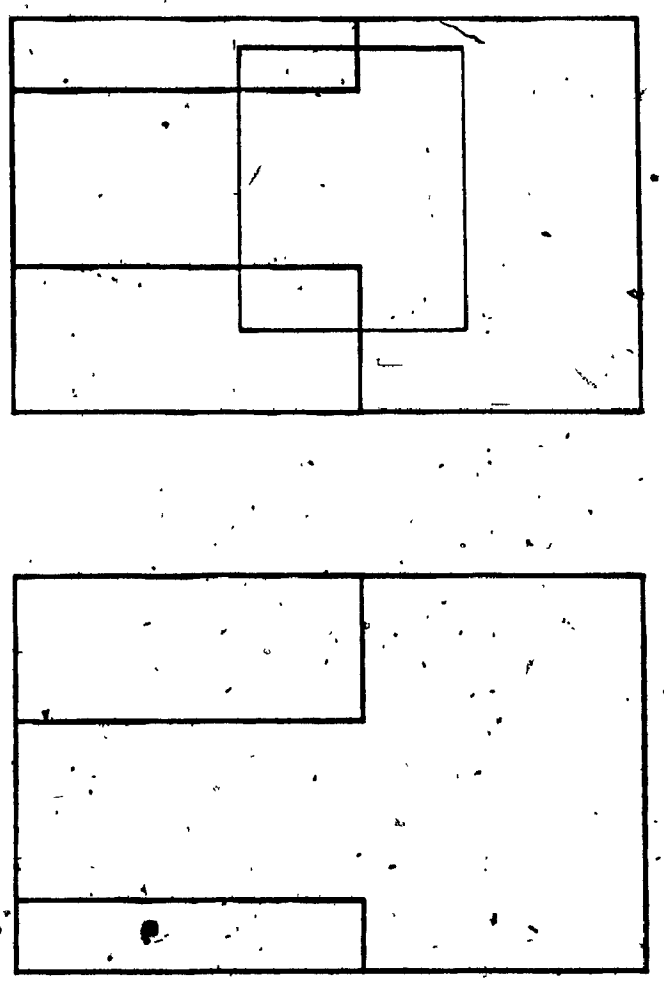

Fig. 6.24 Outline of longitudinal slice, showing zoom area

Unaligned position

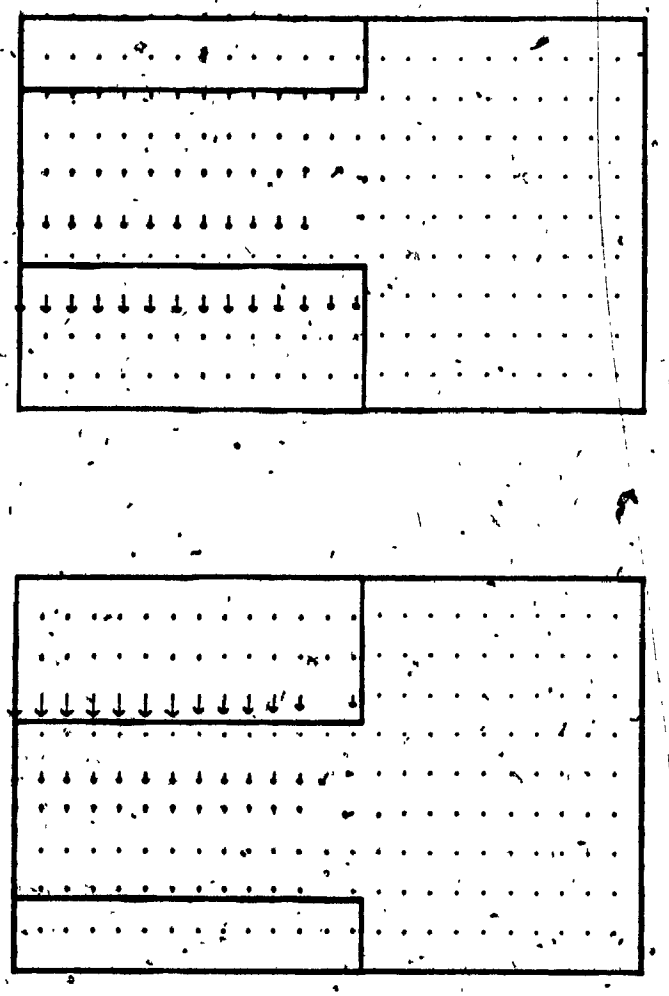

Fig. 6.25 Flux density plot along longitudinal slice

Unaligned position

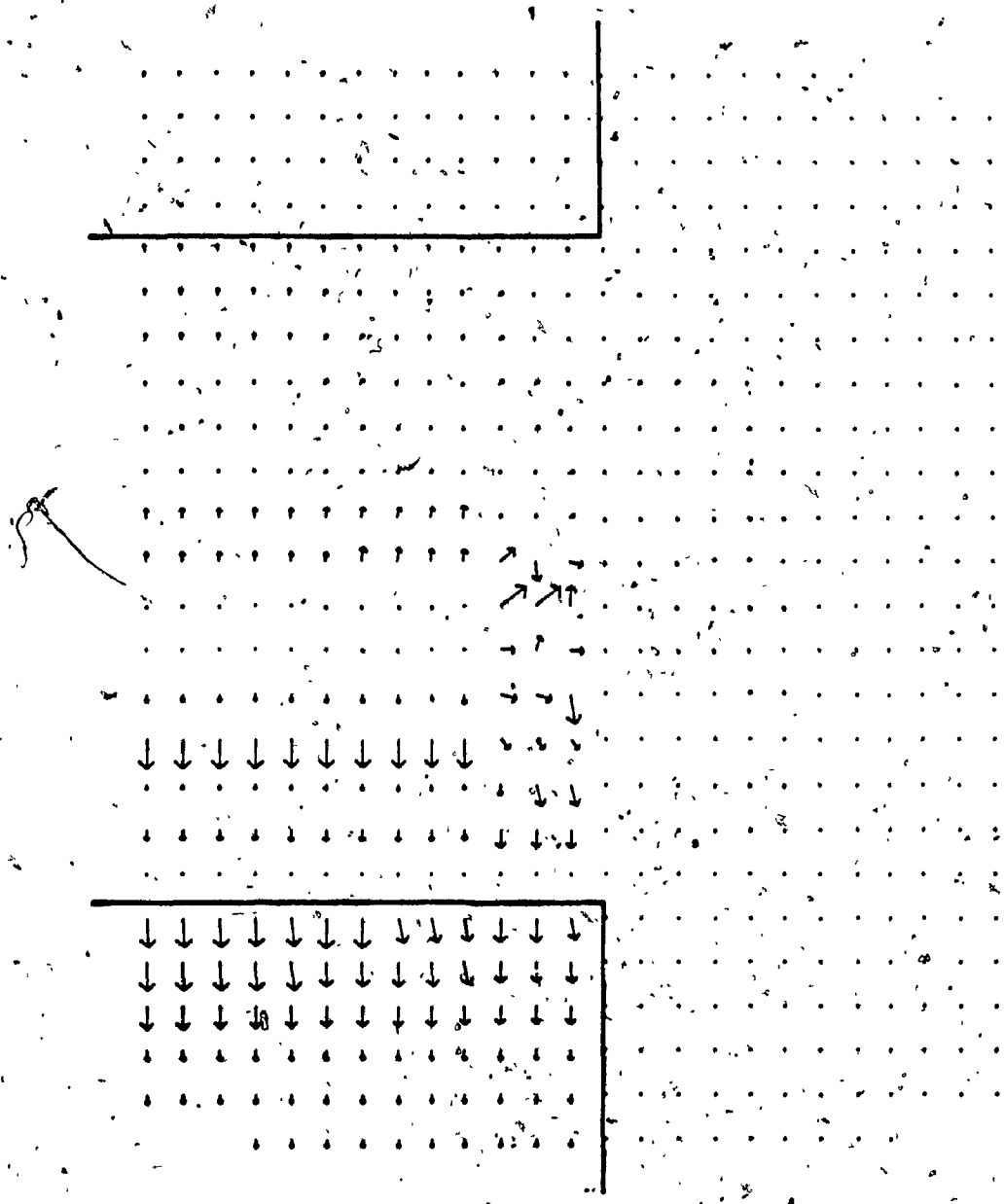

Fig. 6.26 Flux density plot over zoomed area

Unaligned position

CHAPTER 7

CONCLUSIONS

7.1 Conclusions

The analysis of the magnetic field to determine the performance of SR motors is presented in this thesis. In addition, a design procedure is developed.

The first serious work using a two dimensional finite element formulation to determine the performance of SR motor is described. Various steps involved in the use of a CAD package such as MagNet are described briefly. Due to the position dependence of the torque developed by the SR motor, the necessity of calculating field solutions at several rotor positions is demonstrated. Though alternative approaches are being developed to incorporate the time stepping nature of the magnetic field in finite element analysis [74],[75], the method adopted in this thesis to obtain the field solutions provides one of the alternatives that are being used.

In order to save computational effort and cost, the magnetic and geometric symmetries are identified. This enables the use of one quarter of the motor geometry for field solutions in the aligned and unaligned positions. For other intermediate rotor positions, one half of the motor geometry is used exploiting the periodic nature of the magnetic field, when the diametrically opposite pole windings are excited. The setting up of the boundary conditions for each case of study is discussed. A brief summary of the various methods of modeling the B-H curve of magnetic materials is given. The basic electromagnetic principles involved to obtain certain parameters of SR motor such as the flux linkages, inductances, coenergy and torque from the finite element field solutions are described.

One of the methods of checking the effectiveness of the procedures used in finite element analysis is by predicting the performance of an experimental motor and comparing the results with the experimental values those are already available. In this thesis, one of the motors considered for analysis is the 12/10 motor, described in Chapter 3, whose experimental values are already reported in the literature. The flux linkages vs current characteristics obtained by finite element analysis agree satisfactorily with the experimental values reported by Finch et al. [57] for the 12/10 motor (refer Fig. 3.22). The difference between the predicted and experimental values is very small and could be due to the use of magnetic material having a slightly different magnetization characteristic in the finite element analysis.

In order to investigate the relative performances of different configurations for SR motors, at the design stage, two motors are considered. Both are three phase motors and are described in Chapter 3. One of them is the 12/10 motor which has two teeth per stator pole and the other is the 6/4 motor having a single tooth per stator pole. The finite element analysis is used to evaluate the performances of these two motors. The performance parameters considered for evaluation and comparison are the flux linkages, terminal inductances, leakage inductances and the torque per ampere characteristics. All these parameters are found to be dependent on the rotor position and excitation current.

From the flux linkages vs current characteristics, it is observed that the change in coenergy when the rotor is nearer to the aligned position is small compared with that when the rotor is in partial overlap positions. Hence, the excitation of the phase winding can be switched off before the rotor reaches full alignment. Increasing the excitation current beyond saturation does not produce increased incremental torque. This indicates that at higher values of

excitation currents, well beyond saturation, the efficiency of the motor may decrease due to increased losses.

The unsaturated inductance of the 12/10 motor is greater than that of the 6/4 motor. The higher rate of change of inductance with rotor position in the 12/10 motor results in a greater torque being developed than that in the 6/4 motor.

In the SR motor, the winding is excited well in advance of the onset of the increasing inductance period in order to allow the winding current to reach its maximum value [1]. This is desirable since it maximizes the torque development. The relatively higher value of inductance in the unaligned position of the 12/10 motor may inhibit the faster rise of current in the phase windings.

In earlier investigations, a detailed analysis of the nature of leakages was not undertaken and reported. The assumed flux path method proposed by Corda et al. [38] attempts to consider the leakages, but the results of their study have an error of about 14.5 percent for the unaligned position values compared with those obtained using two dimensional field analysis. A significant outcome of this research is the identification and determination of the leakage inductances in SR motors. The total leakage inductance shows a slight increase in partial pole overlap positions compared with that in the aligned and unaligned positions. When compared with the terminal inductance of the phase winding, for a given excitation, the change in leakage inductance is very small.

It is clearly shown that the torque is a function of rotor position and excitation. The SR motor produces a pulsating torque even with steady excitation currents. The magnitude of the torque pulsation may be controlled by switching currents at appropriate rotor angles.

The higher number of teeth on the stator pole of the 12/10 motor has the effect of saturating the magnetic circuit at a smaller excitation current. As a consequence, the 12/10 motor has a higher torque per ampere capability than the 6/4 motor. On the other hand, in the 12/10 motor, the switching frequency is doubled compared with that of the 6/4 motor, due to its two teeth per stator pole construction. This results in increased iron losses which limits the operation of the 12/10 motor at higher speeds.

This thesis presents the first serious investigation to be directly concerned with the influence of the airgap geometry on the SR motor performance. It is observed that the changes in the stator pole arc/pole pitch ratio greatly affects the torque development than that in the rotor pole arc/pole pitch ratio. Also, a pole arc/pole pitch ratio of 0.4 suggested by some investigators need not necessarily be an optimum design value for SR motors.

It is desirable to have a greater pole arc/pole pitch ratio for the stator, keeping winding considerations in mind, and a smaller pole arc/pole pitch ratio for the rotor such that the rotor pole arc is always greater than the stator pole arc. Thus, the pole arc/pole pitch ratio for the stator and rotor can be different. From the investigation of this research, it can be recommended that the pole arc/pole pitch ratio for the stator may be 0.35 to 0.5 and that for the rotor may be 0.3 to 0.45 , for a motor having more poles on the stator than on the rotor.

A step by step design procedure for the design of a non-servo SR motor is described. The design is based on the output equation developed which is very similar to that used for conventional electrical machines. The influence of certain design parameters on the SR motor design is discussed. Selection of values for the design parameters and verification of the design through finite element

analysis are given. It is shown that the output calculated is not affected appreciably by the error in the unaligned inductance value. A criterion to evaluate the operational limit is developed. The limiting value of the incremental power output is found to occur when the incremental aligned inductance is equal to the value of the unaligned inductance.

The postprocessing of 3D finite element analysis indicates a difference in the results obtained by using a 2D analysis on a motor model with the same degree of fineness in the finite element mesh. From a comparison of the results such as the inductance and the flux density values it is observed that the 2D approximation in the aligned position agrees favorably with the 3D analysis. On the other hand, the results for the unaligned position differ considerably. These are due to the end effects when the rotor is in the unaligned position and the longer airgap in the magnetic circuit than that in the aligned position. It has already been seen that an error in the unaligned inductance value can be tolerated as it does not affect the performance prediction greatly.

7.2 Recommendations for Future Work

A suitable electric circuit model similar to that of conventional electrical machines will be useful for further understanding and control of SR machines. The behaviour of these machines under steady state and dynamic conditions can be investigated. Torque pulsations and noise are the problems associated with SR motors. The possibility of reducing them by controlling the motor input current waveforms or by shaping the poles at the motor design stage can be studied. Improvements in the design of power conditioner may enhance the ease of motor control for a desired application.

CHAPTER 8

REFERENCES

1. Lawrenson,P.J., Stephenson,J.M., Blenkinsop,P.T., Corda,J., and Fulton,N.N., "Variable speed switched reluctance motors", Proc.IEE, Vol 127, No.4, April 1980, pp. 253-265.

2. Bedford,B.D., "Compatible brushless reluctance motors and controlled switch circuits", U.S. Patent 3679953, July 25, 1972.

3. Unnewehr,L.E., "Sine pulse controller for variable reluctance motor", U.S. Patent 3714533, Jan. 30, 1973.

4. Byrne,J., and Lacy,J.C., "Electrodynamic system comprising a variable reluctance machine", U.S.Patent 3956678, May 11, 1976.

5. Discussion on "Variable speed switched reluctance motor Systems", Proc. IEE, Vol.128, Pt.B, No.5, Sept., 1981, pp. 260-268.

6. Ray,W.F., Davis,R.M., "Inverter drive for doubly salient reluctance motor: Its fundamental behaviour, linear analysis and cost implications", IEE Electrical Power Applications, Vol 2, No.6, Dec. 1979, pp. 185-193.

7. Davis,R.M., Ray,W.F., and Blake,R.J., "Inverter drive for switched reluctance motor: Circuits and component ratings", Proc.IEE, Vol 128, No.2, March 1981, pp. 126-136.

8. Byrne,J.V., "Tangential forces in overlapped pole geometries incorporating ideally saturable material", IEEE Trans. on Magnetics, Vol.MAG-8, 1972, pp. 2-9.

9. Brian Bowers, "The eccentric electromagnetic engine- a chapter from the very early history of the electric motor", Electronics and Power, July, 1972, pp. 269-272.

10. Anderson,A.F., "Robert Davidson - father of electric locomotive", Proc.IEE History of electrical engineering conference 1975.

11. Post,R.C., "The Page locomotive - federal sponsorship of invention in mid 19th century America", Technol. Culture, 1973, Vol.13, pp. 140-169.

12. Walker,J.H., "High frequency alternators", JIEE, 1946, Part II, pp. 67-80.

13. Pohl,R., "Theory of pulsating field machines", JIEE, 1946, Part II, pp. 37-47.

14. Mukherji,K.C., and Tustin,A., "Vernier reluctance motor", Proc. IEE, Vol.121, No.9, Sept. 1974, pp. 965-974.

15. Lawrenson,P.J., and Agu,L.A., "Theory and performance of polyphase reluctance machines", Proc. IEE, Vol.111, No.8, Aug. 1964, pp. 1435-1445.

16. Lawrenson,P.J., and Agu,L.A., "Low inertia reluctance machines", Proc. IEE, Vol.111, No.12, Dec. 1964, pp. 2017-2025.

17. Lawrenson,P.J., "Two speed operation of salient pole reluctance machines", Proc. IEE, Vol.112, No.12, Dec. 1965, pp. 2311-2316.

18. Lawrenson,P.J., "Development and application of reluctance motors", Electronics and Power, June 1965, pp. 195-198.

19. Harris,M.R., and Andjargholi,V., "Torque production in the hybrid motor", Proc. of the International Conference on Stepping Motors and Systems, July, 1974, pp. 148-157.

20. Harris,M.R., Andjargholi,V., Hughes,A., Lawrenson,P.J., and Ertan,B., "Limitations of reluctance torque in doubly salient structures", Proc. of the International Conference on Stepping Motors and Systems, July, 1974, pp. 158-168.

21. Harris,M.R., Andjargholi,V., Lawrenson,P.J., Hughes,A., and Ertan,B., "Static torque in PM and VR stepping motors: A comparative review", IEE Conf. Publ. No.136, Small Electrical Machines, March, 1976, pp. 100-103.

22. Harris,M.R., Hughes,A., and Lawrenson,P.J., "Static torque production in saturated double salient machines", Proc.IEE, vol 122,No.10, Oct.1975, pp. 1121-1127.

23. Harris,M.R., Andjargholi,V., Lawrenson,P.J., Hughes,A., and Ertan,B., "Unifying approach to the static torque of stepping motor structures", Proc.IEE, Vol 124, No.12, Dec.1977, pp. 1215-1224.

24. Acarnley,P.P., "Analysis and improvement of the steady state performance of variable reluctance stepping motors", Ph.D Thesis, Leeds University, 1977.

25. Byrne,J.V., and Lacy,J.G., "Characteristics of saturable stepper and reluctance motors", Small Electrical Machines, IEE Conf. Publ. No.136, 1976, pp. 93-96.

26. O'Connor,W.J., "Magnetic forces in idealised saturable-pole configurations", Proc. IEE, Vol.127, Pt.B, No.1, Jan. 1980, pp. 29-33.

27. Jarret,J., "Machines electriques a reluctance variable et a dents saturees", Tech. Mod., 1976, 2, pp. 78-80.

28. Unnewehr,L.E., and Koch,W.H., "An axial air-gap reluctance motor for variable speed applications", IEEE Trans. PAS-93, 1974, pp. 367-376.

29. Koch,W.H., "Thyristor controlled pulsating field reluctance motor system", Electric Machines and Electromechanics, 1977, 1, pp. 201-215.

30. Mukherji,K.C., and Neville,S., "Magnetic permeance of identical double slotting", Proc.IEE, Vol 118, No.9, Sept. 1971, pp. 1257-1268.

31. Bausch,H., and Rieke,B., "Speed and torque control of thyristor-fed reluctance motors", Proc. of the international conference on electrical machines, Vienna, 1976, Part I, pp. 128-1-128-10.

32. Bausch,H., and Rieke,B., "Performance of thyristor-fed electric car reluctance machines", Proc. of the international conference on electrical machines, Brussels, 1978, pp. E4/2-1-E4/2-10.

33. Lawrenson,P.J., "Switched reluctance motor drives.", Electronics and Power, Feb 1983, pp. 144-147.

34. Reed,J., "Switched reluctance drive systems", Proc. on Drives/Motors/Controls, Harrogate, Oct. 1983, pp. 118-121.

35. Davis,R.M., "Switched reluctance drive", Proc. on Drives/Motors/Controls, Harrogate, Oct. 1983, pp. 188-191.

36. Stephenson,J.M., and Corda,J., "Computation of torque and current in doubly salient inductance motors from nonlinear magnetisation data", Proc. IEE, Vol.126, No.5, May, 1979, pp. 393-396.

37. Ward,P.A., and Lawrenson,P.J., "Magnetic permeance of doubly salient airgaps", Proc.IEE, Vol 126, No.6, June 1977, pp. 542-543.

38. Corda,J., and Stephenson,J.M., "An analytical estimation of the minimum and maximum inductances of a double salient motor", Proc. Int. Conf. on Stepping motors and systems, University of Leeds, 1979, pp. 50-59.

39. Chai,H.D., "Permeance model and reluctance force between toothed structures", Proc. of the 2nd Symposium on incremental motion control system and devices, University of Illinois, May 1973, paper K.

40. Lawrenson,P.J., Stephenson,J.M., and Corda,J., "Switched reluctance motors for traction drives", Proceedings of the International Conference on Electrical Machines, Athens, Greece, 1980, pp. 410-417.

41. Davis,R.M., Ray,W.F., and Blake,R.J., "An inverter for a switched reluctance motor", Proc. of the International Conference on Electrical Machines, Athens, Greece, 1980, pp. 1206-1214.

42. Corda,J., and Stephenson,J.M., "Speed control of switched reluctance motors", Proc. of the International Conference on Electrical Machines, Budapest, Hungary, 1982, pp. 235-238.

43. Lawrenson,P.J., Ray,W.F., Davis,R.M., Stephenson,J.M., Fulton.N.N., and Blake,R.J., "Controlled-speed switched-reluctance motors: Present status and future potentials", Drives/Motors/Control '82, Leeds, 1982, pp. 23-31.

44. Fulton,N.N., Lawrenson,P.J., Stephenson,J.M., Blake,R.J., Davis,R.M., and Ray,W.F., "Some recent experience with switched reluctance motor drives", IEE Int. Conf. on Eleetrical Machines, Conf. Publ. 213, July 1982, pp. 254-256.

45. Ray,W.F., Davis,R.M., Stephenson,J.M., Lawrenson,P.J., Blake,R.J., and Fulton,N.N., "Industrial switched reluctance drives - Concepts and performance", Proc. of IEE Conf. on Power Electronics and Variable Speed Drives, London, 1984, pp. 357-360.

46. Blake,R.J., Davis,R.M., Ray,W.F., Fulton,N.N., Lawrenson,P.J., and Stephenson,J.M., "The control of switched reluctance motors for battery electric road vehicles", Proc. of IEE Conf. on Power Electronics and Variable Speed Drives, London, 1984, pp. 361-364.

47. French,J.R., "Switched reluctance motor drives for rail traction: relative assessment", Proc.IEE, Vol 131, Pt.B, No.5, Sept. 1984, pp. 209-219.

48. Ray,W.F., Davis,R.M., Lawrenson,P.J., Stephenson,J.M., Fulton,N.N., and Blake,R.J., "Switched reluctance motor drives for rail traction; a second view", Proc.IEE, Vol 131, Pt.B, No.5, Sept. 1984, pp. 220-225.

49. Fulton,N.N., Lawrenson,P.J., Stephenson,J.M., Blake,R.J., Davis,R.M., and Ray,W.F., "Recent developments in high performance switched reluctance drives", Second Int. Conf. on Electrical Machines - Design and Applications, Sept. 1985, pp. 130-133.

50. Ray,W.F., Lawrenson,P.J., Davis,R.M., Stephenson,J.M., Fulton,N.N., and Blake,R.J., "High performance switched reluctance brushless drives", IEEE Trans. on Industry Applications, Vol IA22, No.4, July/Aug. 1986, pp. 722-730.

51. Ray,W.F., Davis,R.M., and Blake,R.J., "The control of SR motors", Proc. of the Conference on Applied Motion Control 1986, Minneapolis, Minnesota, June 1986, pp. 137-145.

52. Davis,R.M., and Ray,W.F., British Patent 13415, 1977.

53. Davis,R.M., and Ray,W.F., British Patent 13416, 1977.

54. Stephenson,J.M., British Patent 22891, 1978.

55. Davis,R.M., and Ray,W.F., British Patent 22892, 1978.

56. Davis,R.M., and Ray,W.F., British Patent 22893, 1978.

57. Finch,J.W., Harris,M.R., Musoke,A., and Metwally,H.M.B., "Variable speed drives using multi-tooth per pole switched reluctance motors", Proc. 13th Annual Symposium on Incremental Motion Control Systems and Devices, May 1984, pp. 293-301.

58. Finch,J.W., Harris,M.R., Metwally,H.M.B., and Musoke,A., "Switched Reluctance motors with multiple teeth per pole: Philosophy of design", Second Int. Conf. on Electrical Machines - Design and Applications, Sept. 1985, pp. 134-138.

59. Miller,T.J.E., "Converter volt-ampere requirements of the switched reluctance motor drive", IEEE Trans. on Industry Applications, Vol IA21, No.5, Sept/Oct. 1985, pp. 1136-1144.

60. Bose,B.K., Miller,T.J.E., and Szczesny,P.M., and Bicknell,W.H., "Microprocessor control of switched reluctance motor", IEEE Trans. on Industry Applications, Vol IA22, No.4, July/Aug. 1986, pp. 708-715.

61. Harris,M.R., Finch,J.W., Mallick,J.A., and Miller,T.J.E., "A review of the integral horsepower switched reluctance drive", IEEE Trans. on Industry Applications, Vol.IA22, No.4, July/Aug. 1986, pp. 716-721.

62. Bass,J.T., Ehsani,M, Miller,T.J.E., and Steigerwald,R.L., "Development of a unipolar converter for variable reluctance motor drives", IEEE Industry Applications Society Annual Meeting, Oct. 1985, pp. 1062-1068.

63. Carter.F.W., "The magnetic field of the dynamoelectric machine", Jour. IEE, 1926, pp. 1115-1138.

64. Mukherji,K.C., and Neville,S., "Magnetic permeance of identical double slotting", Proc. IEE, Vol. 118, No.9, Sept. 1971, pp. 1257-1268.

65. Silvester,P.P., and Chari,M.V.K., "Finite element solution of saturable magnetic field problems", IEEE Trans. on Power Apparatus and Systems, Vol. PAS-89, No.7, Sept/Oct. 1970, pp. 1642-1651.

66. Chari,M.V.K., "Finite element analysis of nonlinear magnetic fields in electrical machines", Ph.D Thesis, McGill University, Montreal, Canada, 1970.

67. Trutt,F.C., Erdelyi,E.A., and Hopkins,R.E., "Representation of the magnetization characteristic of dc machines for computer use", IEEE Trans. on Power Apparatus and Systems, Vol. PAS-87, No.3, March 1968, pp. 665-669.

68. El-Sherbiny,M.K., "Representation of the magnetization characteristic by a sum of exponentials", IEEE Trans. on Magnetics, Vol. MAG-9, No.1, March 1973, pp. 60-61.

69. Silvester,P.P., Cabayan,H.S., and Browne,B.T., "Efficient techniques for finite element analysis of electrical machines", IEEE Trans. on Power Apparatus and Systems, Vol. PAS-92, July/Aug. 1973, pp. 1274-1281.

70. Brauer,J.R., "Simple equations for the magnetization and reluctivity curves of steel", IEEE Trans. on Magnetics, Vol. MAG-11, No.1, Jan. 1975, p. 81.

71. Hoole,S.R.H., and Hoole,N.R.G., "Reluctivity characteristics in nonlinear finite element analysis of magnetostatic fields", IEEE Trans. on Magnetics, Vol. MAG-22, No.5, Sept. 1986, pp. 1352-1353.

72. Arumugam,R., Lowther,D.A., Krishnan,R., and Lindsay,J.F., "Magnetic field analysis of a switched reluctance motor using a two dimensional finite element model", IEEE Trans. on Magnetics, Vol.MAG-21, No.5, Sep. 1985, pp. 1883-1885.

73. Simkin,J., and Trowbridge,C.W., "Three dimensional nonlinear electromagnetic field computations using scalar potentials", Proc.IEE, Vol.127, Pt.B, No.6, Nov. 1980, pp. 368-374.

74. Hoole,S.R.H., "Rotor motion in the dynamic finite element analysis of rotating electrical machinery", IEEE Trans. on Magnetics, Vol.MAG-21, No.6, Nov. 1985, pp. 2292-2295.

75. Davat,B., Ren,Z., and Lajoie-Mazenc,M., "The movement in field modelling", IEEE Trans. on Magnetics, Vol.MAG-21, No.6, Nov. 1985, pp. 2296-2298.

APPENDIX I

Consider, Fig. 5.2, redrawn below to derive an expression for the operational limit of SR motors. For a stator operating current of i_{so} amperes, the mechanical power output is given by the area OABCO. If the current i_{so} is incremented by Δi, then the change in mechanical power output $\Delta\omega_m$ will be given by the area ADEBA.

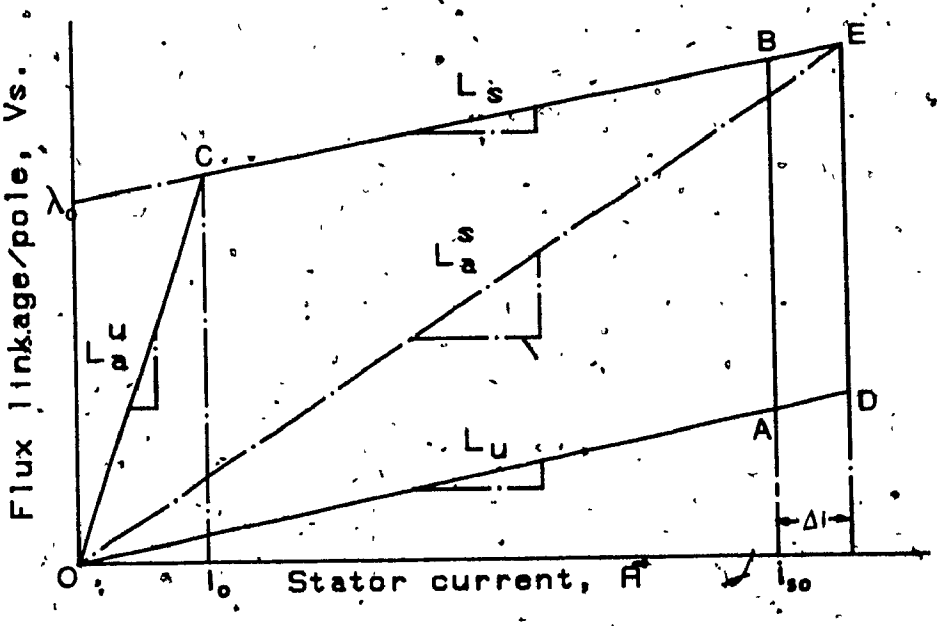

When expressed in terms of the inductances L_u and L_s,

$$Area\ OABCO = \lambda_0 i_{so} + \frac{1}{2}L_s i_{so}^2 - \frac{1}{2}L_u i_{so}^2 - \frac{1}{2}\lambda_0 I_0$$

If the current is incremented to $(i_{so}+\Delta i)$, then

$$Area\ ODECO = \lambda_0 (i_{so} + \Delta i) + \frac{1}{2}(L_s - L_u)(i_{so} + \Delta i)^2 - \frac{1}{2}\lambda_0 I_0$$

The change in area due to Δi,

$$\Delta W = Area\ ODECO - Area\ OABCO$$
$$= \lambda_0 \Delta i + (L_s - L_u) i_{so} \Delta i + \frac{1}{2}(L_s - L_u)\Delta i^2$$

The incremental mechanical energy per unit input current,

$$g_{mi} = \frac{\Delta W}{\Delta i}$$

$$= \lambda_o + (L_s - L_u) i_{so} + (L_s - L_u)\frac{\Delta i}{2}$$

For the motor considered in the design $L_u > L_s$. Hence,

$$g_{mi} = \lambda_o - (L_u - L_s) i_{so} - (L_u - L_s)\frac{\Delta i}{2}$$

This is maximum when $L_u = L_s$ and its value will be

$$g_{mi}(max) = \lambda_o$$